

# Development of a Human Mesenchymal Stem Cell and Pluripotent Stem Cell Derived Cardiomyocyte Seeded Biological Suture for Cell Delivery to Cardiac Tissue for Cardiac Regeneration Applications

---

A Dissertation  
Submitted to the Faculty of the  
WORCESTER POLYTECHNIC INSTITUTE  
In partial fulfillment of the requirements for the Degree of  
Doctorate of Philosophy in Biomedical Engineering

October 10<sup>th</sup> 2017

By



Katrina J. Hansen



Glenn R. Gaudette, Ph.D.

Professor, Advisor

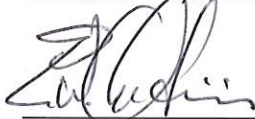
Department of Biomedical Engineering  
Worcester Polytechnic Institute



Marsha W. Rolle, Ph.D.

Associate Professor

Department of Biomedical Engineering  
Worcester Polytechnic Institute



Eric W. Overstrom, Ph.D.

Professor, Provost and Senior Vice President  
Wentworth Institute of Technology



George D. Pins, Ph.D.

Associate Professor

Department of Biomedical Engineering  
Worcester Polytechnic Institute



Michael A. Laflamme, M.D., Ph.D.

Senior Scientist

Toronto General Hospital Research Institute

## Acknowledgements

I have a number of people I would like to thank in the completion of this dissertation work. First and foremost, I would like to thank my advisor, Glenn Gaudette, PhD, for his unwavering support and mentorship. Glenn gave me one of my first real research experiences as an REU student and he gave me the opportunity to complete my PhD in a lab working on cardiovascular regeneration, which has been a goal of mine since high school. He has been a wonderful advisor who has given me numerous opportunities to grow as a researcher and leader. From learning new surgical techniques, grant writing and manuscript reviews, advising undergraduates, running outreach activities, and presenting my work at various conferences I have been allowed to develop as a scientist, mentor, and leader under his mentorship.

In addition to Dr. Gaudette, I would like to recognize and thank my dissertation committee. Michael Laflamme from the University of Toronto allowed me to train in his lab and he has always made himself available for skype meetings to discuss my most recent results and has always provided invaluable suggestions and insights. Drs. Marsha Rolle, George Pins, and Eric Overstrom from WPI have been wonderful sources of support and knowledge throughout the last few years and I am ever thankful for their insights and guidance.

The completion of this work would not have been possible without the help from members of my lab. Through laying the groundwork for my research, providing critical feedback on my work, and just being supportive they have been instrumental in my time in the lab. One of my greatest joys from my time at WPI are all of the phenomenal undergraduate students I have gotten to meet and mentor over the years. Without their hard work sectioning and staining or analyzing hundreds of datasets I could not have completed much of this work.

I, of course, want to thank all of the amazing graduate students at WPI. You guys have become wonderful friends with whom I have been able to share the failures and successes that come along with graduate school.

Lastly, I want to thank my friends and family. Thank you for always supporting me in this process, for encouraging me when I was discouraged and/or uninspired, for letting me vent when an experiment failed, and for celebrating my successes. I want to thank my father for instilling in me a love for science, from putting a freshly excised, still beating fish heart in my hand to teaching me the constellations. He showed me how cool the world is and I so wish he was here to see me complete this body of work. I reserve my last thank you for my mother, my nana, and my sister, I simply could not have done this without you.

## Table of Contents

Acknowledgements.....	ii
Table of Figures.....	vii
Table of Tables.....	ix
Abbreviations .....	x
Abstract.....	xii
<b>1 Overview .....</b>	<b>1</b>
<b>1.1 Introduction .....</b>	<b>1</b>
<b>1.2 Overall goal and hypothesis .....</b>	<b>3</b>
<b>1.3 Specific Aim 1. Determine the effects of hMSCs delivered via a fibrin suture on mechanical function of an infarcted heart. ....</b>	<b>4</b>
1.3.1 Objective 1a: Investigate cell seeding conditions to improve attachment of hMSCs onto fibrin microthread sutures. ....	4
1.3.2 Objective 1b: Evaluate changes in mechanical function when hMSC seeded fibrin sutures are implanted in the infarct zone. ....	4
<b>1.4 Specific Aim 2. Produce and characterize contractile hPS-CM seeded fibrin microthreads. ....</b>	<b>4</b>
1.4.1 Objective 2a: Develop a method to characterize the contractile behavior of hPS-CM.....	5
1.4.2 Objective 2b: Produce and characterize contractile hPS-CM seeded microthreads. ....	5
<b>1.5 Specific Aim 3. Evaluate the use of fibrin microthread sutures to deliver hPS-CM to healthy cardiac tissue. ....</b>	<b>6</b>
<b>1.6 References .....</b>	<b>8</b>
<b>2 Background.....</b>	<b>9</b>
<b>2.1 Introduction .....</b>	<b>9</b>
2.1.1 The cardiovascular system .....	9
<b>2.2 Cardiovascular disease.....</b>	<b>10</b>
2.2.1 Myocardial infarction .....	11
2.2.2 Therapeutic treatment strategies for MI.....	12
2.2.3 Techniques to measure and assess cardiovascular function .....	12
<b>2.3 Cardiovascular regeneration .....</b>	<b>15</b>
2.3.1 Material based.....	16
2.3.2 Cell based .....	17
2.3.2.1 Skeletal myoblasts.....	18
2.3.2.2 Cardiac progenitor cells.....	18
2.3.2.3 Bone marrow derived cells.....	19
2.3.2.4 Pluripotent stem cells.....	20
2.3.3 Cell delivery methods.....	22
2.3.4 Fibrin microthreads for cell delivery.....	23
<b>2.4 References .....</b>	<b>25</b>
<b>3 Objective 1a: Investigate cell seeding conditions to improve attachment of hMSCs onto fibrin microthread sutures. ....</b>	<b>33</b>
<b>3.1 Introduction .....</b>	<b>33</b>
<b>3.2 Materials and methods.....</b>	<b>34</b>
3.2.1 Fibrin microthread production .....	34
3.2.2 Human MSC culture .....	35
3.2.3 Biological suture seeding .....	35
3.2.4 hMSC cell attachment quantification .....	36

3.2.5	Histological data.....	36
3.2.6	Statistical analysis .....	36
<b>3.3</b>	<b>Results .....</b>	<b>37</b>
3.3.1	Effect of cell seeding concentration on hMSC attachment to biological sutures.....	37
3.3.2	Effect of incubation time on hMSC attachment to biological sutures.....	37
<b>3.4</b>	<b>Discussion .....</b>	<b>38</b>
<b>3.5</b>	<b>References .....</b>	<b>40</b>
<b>4</b>	<b>Objective 1b: Evaluate changes in mechanical function when hMSC seeded fibrin sutures are implanted in the infarct zone.....</b>	<b>42</b>
<b>4.1</b>	<b>Introduction .....</b>	<b>42</b>
<b>4.2</b>	<b>Materials and methods.....</b>	<b>42</b>
4.2.1	Infarct model.....	42
4.2.2	Terminal surgery .....	43
4.2.3	Assessment of global and regional mechanical function.....	44
4.2.4	Histological data.....	44
4.2.5	Infarct region and suture area quantification.....	45
4.2.6	Statistical analysis .....	46
<b>4.3</b>	<b>Results .....</b>	<b>46</b>
4.3.1	hMSC seeded biological sutures do not improve global function after infarction .....	46
4.3.2	hMSC seeded biological sutures improve regional mechanical function after infarction..	47
4.3.3	Cells delivered via the suture remain in the heart at least one week after delivery.....	48
4.3.4	Infarct size is reduced using unseeded and hMSC seeded sutures .....	49
4.3.5	hMSCs preserve suture area in infarct.....	50
<b>4.4</b>	<b>Discussion .....</b>	<b>50</b>
<b>4.5</b>	<b>References .....</b>	<b>53</b>
<b>5</b>	<b>Objective 2a: Develop a method to characterize the contractile behavior of hPS-CM .</b>	<b>56</b>
<b>5.1</b>	<b>Introduction .....</b>	<b>56</b>
<b>5.2</b>	<b>Materials and methods.....</b>	<b>57</b>
5.2.1	Generation and culture of pluripotent stem cell derived cardiomyocytes.....	57
5.2.2	High density mapping analysis of cardiomyocyte contraction .....	58
5.2.3	Brightfield and fluorescent imaging acquisition .....	59
5.2.4	Loading iPS-CM with fluo-4 AM.....	61
5.2.5	Calcium transient analysis .....	61
5.2.6	Infusion of chemical stimulation via epinephrine.....	62
5.2.7	Statistical analysis.....	62
<b>5.3</b>	<b>Results .....</b>	<b>62</b>
5.3.1	Effect of spatial resolution on determining contraction in hPS-CM .....	62
5.3.2	Contractile mechanics of hPS-CM can be monitored over 21 days.....	63
5.3.3	Measurements of calcium transients and mechanical contraction in hPS-CM .....	64
5.3.4	Isoproterenol simulation increases contractile strain and beat frequency .....	67
<b>5.4</b>	<b>Discussion .....</b>	<b>68</b>
<b>5.5</b>	<b>References .....</b>	<b>74</b>
<b>6</b>	<b>Objective 2b: Produce and characterize contractile hPS-CM seeded microthreads.....</b>	<b>78</b>
<b>6.1</b>	<b>Introduction .....</b>	<b>78</b>
<b>6.2</b>	<b>Materials and methods.....</b>	<b>80</b>
6.2.1	Seeding platform for hPS-CM attachment to fibrin microthreads .....	80

6.2.2	Effect of ECM surface coatings on hPS-CM attachment.....	81
6.2.3	Viability of hPS-CM attachment on fibrin microthreads.....	81
6.2.4	Capturing contraction of hPS-CM seeded microthreads.....	82
6.2.5	Immunocytochemistry.....	83
6.2.6	Conduction velocity measurements.....	83
6.2.7	Alpha-actinin fiber alignment.....	83
6.2.8	Statistical analysis.....	83
<b>6.3</b>	<b>Results.....</b>	<b>84</b>
6.3.1	Collagen IV coating improves hPS-CM attachment to fibrin microthreads.....	84
6.3.2	hPS-CM exhibit opposite temporal trends in contractile and maximum strains when cultured on TCP and fibrin microthreads.....	85
6.3.3	Contractile frequency increases over 21 days for hPS-CM cultured on TCP and microthreads.....	87
6.3.4	hPS-CM contraction direction becomes more aligned with the thread over 21 days in culture	88
6.3.5	hPS-CM become more aligned along the microthread over 21 days in culture.....	90
6.3.6	hPS-CM seeded on microthreads increase conduction velocity over 21 days in culture...	91
<b>6.4</b>	<b>Discussion.....</b>	<b>92</b>
<b>6.5</b>	<b>References.....</b>	<b>97</b>
<b>7</b>	<b>Specific Aim 3: Evaluate the use of fibrin microthread sutures to deliver hPS-CM to healthy cardiac tissue.....</b>	<b>100</b>
<b>7.1</b>	<b>Introduction.....</b>	<b>100</b>
<b>7.2</b>	<b>Materials and methods.....</b>	<b>102</b>
7.2.1	Implant model.....	102
7.2.2	Histological analysis.....	102
7.2.3	<i>In vitro</i> cell delivery assay.....	103
7.2.4	Statistical analysis.....	105
<b>7.3</b>	<b>Results.....</b>	<b>105</b>
7.3.1	Cell retention at 1 hour, 8 hours, 1 day, and 3 days.....	105
7.3.2	Cell distribution across the delivered area.....	107
7.3.3	Cell morphology after delivery.....	108
7.3.4	<i>In vitro</i> cell delivery assay indicates apoptotic cells as early as 30 minutes post-delivery	109
<b>7.4</b>	<b>Discussion.....</b>	<b>112</b>
<b>7.5</b>	<b>References.....</b>	<b>118</b>
<b>8</b>	<b>Conclusions and future work.....</b>	<b>121</b>
<b>8.1</b>	<b>Conclusions.....</b>	<b>121</b>
<b>8.2</b>	<b>Future work.....</b>	<b>125</b>
<b>8.3</b>	<b>References.....</b>	<b>129</b>
<b>9</b>	<b>Appendix.....</b>	<b>132</b>
<b>9.1</b>	<b>Reprint Permissions.....</b>	<b>132</b>
<b>9.2</b>	<b>Protocols.....</b>	<b>132</b>
9.2.1	Protocol for seeding fibrin sutures using rotator method.....	132
9.2.2	Masson's Trichrome staining.....	133
9.2.3	High density mapping for regional cardiac function analysis.....	134
9.2.4	Dual imaging scope/setup parameters and analysis.....	135

9.2.5	High density mapping for contractile cell analysis.....	136
9.2.6	Protocol for seeding microthreads with hPS-CM.....	137
9.2.7	Ku80, Alpha-actinin, and Connexin 43 staining .....	137
9.2.8	Annexin V Assay .....	138

Table of Figures

Figure 2-1. Pressure volume work loop. ....9

Figure 2-2. Description of HDM method. a .....14

Figure 2-3. Schematic of cardiovascular regeneration techniques.. .....16

Figure 2-4. Fibrin microthread suture delivery to the heart.. .....24

Figure 3-1. Fibrin suture seeding.....35

Figure 3-2. Effect of cell seeding concentration on hMSC attachment to biological suture.. .....37

Figure 3-3. Effect of seeding time on hMSC attachment to biological suture. ....38

Figure 4-1. Implanted hMSC seeded suture.....43

Figure 4-2. Global function is not impacted by hMSC seeded biological suture treatment after infarct.  
.....46

Figure 4-3. hMSC seeded biological sutures improve regional mechanical function after infarct.. .....47

Figure 4-4. hMSCs persist in myocardium 1 week after delivery.....48

Figure 4-5. Infarct size and suture area.. .....49

Figure 5-1 Use of High Density Mapping to determine displacement fields of contracting hPS-CM. ....59

Figure 5-2. Image acquisition schematic with temporal control of fluorescence or brightfield  
illumination. ....60

Figure 5-3. The effect of window size and window spacing on reported contractile strain values.....63

Figure 5-4. Representative distribution of strain within clusters. ....63

Figure 5-5. HDM can be used to quantify contraction of hPS-CM seeded on collagen IV coated plates  
over 21 days. ....64

Figure 5-6. Overlay of mechanical contraction and calcium transients in iPS-CM. ....65

Figure 5-7. Overlay of mechanical contraction and calcium transients in ES-CM. ....65

Figure 5-8. Deconvolved GCaMP calcium transient traces.....66

Figure 5-9. Isoproterenol stimulation of hPS-CM. ....67

Figure 6-1. Seeding schematic to seed hPS-CM onto fibrin microthreads.....80

Figure 6-2. Collagen IV ECM coating enhances hPS-CM attachment to fibrin microthreads.. .....84

Figure 6-3. hPS-CM seeded onto fibrin microthreads remain viable. ....85

Figure 6-4. hPS-CM exhibit opposite trends in contractile and maximum strains when cultured on TCP  
and fibrin microthreads over 21 days.....85

Figure 6-5. hPS-CM exhibit significantly higher contractile and maximum strains when cultured on  
fibrin microthread compared to TCP by 21 days.. .....86

Figure 6-6. Contractile frequency increased over 21 days for hPS-CM cultured on TCP and fibrin  
microthreads.. .....87

Figure 6-7. hPS-CM contract with higher alignment to the microthread at later timepoints.....88

Figure 6-8 A linear relationship exists between contractile alignment and contractile strain for hPS-CM  
seeded on fibrin sutures, not on TCP.. .....89

Figure 6-9. hPS-CM seeded onto fibrin microthreads express alpha-actinin and connexin 43.....90

Figure 6-10. hPS-CM demonstrate better alignment to the microthread at later timepoints.. .....90

Figure 6-11. Representative images of connexin 43 at day 21.. .....91

Figure 6-12. Conduction velocity of hPS-CM seeded sutures.. .....91

Figure 7-1. Construct for implantation sutures.. .....102

Figure 7-2 hPS-CM persist in ventricular myocardium up to 3 days after delivery via a fibrin  
microthread suture. ....105

Figure 7-3. hPS-CM can be delivered to healthy myocardium with a 67% delivery efficiency. ....106

Figure 7-4 Representative histograms indicate cells are distributed throughout the delivery track. ...107

Figure 7-5. Limited evidence of positive Connexin 43 staining between host tissue and graft tissue at 1 hour and 3 hours.....	108
Figure 7-6. Representative Hematoxylin and Eosin staining.....	108
Figure 7-7. Representative Masson’s Trichrome stained sections.....	109
Figure 7-8. In vitro cell delivery assay utilizing Annexin V to examine cell apoptosis.....	110
Figure 7-9. Percentage quantification of the <i>in vitro</i> cell delivery assay utilizing Annexin V to examine cell apoptosis.....	112
Figure 7-10. Cell number quantification of the <i>in vitro</i> cell delivery assay utilizing Annexin V to examine cell apoptosis.....	113



Table of Tables

**Table 1-1. Table showing possible combinations of optical system parameters and each resultant frame rate..... 61**

## Abbreviations

**ACE**- angiotensin- converting enzyme  
**AHA**– American Heart Association  
**ANOVA**- analysis of variance  
**BMCs**- bone marrow derived cells  
**BM-MNCs**- bone marrow mononuclear cells  
**Bpm**- beats per minute  
**Ca<sup>2+</sup>**- calcium  
**cTnT**– cardiac troponin T  
**CVD**- cardiovascular disease  
**DNA**- deoxyribonucleic acid  
**dP/dt**– change in ventricular pressure over time  
**IM**- intramyocardial  
**iPS**- induced pluripotent stem cells  
**iPS-CM**- induced pluripotent stem cell derived cardiomyocytes  
**ECM**– extracellular matrix  
**EDA**– end diastolic area  
**ESA**– end systolic area  
**ESC**- embryonic stem cells  
**EF**- ejection fraction  
**Fps**- frames per second  
**FS**- fractional shortening  
**GCaMP**- genetically encoded calcium sensor  
**HDM**– high density mapping  
**H&E**– Hematoxylin and Eosin  
**hES-CM**- human embryonic stem cell derived cardiomyocytes  
**hPS-CM**- human pluripotent stem cell derived cardiomyocytes  
**HF**- heart failure  
**hMSCs**- human mesenchymal stem cells  
**LAD**- left anterior descending coronary artery  
**LEDD**- left ventricular end diastolic diameter  
**LEDV**- left ventricular end diastolic volume  
**LESD** – left ventricular end systolic volume  
**LESV**- left ventricular end systolic volume  
**LV**- left ventricle  
**MHC**– myosin heavy chain  
**MI**- myocardial infarction  
**mg**- milligram  
**mm**- millimeter  
**mL**- milliliter  
**MSC**- mesenchymal stem cell

**MSCGM**- mesenchymal stem cell growth medium  
**NANOG**- transcription factor involved with self-renewal of ESCs  
**NIS**- sodium iodide symporter transgene  
**OCT** – medium used to embed tissue for cyrosectioning  
**OCT 4**- transcription factor involved with self-renewal of ESCs  
**dpBS**- Dulbecco’s phosphate buffered saline  
**PBS**– phosphate buffered saline  
**PCI**- Percutaneous Coronary Intervention  
**PI**- Propidium Iodide  
**PIV**– particle image velocimetry  
**PTFE** – polytetrafluoroethylene; Teflon  
**Qdots**– quantum dots  
**ROI**- region of interest  
**RPMI**- Roswell Park Memorial Institute medium; cell culture basal medium  
**RSW**– regional stroke work  
**sCMOS**- high speed camera  
**SAC**– systolic area of contraction  
**SD**- standard deviation  
**SEM** – standard error of the mean  
**SV**- stroke volume  
**TCP**– tissue culture plastic  
**TFM**– traction force microscopy  
**µg**- microgram  
**µL**- microliter  
**µm**- micrometer, micron  
**µM**- micromolar

## Abstract

Recent data show that 7.6 million Americans have survived a myocardial infarction (MI), and 5.1 million Americans suffer from severe heart failure. Stem cell therapy has the potential to improve cardiac function after MI. Two promising cells for cardiovascular regeneration therapies include human mesenchymal stem cells (hMSCs) and pluripotent stem cell derived cardiomyocytes (hPS-CM) each with their own unique method for improving cardiac function post-infarct. However, a limiting factor to cell therapies is that the methods currently used to deliver cells to the myocardium, including intramyocardial injection (considered the gold standard), suffer from low retention rates. To promote localization of delivered cells to the infarct and increase retention rates, our lab has developed a fibrin biological suture that can deliver human mesenchymal stem cells (hMSCs) with an efficiency of 64% compared to just 11% with intramyocardial injection in the normal rat heart.

In this dissertation we sought to examine the functionality of hMSC and hPS-CM seeded sutures and their impact on cardiovascular regeneration applications. We began by delivering hMSC seeded fibrin sutures to an infarcted rat heart and found that the sutures are an effective method to deliver cells to the infarcted myocardium and demonstrated a trend towards improved regional mechanical function in the infarct region over infarct alone. Next, we transitioned to using hPS-CM and developed methods to seed the sutures, as well as a method to measure hPS-CM contractility with high spatial and temporal resolution, while concurrently capturing calcium transients. This technique allowed us to examine the contractile behavior in terms of contractile strain and conduction velocity of hPS-CM seeded on fibrin microthreads over 21 days in culture. We found that the fibrin microthread is a suitable scaffold for hPS-CM attachment and contraction and that extended culture promotes cell alignment along the length of the suture as well as improvements in contractile function in terms of increases in contractile strain and conduction velocity. Finally, we delivered the hPS-CM seeded microthreads to an uninjured rat heart and found a delivery efficiency of 67%. Overall, we further demonstrated the technology of the fibrin suture to deliver cells to an infarct as well as the ability to support the attachment, contraction and delivery of hPS-CM to cardiac tissue.

## 1 Overview

### 1.1 Introduction

The American Heart Association reported in the 2015 update of the heart disease and stroke statistics that 85.6 million Americans, over 33% of the population, exhibit a form of cardiovascular disease (CVD)<sup>1</sup>. In 2011, CVD was implicated in 54% of total deaths. The death rates attributable to CVD have decreased 30% from 2001 to 2011, however there is still a 47% probability at birth of dying from a major cardiovascular event, compared to only 22% by cancer<sup>1</sup>. CVD is estimated to have a total direct cost of \$320 billion, which is projected to rise to \$918 billion by 2030<sup>1</sup>. These statistics and findings indicate a real clinical need to continue to decrease the probability of death by CVD through improving treatments and understanding of the disease.

Of the 85.6 million Americans who suffer from CVD, 15.5 million specifically suffer from coronary heart disease<sup>1</sup>. CHD results in myocardial infarction (MI) for 7.6 million Americans causing 5.7 million Americans to suffer from heart failure (HF) a condition characterized by the inability of the heart to pump enough blood to support other organs<sup>1</sup>. The number of patients with HF is expected to rise to 8.4 million Americans by 2030<sup>2</sup>. Currently, the total cost of care for HF is \$31 billion, which is expected to increase to \$70 billion by 2030<sup>2</sup>.

The rate of hospitalizations for HF have slightly decreased over time, however, there is still a 50% mortality associated with HF 3 years after the first hospitalization<sup>2</sup>. The only true cure for end stage heart failure is a heart transplant; however, due to limited donor availability and the potential for immune rejection, a heart transplant is not an ideal treatment option<sup>3,4</sup>

Myocardial infarction occurs due to an occlusion of blood flow, caused by atherosclerosis in the coronary arteries. Clinically, MI is treated by resuming blood flow using drugs, catheterization techniques to open blocked arteries, or a coronary artery bypass graft. If treatment does not occur within the first 30-60 minutes after an MI, irreversible damage to the myocardium can occur<sup>5</sup>. After an MI, an inflammatory response is initiated that promotes healing and scar formation. As the myocardium does

not possess a proliferative cardiomyocyte population the injured tissue is replaced with a collagenous scar<sup>6, 7</sup>. The replacement of healthy, contractile myocardium with non-contractile, stiff scar tissue ultimately decreases cardiac output, putting the patient at risk of severe heart failure.

Current treatments for patients who have survived an MI are palliative in nature and only treat the symptoms. These treatments occur after the initial MI event and include aspirin,  $\beta$ -adrenergic blockers, and angiotensin-converting enzyme (ACE) inhibitors<sup>8</sup>. Further management of symptoms can be done through cholesterol and weight management along with exercise routines<sup>8</sup>. These treatments may improve immediate symptoms, however they are unable to restore functional tissue lost during the injury.

Consequently, researchers have investigated other therapeutic options for heart failure, such as cellular therapy. There are two main paradigms regarding cellular therapy for cardiac regeneration, the first is that the delivered cell, such as a mesenchymal stem cell, can provide a *pro-healing environment* for the heart to heal<sup>4</sup>. The second is the delivery of a contractile cell, such as a stem cell derived cardiomyocyte, could provide an integrative *restoration in contractile function* lost after an MI<sup>4</sup>. Clinical trials delivering bone marrow mononuclear cells, CD34<sup>+</sup> cells, and mesenchymal stem cells have demonstrated efficacy in increasing cardiac function after a myocardial infarction<sup>9</sup>. However, all cell delivery methods suffer from low retention (0-19%)<sup>10, 11</sup>.

Previously, we have developed a fibrin microthread suture that can be used for efficient cell delivery to the myocardium<sup>12</sup>. We have shown that human mesenchymal stem cells (hMSCs) can be seeded onto the fibrin suture, with a loading efficiency of up to 70%, and successfully implanted into the rat heart with a 63.6 $\pm$ 10.6% retention<sup>12</sup>. Delivering hMSCs to an infarct area with higher efficiency may improve mechanical function post-infarct. Other cell types being investigated for myocardial regeneration include human pluripotent stem cell derived cardiomyocytes (hPS-CM). The hPS-CM is not a mature cardiomyocyte; however, this cell type offers more similarities to the host tissue than a MSC, which may allow for better functional restoration of the infarcted region<sup>13</sup>. Herein, we deliver hMSCs using the fibrin

microthread platform to an infarcted rat heart and assess the effect on mechanical function. Additionally, we examine hPS-CM seeding onto the fibrin microthreads and examine the function of seeded cells over time in culture. Finally, we deliver the hPS-CM seeded microthreads to an uninjured rat heart and examine cell retention.

## 1.2 Overall goal and hypothesis

The overall goal of this dissertation is to develop a cell seeded fiber for cardiac cellular therapy. Utilizing the fibrin microthread technology, we hypothesize that a fibrin suture can support human mesenchymal stem cell and pluripotent stem cell derived cardiomyocyte attachment and subsequent delivery to cardiac tissue. The expected outcome of this dissertation work is to understand the conditions necessary to seed hMSCs and hPS-CM onto fibrin microthreads, how the fibrin microthread mediated delivery of hMSCs affects mechanical function in a rat model of myocardial infarction, and to characterize the contractile behavior of hPS-CM seeded microthreads and their ability to be delivered to healthy cardiac tissue. The first portion of the dissertation work seeks to create a pro-healing environment by delivering hMSCs to the infarct via fibrin sutures. The second portion will assess if the fibrin microthreads are capable of supporting hPS-CM attachment and delivery in such a fashion that in the correct environment the cells can integrate into the damaged tissue and restore contractile function.

To test this hypothesis, this proposal was divided into three specific aims comprising five objectives. We aim to understand hMSC attachment to fibrin sutures and subsequently deliver hMSC seeded fibrin sutures to a rat infarct model and examine the effects on regional mechanical function. Next, we aim to develop a method with high spatial and temporal resolution to concurrently measure mechanical contraction and calcium transient activity of hPS-CM. We aim to determine seeding parameters to allow hPS-CM attachment on fibrin microthreads and characterize their contractile behavior when attached to the fibrin microthreads. Finally, we aim to deliver hPS-CM to healthy cardiac tissue to examine retention of hPS-CM delivered via fibrin microthread sutures.

### 1.3 Specific Aim 1. Determine the effects of hMSCs delivered via a fibrin suture on mechanical function of an infarcted heart.

Recent findings in clinical trials suggest the delivery of MSCs to an infarct will promote myocardial repair.

However, these studies used cell delivery methods that inefficiently delivered cells to the infarcted tissue.

In this aim we propose that the efficient delivery of hMSCs via fibrin sutures to an infarcted rat model will impact mechanical function post infarct.

#### 1.3.1 Objective 1a: Investigate cell seeding conditions to improve attachment of hMSCs onto fibrin microthread sutures.

In this objective, we investigated varying seeding concentrations and seeding times of hMSCs onto the fibrin sutures to understand how seeding conditions affect the numbers of hMSC attached to the suture.

The ideal seeding conditions were found to occur using 100,000 cells per suture seeded for 12-24 hours.

#### 1.3.2 Objective 1b: Evaluate changes in mechanical function when hMSC seeded fibrin sutures are implanted in the infarct zone.

In this objective we employed fibrin sutures to deliver hMSCs to the infarct zone in a rat infarct model.

We hypothesized that delivering hMSCs with high efficiency and targeted localization would improve regional mechanical function compared to the delivery of unseeded sutures and infarct alone. The results of the objective indicate that the delivery of hMSC seeded biological sutures exert a trend towards increased regional mechanical function compared to infarct alone. Additionally, histology demonstrated that Quantum dot loaded hMSCs remained present in the infarcted myocardium after one week and migrated off of the suture. The remaining suture area after 1 week was significantly increased for hMSC-seeded sutures over unseeded sutures. As both the unseeded and hMSC-seeded suture groups had similar infarct sizes, the suture area being significantly increased for the hMSC-seeded group may explain the improvement in regional mechanical function for the hMSC-seeded group, compared to the unseeded group.

### 1.4 Specific Aim 2. Produce and characterize contractile hPS-CM seeded fibrin microthreads.

The discovery of iPS cells and their subsequent ability to be differentiated into contractile cardiomyocytes presents a new cell type to be explored for cardiovascular regeneration endeavors. In this



aim, we hypothesized that hPS-CM would attach to fibrin microthreads in a manner that would not inhibit mechanical contraction or calcium transients. In order to test this hypothesis, in objective 2a we created a method to near simultaneously measure and quantify mechanical contraction and calcium transients by applying HDM to contracting hPS-CM. In objective 2b we examined seeding conditions to allow hPS-CM attachment on fibrin microthreads and applied the quantification method developed in objective 2a to characterize the contractile behavior of hPS-CM seeded on fibrin microthreads over 21 days in culture. The results of this aim suggest that hPS-CM can readily adhere to fibrin microthreads, align along the microthreads, and maintain the ability to contract over several weeks in culture.

#### 1.4.1 Objective 2a: Develop a method to characterize the contractile behavior of hPS-CM

Currently there are no existing systems to measure the simultaneous mechanical contraction and calcium transients of clusters of hPS-CM. In this objective we developed a method combining light and fluorescent microscopy to near simultaneously record brightfield and fluorescent images. Analysis of these high speed videos allow us to determine contractile behavior of hPS-CM in terms of contractile strain, beat frequency, and calcium transient waveforms. We applied our speckle tracking algorithm to contracting clusters of hPS-CM to determine the parameters needed to quantify contractile strain produced by hPS-CM. By analyzing the fluorescent channel, we are capable of producing the calcium transient waveform, which can be overlaid with the contractile strain waveform to examine their temporal relationship.

#### 1.4.2 Objective 2b: Produce and characterize contractile hPS-CM seeded microthreads.

In this objective we demonstrated that higher numbers of hPS-CM attached to collagen IV coated microthreads, but that hPS-CM attached and contracted on fibrin only, fibronectin, and collagen IV coated microthreads. Next, using the method developed in objective 2a, we sought to characterize hPS-CM contractile behavior, in terms of contractile strain, beat frequency, contractile direction, and conduction velocity when adhered to the fibrin suture. No major differences were found in the contractile behaviour of hPS-CM seeded on coated or uncoated microthreads. Cells seeded on tissue culture plastic increased

beat frequency, but decreased contractile and maximum strains over 21 days. The contractile strains produced by hPS-CM on TCP at day 21 were significantly reduced compared to the strains hPS-CM seeded on microthreads produced. hPS-CM seeded on the microthreads increased beat frequency and contractile and maximum strains over 21 days in culture. In regards to alignment, both immunohistochemical staining and contraction angle indicated that the cells contracted in a manner that was more aligned to the microthread at later time points. Cell seeded on tissue culture plastic did not exhibit a dominate contraction angle over 21 days indicating that they remained unaligned in culture. Additionally, calcium transient analysis demonstrated a significant increase in conduction velocities of hPS-CM seeded microthreads up to  $24.26 \pm 8.42 \text{ cm/s}$  by day 21.

These data indicate that major differences in contractile behaviour do not exist between cell seeded TCP and fibrin microthreads; however the microthread provided a scaffold for the hPS-CM to align along and subsequently produce higher strains over 21 days. Additionally, the contraction and alignment data would suggest that delivery of hPS-CM seeded microthreads to cardiac tissue should occur 14-21 days after seeding in order to deliver a higher functioning suture.

### 1.5 Specific Aim 3. Evaluate the use of fibrin microthread sutures to deliver hPS-CM to healthy cardiac tissue.

In this aim we will deliver hPS-CM seeded on fibrin microthreads to cardiac tissue and assess cell retention at 1 hour, 8 hours, 1 day, and 3 days post-delivery. Cells were seeded and cultured for 14 days as described in objective 2b and delivered to an uninjured rat heart using the surgical procedure described in objective 1b without the induction of an infarct. After the given time points, the hearts were removed, fixed, sectioned, stained for Ku80, and analyzed for cell retention by counting the cells in a set number of sections. At 1 hour, we delivered an average of  $7602 \pm 2382$  cells with a delivery efficiency of  $67 \pm 17\%$ , which was significantly higher than the average number of cells delivered at 3 days which was  $185 \pm 403$  with a delivery efficiency of  $1.3 \pm 3.9\%$  ( $p < 0.05$ ). To understand why retention significantly decreased out to 3 days post-delivery sections were stained for H&E to examine cell morphology; additionally an *in vitro*

delivery assay was developed to examine apoptosis. The H&E stained sections indicated hyperchromatic cells and nuclear debris after 1 hour with high neutrophil infiltration after 8 hours. The apoptosis assay utilizing Annexin V demonstrated some apoptotic cells on control threads, however when the cell seeded sutures were passed through a fibrin gel the seeded cells expressed Annexin V as early as 30 minutes post-delivery. These results indicate that the cells may be undergoing apoptosis after being stitched through cardiac tissue and as such, fewer cells are being retained at later time points after cell delivery.

## 1.6 References

1. Mozaffarian D, Benjamin EJ, Go AS, Arnett DK, Blaha MJ, Cushman M, de Ferranti S, Després J-P, Fullerton HJ, Howard VJ, Huffman MD, Judd SE, Kissela BM, Lackland DT, Lichtman JH, Lisabeth LD, Liu S, Mackey RH, Matchar DB, McGuire DK, Mohler ER, Moy CS, Muntner P, Mussolino ME, Nasir K, Neumar RW, Nichol G, Palaniappan L, Pandey DK, Reeves MJ, Rodriguez CJ, Sorlie PD, Stein J, Towfighi A, Turan TN, Virani SS, Willey JZ, Woo D, Yeh RW, Turner MB, Committee AHAS and Subcommittee SS. Heart disease and stroke statistics--2015 update: a report from the American Heart Association. *Circulation*. 2015;131:e29-322.
2. Heidenreich PA, Albert NM, Allen LA, Bluemke DA, Butler J, Fonarow GC, Ikonomidis JS, Khavjou O, Konstam MA, Maddox TM, Nichol G, Pham M, Pina IL, Trogdon JG, American Heart Association Advocacy Coordinating C, Council on Arteriosclerosis T, Vascular B, Council on Cardiovascular R, Intervention, Council on Clinical C, Council on E, Prevention and Stroke C. Forecasting the impact of heart failure in the United States: a policy statement from the American Heart Association. *Circulation Heart failure*. 2013;6:606-19.
3. Evans RW, Manninen DL, Garrison LP, Jr. and Maier AM. Donor availability as the primary determinant of the future of heart transplantation. *JAMA : the journal of the American Medical Association*. 1986;255:1892-8.
4. Jakob P and Landmesser U. Current status of cell-based therapy for heart failure. *Current heart failure reports*. 2013;10:165-76.
5. Zou Y and Zhang Y. The orthotropic viscoelastic behavior of aortic elastin. *Biomech Model Mechanobiol*. 2011;10:613-25.
6. Bergmann O, Bhardwaj RD, Bernard S, Zdunek S, Barnabe-Heider F, Walsh S, Zupicich J, Alkass K, Buchholz BA, Druid H, Jovinge S and Frisen J. Evidence for cardiomyocyte renewal in humans. *Science*. 2009;324:98-102.
7. Chow M-J, Choi M, Yun SH and Zhang Y. The effect of static stretch on elastin degradation in arteries. *PLoS One*. 2013;8:e81951.
8. Ryan TJ, Antman EM, Brooks NH, Califf RM, Hillis LD, Hiratzka LF, Rapaport E, Riegel B, Russell RO, Smith EE, Weaver WD, Gibbons RJ, Alpert JS, Eagle KA, Gardner TJ, Garson A, Gregoratos G and Smith SC. 1999 update: ACC/AHA Guidelines for the Management of Patients With Acute Myocardial Infarction: Executive Summary and Recommendations: A report of the American College of Cardiology/American Heart Association Task Force on Practice Guidelines (Committee on Management of Acute Myocardial Infarction). *Circulation*. 1999;100:1016-30.
9. Menasche P. Cardiac cell therapy: lessons from clinical trials. *Journal of molecular and cellular cardiology*. 2011;50:258-65.
10. Vrtovec B, Poglajen G, Lezaic L, Sever M, Socan A, Domanovic D, Cernelc P, Torre-Amione G, Haddad F and Wu JC. Comparison of transendocardial and intracoronary CD34+ cell transplantation in patients with nonischemic dilated cardiomyopathy. *Circulation*. 2013;128:S42-9.
11. Hou D, Youssef EA, Brinton TJ, Zhang P, Rogers P, Price ET, Yeung AC, Johnstone BH, Yock PG and March KL. Radiolabeled cell distribution after intramyocardial, intracoronary, and interstitial retrograde coronary venous delivery: implications for current clinical trials. *Circulation*. 2005;112:I150-6.
12. Guyette JP, Fakhrazadeh M, Burford EJ, Tao ZW, Pins GD, Rolle MW and Gaudette GR. A novel suture-based method for efficient transplantation of stem cells. *Journal of biomedical materials research Part A*. 2013;101:809-18.
13. Yang X, Pabon L and Murry CE. Engineering adolescence: maturation of human pluripotent stem cell-derived cardiomyocytes. *Circ Res*. 2014;114:511-23.

## 2 Background

### 2.1 Introduction

#### 2.1.1 The cardiovascular system

The cardiovascular system is responsible for carrying nutrients and oxygen to the body while removing carbon dioxide and other waste products. The primary components of the cardiovascular system are the heart and the blood vessels. The heart is a multichamber muscular organ that serves as an electromechanical pump to deliver blood through the body's vascular network. It is a dynamic organ that beats over 100,000 times a day resulting in over 2 billion beats in a humans lifetime<sup>1</sup>.

There are four chambers within the human heart, the two atria are positioned superior to the two ventricles. An atria and a ventricle each compose the left and right side of the heart, which serve separate functions. The primary responsibility of the right side is to carry deoxygenated blood from the body to the lungs to be re-oxygenated. The left side of the heart then receives oxygenated blood from the lungs and delivers it to the rest of the body. Ventricular tissue is thicker than atrial tissue as atrial myocardium only acts to pass blood a relatively short distance to the ventricles. The left ventricle (LV) is more muscular than the right ventricle as the left ventricle must drive blood throughout the body, whereas the right ventricle pumps blood only to the lungs.

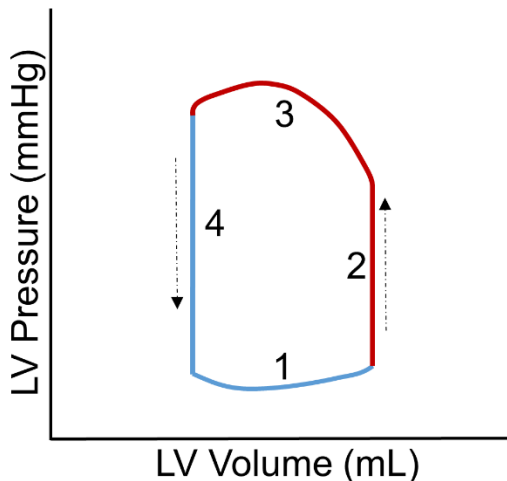


**Figure 2-1. Pressure volume work loop.** 1- diastolic filling. 2- isovolumic contraction, 3- ejection, 4 – isovolumic relaxation. Red indicates systole and blue indicates diastole. Arrows indicate loop direction.

The heart pumps blood through the body over the cardiac cycle, which is composed of two phases: diastole and systole. In diastole the ventricles fill with blood from the left and right atria, pressures are low and the volume within the ventricle increases over diastole as seen in part 1 of the pressure volume work loop in Figure 2-1. During systole pressure rises within the ventricles until the valves open (Figure 2-1) and blood is ejected out of the ventricles to the body

(Figure 2-1). As the pressure and volume decrease in the ventricles after systole (Figure 2-1), the valves close until pressures are low enough to allow the valves to reopen enabling the ventricles to refill.

The heart itself is a muscular organ that has a high metabolic demand required to sustain normal cardiac function. It is served by the coronary arteries that branch from the aorta. The left side of the heart is supplied from the left anterior descending coronary artery (LAD) and the circumflex coronary artery that branch from the left coronary artery. The right coronary artery supplies blood to the right side of the heart.

There are several type of cells that make up cardiac tissue such as, cardiomyocytes, endothelial cells, smooth muscle cells, and pacemaker cells, which lie within an extracellular matrix comprised of collagen (types I,III, and IV), fibronectin, elastin and laminin, which serve to provide structure for cardiac cells. The workhorse of cardiac tissue is the cardiac muscle cell, or cardiomyocyte. Cardiomyocytes form branched muscle fibers that are electrically coupled at their intercalated disks, which are made of gap junctions comprised of connexin proteins. Gap junctions facilitate rapid action potential conduction through the entire myocardium. When the action potential is initiated, calcium is released into the cardiomyocyte. Calcium then binds troponin resulting in a conformational change allowing actin to be bound by myosin. Subsequent ATP hydrolysis induces cross-bridge formation between actin and myosin and results in the power stroke, which moves actin. As cardiomyocytes are electrically coupled, they act as a syncytium that results in a synchronized contraction. This synchronized contraction allows atrial and ventricular contraction which pumps blood through the body.

## 2.2 Cardiovascular disease

The AHA reported that in 2015 85.6 million Americans, over 33% of the population, exhibit a form of cardiovascular disease (CVD)<sup>2</sup>. Of the 85.6 million Americans who suffer from CVD, 7.6 million will suffer a myocardial infarction (MI) resulting in 5.7 million Americans suffering from heart failure (HF), a condition characterized by the inability of the heart to pump enough blood to support other organs<sup>2,3</sup>.

### 2.2.1 Myocardial infarction

A myocardial infarction generally occurs from narrowing of the coronary arteries resulting in complete or partial occlusion causing ischemia to downstream cardiac tissue. If treatment is not immediately obtained, the ischemia results in myocyte death. Infarcts primarily occur in the left ventricle; it has been suggested that over a quarter (1 billion) of a patient's left ventricular myocytes can die during an MI<sup>4</sup>. Not only do infarcts cause massive cardiomyocyte death, thus decreasing the available number of contractile units, but an inflammatory cascade is triggered that results in infarct expansion and the formation of scar tissue<sup>5</sup>.

During the inflammatory process post-infarct, initially neutrophils infiltrate the infarct regions and recruit resident monocytes and lymphocytes<sup>6, 7</sup>. These cells remove necrotic myocardium, but inflammatory cytokines are secreted in the process. The release of inflammatory cytokines and increased infiltration of inflammatory cells causes infarct expansion and further damages the myocardium. The end of the inflammatory phase is characterized by the presence of anti-inflammatory cytokines and growth factors, released by apoptotic neutrophils and anti-inflammatory macrophages, that promote fibroblast proliferation and neovascularization<sup>8</sup>. As there is a less than 1% self-renewal of cardiomyocytes the injured tissue is replaced with scar tissue<sup>9</sup>.

The scar tissue that replaces healthy contractile myocardium after an infarct negatively affects the active mechanical function of the heart. Contraction is inhibited as the scar tissue creates a stiff region, which works against the active contraction of cardiac tissue. Additionally, myocardial ischemia decreases the number of contractile units resulting in reduced active contraction. All together, these changes result in a reduced cardiac output that is detrimental to a patient's quality of life. The impairment of the left ventricular myocardial function resulting from a MI can cause the patient to suffer from HF. HF from MI is a progressive disorder where the heart remodels and weakens over time to the point where the heart

cannot deliver a sufficient amount of blood to sustain the rest of the bodies organs<sup>10</sup> There are currently 915,000 new cases of HF annually, with a 5 year mortality rate of 50%<sup>11</sup>.

### 2.2.2 Therapeutic treatment strategies for MI

Despite medical advances, there have been few improvements in treatment options for patients who have suffered an MI. Options for treating patients in HF are limited, however current treatments have been attributed to a decline in mortality associated with HF<sup>11</sup>. These treatment options include pharmacological treatments such as ACE inhibitors and beta-blockers, as well as more aggressive techniques such as coronary revascularization, implantation of cardioverter-defibrillators, and cardiac resynchronization strategies<sup>12</sup>. The utilization of these treatments have increased survival rates for patients in HF, however these treatments only treat the symptoms of heart failure and do not treat or restore the damaged myocardium<sup>12</sup>. Without treating the damaged myocardium the patient's heart disease may progress to end stage HF, for which the only treatment is a full heart transplant. However, as there are less than 2,700 donor hearts available each year, and over 4,100 patients needing a heart transplant, not all patients in HF will be adequately treated<sup>11</sup>. Additionally, donor mismatches and the chances for organ rejection make heart transplants a less than ideal treatment option. A left ventricular assist device is an option for extending the time for a patient to receive a heart transplant, however it only serves as a bridge to transplant.

### 2.2.3 Techniques to measure and assess cardiovascular function

In order to appropriately assess and treat a patient who has suffered from an MI it is important to obtain measurements of cardiovascular function. Measurements of cardiac function include left ventricular end diastolic and systolic volumes and diameters (LEDV- left ventricular end diastolic volume, LESV- left ventricular end systolic volume, LEDD- left ventricular end diastolic diameter, LESD – left ventricular end systolic volume). These measurements are used to obtain ejection fraction (EF) and fractional shortening (FS), two major benchmarks for cardiac function. EF is determined by the equation:  $\frac{(LEDV-LESV)}{LEDV} * 100$  and fractional shortening is determined by the equation:  $\frac{(LEDD-LESD)}{LEDD} * 100$ . Stroke volume (SV) is determined



by ( $LEDV - LESV$ ) and gives the volume of blood ejected during systole. Other parameters for cardiac function include left ventricular systolic and diastolic pressure, maximum and minimum pressure development, diastolic relaxation time constant ( $\tau$ ), heart rate, stroke work, and cardiac output ( $SV \times \text{heart rate}$ ).

There are numerous methods for measuring cardiac function. Echocardiography is a widely used system in animal models and humans as it is minimally invasive and can measure ejection fraction and fractional shortening<sup>13</sup>. Cardiac computed tomography and magnetic resonance imaging are two other modalities that can be used to measure left ventricle end points such as FS, EF, and wall thickening<sup>13</sup>. These two modalities are less invasive than echocardiography, but have a higher cost due to the needed imaging machinery. These imaging modalities obtain global cardiac function with little to no ability to decipher functional changes that occur on a regional level.

A method to determine regional cardiac function is the use of a high resolution speckle tracking system – high density mapping (HDM, Figure 2-2)<sup>14</sup>. HDM is a phase correlation technique used to measure sub-pixel displacement fields<sup>14, 15</sup>. For the heart<sup>14, 16</sup>, a mixture of silicon carbide and retroreflective micro particles are applied to the heart wall to create a random light intensity distribution (Figure 2-2) and a 3.5 French size catheter tipped micro manometer is inserted into the left ventricle through the apex to record left ventricular pressures. Then, a high speed (250 frames/second), high resolution (1696x1730 pixels) video of the contracting heart wall is taken simultaneously with pressure measurements. Using the pressure measurements, maximum and minimum rate of pressure change, and the diastolic relaxation time constant are determined. HDM is applied to determine regional changes in the mechanics of the heart wall (Figure 2-2B, C) including regional stroke work (RSW) and systolic area of contraction (SAC) (Figure 2-2D). RSW is an analog to stroke work and is calculated by taking the integral of left ventricular pressure ( $P$ ) with respect to regional area of interest ( $A$ ), normalized over end diastolic area and maximum pressure developed ( $RSW = \int PdA/P_{dev}$ ). SAC is an analog to  $SV$  and is defined as the difference between

regional end diastolic area (EDA) and regional end systolic area (ESA) ( $SAC = EDA - EDS$ ). While the use of HDM is invasive, its high spatial resolution provides a powerful measurement tool as it determines

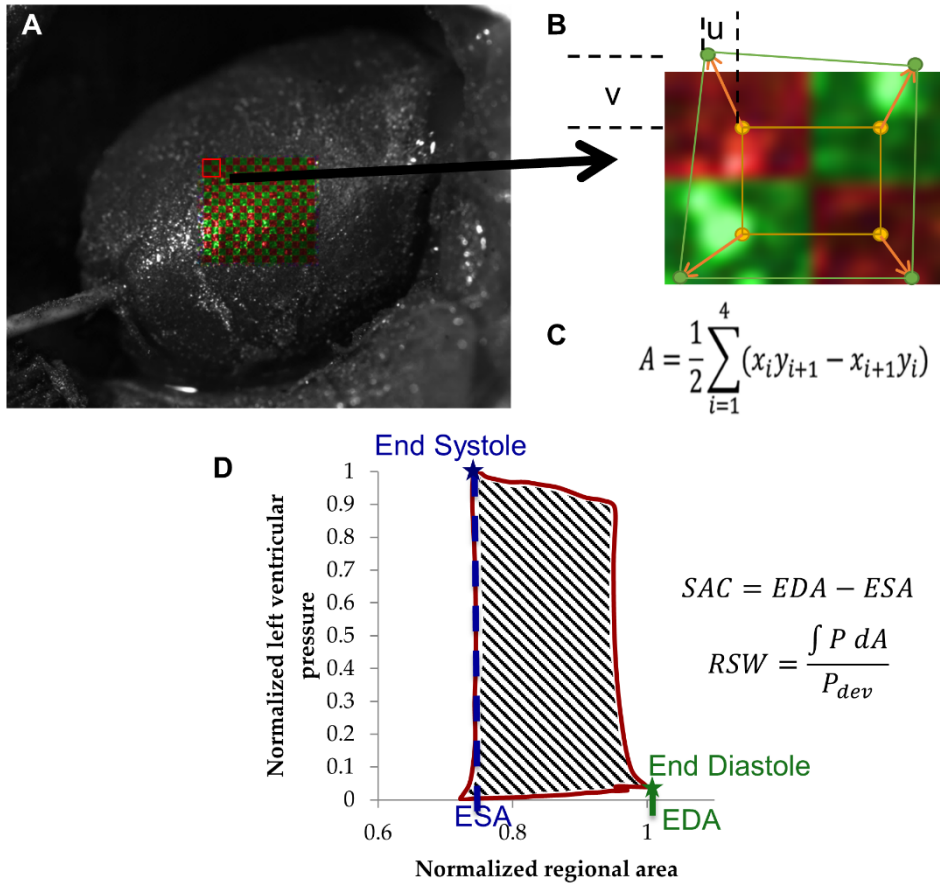


**Figure 2-2. Description of HDM method.** A region of interest is selected across the infarct area and is divided into 32x32 pixel subimages (A). HDM applies a phase correlation to measure displacement fields from frame to frame (B). HDM can measure sub-pixel displacements to obtain changes in area across the cardiac cycle (C). By using corresponding pressure data and area changes regional stroke work (RSW) and systolic area contraction (SAC) can be measured (D). P=pressure, A= area, EDA= end diastolic area, ESA= end systolic area

regional cardiac function. Measurement of regional function is important in MI studies which usually result in regional dysfunction as well as in cell based therapies to determine changes in mechanics where the cells were delivered. The contribution of the cells may be washed out on a global scale, but may impart significant changes on a regional level. As such, this method will be utilized in this dissertation to determine changes in regional cardiac function.

### 2.3 Cardiovascular regeneration

When damage occurs in many systems in the body there is an endogenous system in place to repair the damage. This allows that system to continue to function with little to no impairment, depending on the severity of the damage. For example, skeletal muscle can regenerate through the activation of resident satellite cells, which have the ability to form functional mature myotubes allowing muscle to return to its pre-injured state<sup>17</sup>. Cardiac muscle tissue however is different as it lacks the ability to endogenously repair itself after injury, such as an MI, and restore function to pre-injury levels<sup>18, 19</sup>. Unlike skeletal muscle, cardiac muscle does not contain a resident stem cell population that will repopulate the damaged area after injury. Additionally, cardiomyocytes have a very limited self-renewal, around 1% a year, which decreases even further with age<sup>9</sup>. Over a billion myocytes can be lost after an MI, as the heart does not have the capacity to replace dead myocytes the heart instead replaces functioning myocytes with scar tissue<sup>20</sup>. The remaining cardiac myocytes can compensate to the injury by hypertrophy, however prolonged cardiac hypertrophy can lead to HF<sup>21, 22</sup>. As described above, there are limited options to treat an MI and subsequent HF, which has led researchers to investigate other therapeutic options to improve cardiac function post MI such as cell transplantation and tissue engineering techniques (Figure 2-3).

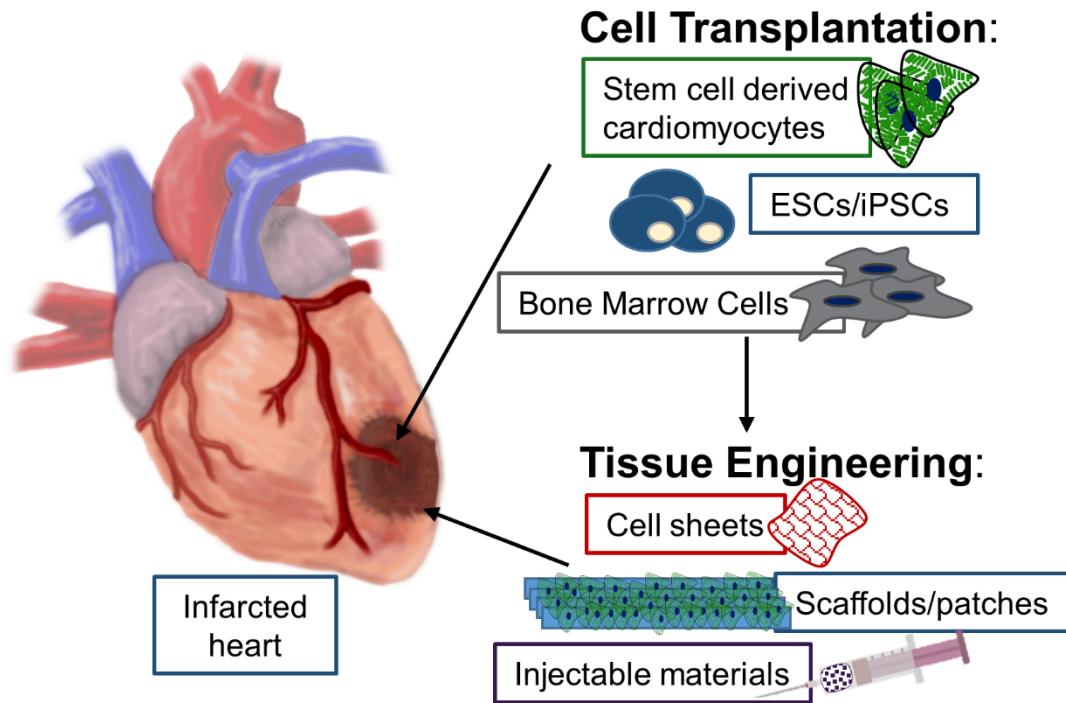


**Figure 2-3. Schematic of cardiovascular regeneration techniques.** Various options to improve cardiac function post infarction including cell transplantation and tissue engineering methods.

### 2.3.1 Material based

A number of material based therapies have been proposed for cardiac regeneration including injectable materials and synthetic and natural polymer based cardiac patches. Injectable materials were first explored as a mechanism to increase cell retention and a number of materials have been utilized including fibrin, collagen, chitosan, gelatin, alginate, matrigel, and PEG based polymers<sup>23</sup>. Exploring the potential of injectable materials for MI has been primarily driven by Dr. Christman's group. Her group has injected fibrin into the infarct zone, but more recently has been focused on decellularized extracellular matrix (ECM) as an injectable. By injecting fibrin into the infarct zone Christman *et al.* demonstrated prevention of LV wall thinning and maintenance of cardiac function post MI, additionally fibrin improves blood flow to the area of injury by increasing the arteriole density<sup>24, 25</sup>. With the discovery and improvement of decellularization techniques the group sought to decellularize cardiac tissue and create an injectable material from the remaining ECM<sup>26</sup>. Safety and efficacy studies using rat and porcine MI models with catheter based myocardial matrix delivery indicate that the material is biocompatible and can improve

cardiac function post-MI<sup>27, 28</sup>. Additionally Masson's Trichrome staining indicated decreased collagen and an increased muscle layer within the infarct zone for animals treated with the myocardial matrix<sup>28</sup>. These findings indicate the safety and efficacy of using injectable biomaterials for the treatment of MI. When combined with the appropriate cell type the use of biomaterials may have an even greater impact on functional cardiac improvement post-MI.

The use of biomaterials for cardiac regeneration strategies has also been explored in the context of creating a patch that can be placed on the epicardial surface of the heart to improve function. Materials used for cardiac patches have ranged from fibrin, alginate, urinary bladder matrix, and small intestine submucosa, to PTFE and polyurethane<sup>23</sup>. Cell seeded and acellular patches have been delivered to infarct zone and studies have demonstrated improved LV wall thickness and improvements in cardiac function in terms of FS and EF<sup>29-31</sup>. Mesenchymal stem cells have predominately been used, however recent studies have explored the use of human pluripotent stem cell derived cardiomyocytes (hPS-CM) seeded patches<sup>32-37</sup>. The hPS-CM patches have utilized fibrin as a base in addition to creating scaffold free cell sheets. Transplantation of hPS-CM patches onto porcine and rat MIs have demonstrated the ability for the patch to attenuate cardiac remodeling as well as improve cardiac performance<sup>34-36</sup>. In the case of Kawamura *et al.* and Wendel *et al.*, functional gains in EF were seen initially, however they were diminished at later time points<sup>34, 36</sup>. Additionally, cardiac patch implantation studies found that the patches have an angiogenic potential, which may contribute to the increase in cardiac function. However, these studies found that the cells either did not survive at later time points or did not migrate from the patch into the host myocardium indicating that these cells did not integrate with the host myocardium to contribute to increases in function.

### 2.3.2 Cell based

There are two main paradigms regarding cellular therapy for cardiac regeneration, the first is that a delivered cell type can provide a pro-healing environment for the heart to heal<sup>38</sup>. The second is that the

delivery of a contractile cell would provide an integrative restoration in contractile function lost after an MI<sup>38</sup>. The cell types used for cardiac based cellular therapy primarily include skeletal myoblasts, mesenchymal stem cells (MSCs), cardiac progenitor cells, and pluripotent stem cells<sup>38-42</sup>. Many of these cells types have been explored in pre-clinical MI animal models as well as in human patients<sup>38, 39, 43, 44</sup>. The following sections describe previous and current cell based efforts for cardiac regeneration.

#### 2.3.2.1 Skeletal myoblasts

Skeletal myoblasts were one of the first cell types explored for cardiac regeneration, as they are a contractile cell type researchers believed they may integrate with the host myocardium to improve function. In early studies, skeletal myoblasts were delivered to rabbit and sheep models of MI<sup>45-47</sup>. These studies demonstrated that skeletal myoblasts could engraft in the infarcted tissue as well as provide improvements to cardiac function post-MI. Due to the initial success of these studies, skeletal myoblasts were examined in clinical trials for MI. The transplantation of skeletal myoblasts in human patients resulted in proarrhythmic events and as such have been deemed an inappropriate cell type for cardiac regeneration purposes<sup>48</sup>.

#### 2.3.2.2 Cardiac progenitor cells

There is a controversial set of data suggesting the existence of cardiac progenitors within cardiac tissue that are capable of dividing and differentiating into cardiac cells. These cells have been isolated from cardiac tissue and identified based on their positive expression of tyrosine kinase c-kit, a cell surface receptor<sup>49-51</sup>. Studies where these cells were delivered to animal models of MI indicated their potential to improve cardiac function post injury<sup>42, 52</sup>. These pre-clinical studies laid the ground work for a clinical trial where autologous c-kit positive cells were delivered to patients with ischemic cardiomyopathy in the SCIPIO trial<sup>53</sup>. While the results of this trial were encouraging, reports of misconduct and subsequent paper retractions<sup>54</sup> have called into question the results of this clinical trial and the overall existence and potential for c-kit positive cardiac progenitor cells. Many follow up studies

have indicated that c-kit positive cells cannot contribute enough cardiomyocytes to be considered functionally significant<sup>55, 56</sup>.

### 2.3.2.3 Bone marrow derived cells

Cells derived from the bone marrow (BMC) and used for myocardial repair strategies typically include bone marrow mononuclear cells (BM-MNC) and mesenchymal stem cells (MSCs). BM-MNCs consist of a variety of cell lineages including hematopoietic cells, monocytes, lymphocytes, and progenitor cells<sup>38, 57</sup>. A sub-population of BM-MNCs are MSCs which are a multipotent cell capable of differentiating into many types of cells, notably adipocytes, chondrocytes, and osteoblasts<sup>58-60</sup>. As MSCs possess the capacity to enhance endogenous repair systems through immunomodulation and paracrine effects they became an excellent cell source for cell based therapies targeting a range of diseases including graft versus host, diabetes, bone and cartilage diseases, and neurological diseases<sup>61-66</sup>. BMCs have been explored for myocardial infarction treatment for nearly two decades; a study Orlic *et al.* suggested that the delivery of bone marrow cells to an infarct could create de novo cardiac tissue and promote functional repair<sup>67</sup>. The cells delivered were lin<sup>-</sup>, c-kit<sup>+</sup> GFP labeled cells that were delivered after ischemia was established. The author's results demonstrated that 9 days after injury over 60% of the infarcted tissue was occupied by newly formed cardiomyocytes and left ventricular function has been significantly improved. This study was the first to show promise for BMCs to induce myocardial repair, however many follow up studies were not able to reproduce their results indicating that these stem cells cannot transdifferentiate into cardiomyocytes<sup>68-70</sup>.

However, as BMCs present a promising autologous cell source many studies have continued to explore their potential for myocardial repair. Follow up studies delivering MSCs to animal models of MI indicated that the MSCs participate in angiogenesis and provide an immunomodulatory effect through the secretion of paracrine factors, which helps diminish the pro-inflammatory environment found post-infarct, resulting in decreased infarct expansion and reduction of scar tissue formation<sup>38, 41, 71-73</sup>. These preclinical successes

gave way to the initiation of many clinical trials delivering BMCs to patients who had survived an MI. The initial clinical trials indicated that the delivery of BMCs to a patient's heart was a safe process and showed improvement in left-ventricular function<sup>74-76</sup>. Future studies examined the effect of allogeneic versus autologous cell delivery, different doses of cells, and the effect of cell delivery early or late after an MI<sup>75, 77-80</sup>. The POSIEDON trial examined autologous vs allogeneic MSC delivery and found similar functional improvements after MI with little immune reactions from the allogeneic MSCs<sup>78</sup>. An unexpected finding of this study also indicated that the delivery of smaller numbers (20 million) of MSCs was superior to the delivery of larger numbers (100 million)<sup>78</sup>. The SWISS-AMI, TIME, and LateTIME trials all conducted studies to examine the effect of delivery time on BM-MNC injection after Percutaneous Coronary Intervention (PCI) post-MI. In the SWISS-AMI study, cells were delivered 3-4 days or 5-7 weeks after PCI, in the TIME trial cells were delivered 3 or 7 days after PCI, and in the LateTIME trials cells were delivered 2-3 weeks after PCI<sup>77, 79, 81</sup>. The major findings from these studies were similar, that the timing of cell delivery does not significantly affect global function. Due to the safety profile and therapeutic efficacy demonstrated in the initial clinical trials there are many ongoing clinical trials continuing to investigate the functional effects of MSCs on myocardial repair post-infarction.

#### 2.3.2.4 Pluripotent stem cells

The generation of embryonic stem cells (ESC) by Thomson in 1998<sup>82</sup> and induced pluripotent stem cells (iPS) by Yamanaka in 2006 provides a potential new source of cells for cardiac regeneration<sup>83</sup>. Human derived ESC and iPS cells exhibit many of the same characteristics including morphology, proliferation, pluripotency, and gene expression<sup>84</sup>. Both cell types have the ability to provide a large cell source with cardiac differentiation potential for cell replacement strategies<sup>84, 85</sup>.

Differentiation of ESCs into cardiomyocytes has been achieved by co-culture with mouse visceral endoderm-like (END-2) cells<sup>86</sup> as well as by culturing in embryoid bodies (EB) in the presence of serum<sup>87</sup>, but this results in batch to batch variability with poor differentiation efficiency (<22% contractile population)<sup>88</sup>. More advanced techniques using monolayer culture, instead of EB formation, allow cells



to be cultured under fully defined conditions and have produced cardiomyocytes with a higher differentiation efficiency. One method developed by Lian *et al.* utilized small molecules to regulate canonical Wnt signaling, yielding a 98% (cTnT<sup>+</sup>) pure cardiomyocyte population from ESC and iPS cells<sup>89</sup>. Another method developed by Laflamme *et al.* regulated differentiation by the addition of activin A and bone morphogenetic protein 4 to a monolayer of ESC or iPS cells, which results in cardiomyocyte purity of greater than 95% ( $\beta$ MHC<sup>+</sup>)<sup>90, 91</sup>. These ESC and iPS derived cardiomyocytes (hPS-CM) exhibited down regulation of pluripotent stem cell markers such as NANOG and OCT4, stained positive for cardiac markers cardiac troponin T (cTnT) and  $\alpha$ -actinin, and exhibited ventricular-, atrial-, and nodal-type cardiac electrophysiology<sup>91-93</sup>. cTnT and  $\alpha$ -actinin are regulatory and cytoskeletal proteins, respectively, present in cardiomyocytes and are routinely used to characterize differentiation of hPS-CM<sup>89, 93-95</sup>. Despite the success of cardiac differentiation, these hPS-CM cannot be considered a mature adult cardiomyocyte as they lack the morphology, gap junction expression, contractile apparatus, and functionality of an adult cardiomyocyte<sup>93, 96, 97</sup>.

Many ongoing research efforts are focusing on enhancing the maturity of hPS-CM<sup>98, 99</sup>, however, in the interim, studies have delivered these cells to animal infarct models to assess their regenerative capacity<sup>100, 101</sup>. Initial studies delivered hPS-CM to models of mouse and rat infarctions and demonstrated improved cardiac function in terms of LV dimensions and fractional shortening, attenuated cardiac remodeling, improved vascularization as well as the formation of nascent myocardium<sup>90, 102-106</sup>. Interestingly, the studies by van Laake and Carpenter showed only transient improvement in LV function with improvements being diminished by 10 and 12 weeks, respectively<sup>102, 104</sup>. Additionally, while most studies found that grafts persisted past 4 weeks most studies only found few instances where connections between host and graft tissue were present<sup>90, 103, 104</sup>. Only a few connections between host and graft tissues may have been formed due to the inherent mismatch in beat frequency between graft cells (human, 60-100 beats per minute (bpm)) and host tissue (rodent, 300-600 bpm). Due to these

physiological discrepancies, larger animal studies have been employed to understand hPS-CMs effects on myocardial function in a heart that more closely mimics that of a human heart.

One of the initial larger animal studies was conducted by Menasché and Pucéat where they delivered ESC derived progenitors to the infarcted myocardium of a nonhuman primate<sup>107</sup>. While they did not include any functional endpoints, this study demonstrated that the implanted cardiac progenitors reconstituted 20% of the scar tissue while undifferentiated cells formed teratomas. In 2012, Sawa's group used hPS-CM derived cardiomyocytes to create cell sheets that were delivered to the epicardial surface of a porcine infarct model<sup>36</sup>. This study demonstrated significantly improved systolic function with attenuated ventricular remodeling, however very few cells survived at the 8 week time point. Templin *et al.* developed a sodium iodide symporter (NIS) transgene to improve iPSC cell tracking post-delivery<sup>108</sup>. iPSC-NIS<sup>pos</sup> cells were delivered to a porcine model of infarction, and while no functional endpoints were used, the study was able to demonstrate retention of cells up to the study endpoint at 15 weeks. Additionally these cells were capable of contributing to the vascularization of the infarcted myocardium. A study by the Murry group delivered hPS-CM to a nonhuman primate model of infarction and demonstrated substantial remuscularization of the infarct zone with host vasculature perfusing the grafts<sup>101</sup>. Additionally, calcium transients indicated a 1:1 coupling between host and grafted tissue, but there was evidence on non-fatal ventricular arrhythmias. Further larger studies will need to be done to understand the potential for arrhythmias, however the remuscularization and electrical coupling results are encouraging and support the continued development of hPS-CM for cardiac repair.

### 2.3.3 Cell delivery methods

Substantial progress has been made for cell based therapies, however one inherent limitation with all cell therapies is the method used to deliver the cells to the injured tissue. There are several methods by which researchers have chosen to deliver cells, but none have resulted in the efficient delivery of cells localized to the injured region. Various delivery platforms include systemic delivery by intravenous injection, but this results in cells getting trapped in the lungs and only 1% of these cells engraft in the

heart<sup>109</sup>. Intracoronary delivery, during angioplasty, results in a similarly low retention of about 1% because cells get washed away after blood flow is resumed<sup>109</sup>. The current gold standard for cell delivery is an intramyocardial (IM) injection of cells into and around the epicardial surface of the infarct, yet this only results in a 10% retention of the delivered cells<sup>109</sup>. A recently explored delivery method, transendocardial delivery, has shown promising clinical results with 19% cell retention, but is still relatively inefficient<sup>110</sup>. Such low retention rates result in massive cell loss and would require on the order of 10 billion cells to be delivered, which is prohibitively expensive<sup>111</sup>. This dissertation explores an alternative method for cell delivery using fibrin microthread sutures.

#### 2.3.4 Fibrin microthreads for cell delivery

In the wound healing process fibrin is the first protein deposited in the provisional matrix and recruits the cells that regulate the wound healing cascade<sup>112</sup>. Tissue engineering research has used fibrin to create fibrin glues, hydrogels, and scaffolds that can be used in a variety of applications, including wound sealants, cell delivery, and engineering of adipose, cardiac, bone, and cartilage tissues<sup>113</sup>. Fibrin has been used as a three dimensional (3D) scaffold for cardiac tissue engineering and it supports the survival and contraction of neonatal rat ventricular myocytes and recently hPS-CM<sup>114-117</sup>. This dissertation exploits the natural, biodegradable properties of fibrin and utilizes fibrin as a cell delivery vehicle in the form of fibrin microthreads. Fibrin microthreads are generated by co-extruding fibrinogen and thrombin into a HEPES buffered bath to create discrete fibrin microthreads<sup>118</sup>. Proulx *et al.* demonstrated the ability for the discrete fibrin microthreads to be incorporated into a suture that can support the attachment of human mesenchymal stem cells (hMSCs)<sup>119</sup>. Guyette *et al.* utilized the fibrin suture as a delivery platform to deliver hMSCs to the normal rat heart<sup>120</sup>. A delivery efficiency of  $63.6 \pm 10.6\%$  to the normal rat heart at one hour was achieved by suturing an hMSC seeded fibrin suture into the myocardium (Figure 2-4.). This delivery vehicle presents a promising approach to cell delivery and will be employed in this dissertation.

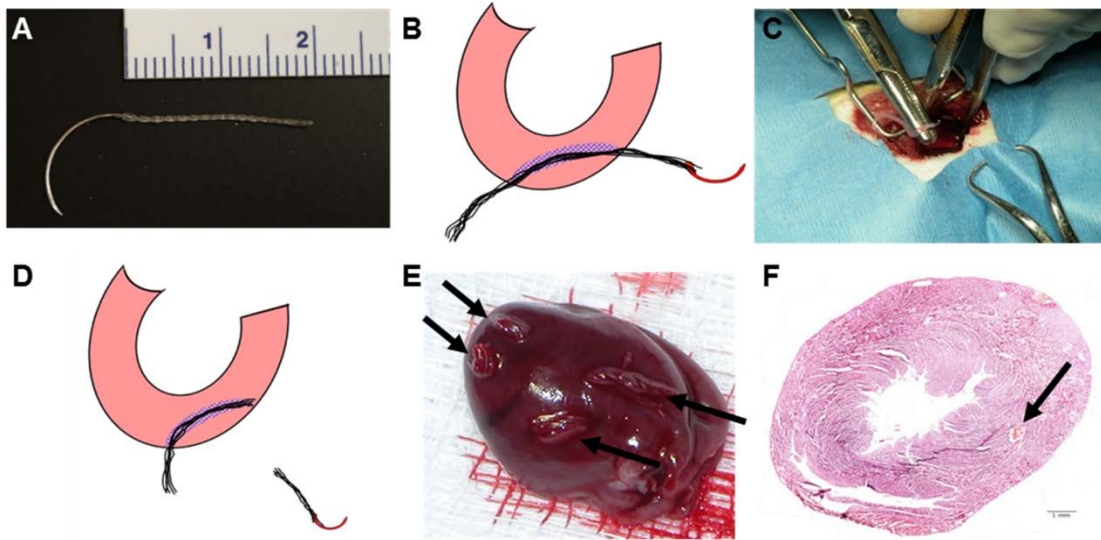


**Figure 2-4. Fibrin microthread suture delivery to the heart.** Fibrin Microthread suture before seeding (A). Suture stitched through myocardium (B, C) Suture needle is removed before animal is closed (D, E). Masson's Trichrome of a cross section of rat heart with a fibrin suture delivered (F). Black arrows indicates fibrin sutures in E and F.

## 2.4 References

1. Jose AD and Collison D. The normal range and determinants of the intrinsic heart rate in man. *Cardiovascular research*. 1970;4:160-7.
2. Mozaffarian D, Benjamin EJ, Go AS, Arnett DK, Blaha MJ, Cushman M, de Ferranti S, Després J-P, Fullerton HJ, Howard VJ, Huffman MD, Judd SE, Kissela BM, Lackland DT, Lichtman JH, Lisabeth LD, Liu S, Mackey RH, Matchar DB, McGuire DK, Mohler ER, Moy CS, Muntner P, Mussolino ME, Nasir K, Neumar RW, Nichol G, Palaniappan L, Pandey DK, Reeves MJ, Rodriguez CJ, Sorlie PD, Stein J, Towfighi A, Turan TN, Virani SS, Willey JZ, Woo D, Yeh RW, Turner MB, Committee AHAS and Subcommittee SS. Heart disease and stroke statistics--2015 update: a report from the American Heart Association. *Circulation*. 2015;131:e29-322.
3. Jessup M and Brozena S. Heart Failure. *New England Journal of Medicine*. 2003;348:2007-2018.
4. Murry CE, Reinecke H and Pabon LM. Regeneration gaps: observations on stem cells and cardiac repair. *Journal of the American College of Cardiology*. 2006;47:1777-85.
5. Frangogiannis NG. The inflammatory response in myocardial injury, repair, and remodelling. *Nat Rev Cardiol*. 2014;11:255-265.
6. Anzai T. Post-Infarction Inflammation and Left Ventricular Remodeling. *Circulation Journal*. 2013;77:580-587.
7. Chow M-J, Choi M, Yun SH and Zhang Y. The effect of static stretch on elastin degradation in arteries. *PLoS One*. 2013;8:e81951.
8. Frangogiannis NG. Regulation of the inflammatory response in cardiac repair. *Circ Res*. 2012;110:159-73.
9. Bergmann O, Bhardwaj RD, Bernard S, Zdunek S, Barnabe-Heider F, Walsh S, Zupicich J, Alkass K, Buchholz BA, Druid H, Jovinge S and Frisen J. Evidence for cardiomyocyte renewal in humans. *Science*. 2009;324:98-102.
10. Mazurek JA and Jessup M. Understanding Heart Failure. *Cardiac Electrophysiology Clinics*. 2015;7:557-575.
11. Mozaffarian D, Benjamin EJ, Go AS, Arnett DK, Blaha MJ, Cushman M, Das SR, de Ferranti S, Després J-P, Fullerton HJ, Howard VJ, Huffman MD, Isasi CR, Jiménez MC, Judd SE, Kissela BM, Lichtman JH, Lisabeth LD, Liu S, Mackey RH, Magid DJ, McGuire DK, Mohler ER, Moy CS, Muntner P, Mussolino ME, Nasir K, Neumar RW, Nichol G, Palaniappan L, Pandey DK, Reeves MJ, Rodriguez CJ, Rosamond W, Sorlie PD, Stein J, Towfighi A, Turan TN, Virani SS, Woo D, Yeh RW and Turner MB. Heart Disease and Stroke Statistics—2016 Update. *Circulation*. 2015.
12. Merlo M, Pivetta A, Pinamonti B, Stolfo D, Zecchin M, Barbati G, Di Lenarda A and Sinagra G. Long-term prognostic impact of therapeutic strategies in patients with idiopathic dilated cardiomyopathy: changing mortality over the last 30 years. *European Journal of Heart Failure*. 2014;16:317-324.
13. Yamamoto M, Yamamoto K and Noumura T. Type I collagen promotes modulation of cultured rabbit arterial smooth muscle cells from a contractile to a synthetic phenotype. *Exp Cell Res*. 1993;204:121-9.
14. Kelly DJ, Azeloglu EU, Kochupura PV, Sharma GS and Gaudette GR. Accuracy and reproducibility of a subpixel extended phase correlation method to determine micron level displacements in the heart. *Med Eng Phys*. 2007;29:154-62.
15. Schuldt AJ, Rosen MR, Gaudette GR and Cohen IS. Repairing damaged myocardium: evaluating cells used for cardiac regeneration. *Current treatment options in cardiovascular medicine*. 2008;10:59-72.
16. Tao ZW, Favreau JT, Guyette JP, Hansen KJ, Lessard J, Burford E, Pins GD and Gaudette GR. Delivering stem cells to the healthy heart on biological sutures: effects on regional mechanical function. *Journal of tissue engineering and regenerative medicine*. 2014.
17. Carlson BM. The regeneration of skeletal muscle — a review. *American Journal of Anatomy*. 1973;137:119-149.

18. Carvalho AB and de Carvalho ACC. Heart regeneration: Past, present and future. *World Journal of Cardiology*. 2010;2:107-111.
19. Laflamme MA and Murry CE. Regenerating the heart. *Nat Biotech*. 2005;23:845-856.
20. Laflamme MA and Murry CE. Heart regeneration. *Nature*. 2011;473:326-35.
21. MEERSON FZ. Compensatory Hyperfunction of the Heart and Cardiac Insufficiency. *Circulation research*. 1962;10:250-258.
22. Selvetella G and Lembo G. Mechanisms of Cardiac Hypertrophy. *Heart Failure Clinics*. 1:263-273.
23. Rane AA and Christman KL. Biomaterials for the Treatment of Myocardial Infarction A 5-Year Update. *Journal of the American College of Cardiology*. 2011;58:2615-2629.
24. Christman KL, Fok HH, Sievers RE, Fang Q and Lee RJ. Fibrin Glue Alone and Skeletal Myoblasts in a Fibrin Scaffold Preserve Cardiac Function after Myocardial Infarction. *Tissue engineering Part A*. 2004;10:403-409.
25. Christman KL, Vardanian AJ, Fang Q, Sievers RE, Fok HH and Lee RJ. Injectable fibrin scaffold improves cell transplant survival, reduces infarct expansion, and induces neovasculture formation in ischemic myocardium. *Journal of the American College of Cardiology*. 2004;44:654-60.
26. Johnson TD, Braden RL and Christman KL. Injectable ECM Scaffolds for Cardiac Repair. *Methods in molecular biology (Clifton, NJ)*. 2014;1181:109-120.
27. Singelyn JM, Sundaramurthy P, Johnson TD, Schup-Magoffin PJ, Hu DP, Faulk DM, Wang J, Mayle KM, Bartels K, Salvatore M, Kinsey AM, DeMaria AN, Dib N and Christman KL. Catheter-deliverable hydrogel derived from decellularized ventricular extracellular matrix increases endogenous cardiomyocytes and preserves cardiac function post-myocardial infarction. *Journal of the American College of Cardiology*. 2012;59:751-763.
28. Seif-Naraghi SB, Singelyn JM, Salvatore MA, Osborn KG, Wang JJ, Sampat U, Kwan OL, Strachan GM, Wong J, Schup-Magoffin PJ, Braden RL, Bartels K, DeQuach JA, Preul M, Kinsey AM, DeMaria AN, Dib N and Christman KL. Safety and efficacy of an injectable extracellular matrix hydrogel for treating myocardial infarction. *Science translational medicine*. 2013;5:10.1126/scitranslmed.3005503.
29. Tan MY, Zhi W, Wei RQ, Huang YC, Zhou KP, Tan B, Deng L, Luo JC, Li XQ, Xie HQ and Yang ZM. Repair of infarcted myocardium using mesenchymal stem cell seeded small intestinal submucosa in rabbits. *Biomaterials*. 2009;30:3234-3240.
30. Fujimoto KL, Tobita K, Merryman WD, Guan J, Momoi N, Stolz DB, Sacks MS, Keller BB and Wagner WR. An Elastic, Biodegradable Cardiac Patch Induces Contractile Smooth Muscle and Improves Cardiac Remodeling and Function in Subacute Myocardial Infarction. *Journal of the American College of Cardiology*. 2007;49:2292-2300.
31. Piao H, Kwon J-S, Piao S, Sohn J-H, Lee Y-S, Bae J-W, Hwang K-K, Kim D-W, Jeon O, Kim B-S, Park Y-B and Cho M-C. Effects of cardiac patches engineered with bone marrow-derived mononuclear cells and PGCL scaffolds in a rat myocardial infarction model. *Biomaterials*. 2007;28:641-649.
32. Liao B, Christoforou N, Leong KW and Bursac N. Pluripotent stem cell-derived cardiac tissue patch with advanced structure and function. *Biomaterials*. 2011;32:9180-7.
33. Zhang D, Shadrin IY, Lam J, Xian HQ, Snodgrass HR and Bursac N. Tissue-engineered cardiac patch for advanced functional maturation of human ESC-derived cardiomyocytes. *Biomaterials*. 2013;34:5813-20.
34. Wendel JS, Ye L, Tao R, Zhang J, Zhang J, Kamp TJ and Tranquillo RT. Functional Effects of a Tissue-Engineered Cardiac Patch From Human Induced Pluripotent Stem Cell-Derived Cardiomyocytes in a Rat Infarct Model. *Stem cells translational medicine*. 2015;4:1324-32.
35. Miki K, Uenaka H, Saito A, Miyagawa S, Sakaguchi T, Higuchi T, Shimizu T, Okano T, Yamanaka S and Sawa Y. Bioengineered Myocardium Derived from Induced Pluripotent Stem Cells Improves Cardiac Function and Attenuates Cardiac Remodeling Following Chronic Myocardial Infarction in Rats. *Stem cells translational medicine*. 2012;1:430-437.

36. Kawamura M, Miyagawa S, Miki K, Saito A, Fukushima S, Higuchi T, Kawamura T, Kuratani T, Daimon T, Shimizu T, Okano T and Sawa Y. Feasibility, Safety, and Therapeutic Efficacy of Human Induced Pluripotent Stem Cell-Derived Cardiomyocyte Sheets in a Porcine Ischemic Cardiomyopathy Model. *Circulation*. 2012;126:S29-S37.
37. Bellamy V, Vanneaux V, Bel A, Nemetalla H, Emmanuelle Boitard S, Farouz Y, Joanne P, Perier M-C, Robidel E, Mandet C, Hagège A, Bruneval P, Larghero J, Agbulut O and Menasché P. Long-term functional benefits of human embryonic stem cell-derived cardiac progenitors embedded into a fibrin scaffold. *The Journal of Heart and Lung Transplantation*. 2015;34:1198-1207.
38. Jakob P and Landmesser U. Current status of cell-based therapy for heart failure. *Current heart failure reports*. 2013;10:165-76.
39. Shah VK and Shalia KK. Stem Cell Therapy in Acute Myocardial Infarction: A Pot of Gold or Pandora's Box. *Stem cells international*. 2011;2011:536758.
40. Tseliou E, de Couto G, Terrovitis J, Sun B, Weixin L, Marban L and Marban E. Angiogenesis, cardiomyocyte proliferation and anti-fibrotic effects underlie structural preservation post-infarction by intramyocardially-injected cardiospheres. *PLoS One*. 2014;9:e88590.
41. Tang J, Xie Q, Pan G, Wang J and Wang M. Mesenchymal stem cells participate in angiogenesis and improve heart function in rat model of myocardial ischemia with reperfusion. *European journal of cardio-thoracic surgery : official journal of the European Association for Cardio-thoracic Surgery*. 2006;30:353-61.
42. Dawn B, Stein AB, Urbanek K, Rota M, Whang B, Rastaldo R, Torella D, Tang XL, Rezazadeh A, Kajstura J, Leri A, Hunt G, Varma J, Prabhu SD, Anversa P and Bolli R. Cardiac stem cells delivered intravascularly traverse the vessel barrier, regenerate infarcted myocardium, and improve cardiac function. *Proc Natl Acad Sci U S A*. 2005;102:3766-71.
43. Menasche P. Cardiac cell therapy: lessons from clinical trials. *Journal of molecular and cellular cardiology*. 2011;50:258-65.
44. Russo V, Young S, Hamilton A, Amsden BG and Flynn LE. Mesenchymal stem cell delivery strategies to promote cardiac regeneration following ischemic injury. *Biomaterials*. 2014;35:3956-3974.
45. Atkins BZ, Hueman MT, Meuchel JM, Cottman MJ, Hutcheson KA and Taylor DA. Myogenic cell transplantation improves in vivo regional performance in infarcted rabbit myocardium. *The Journal of Heart and Lung Transplantation*. 1999;18:1173-1180.
46. Taylor DA, Atkins BZ, Hungspreugs P, Jones TR, Reedy MC, Hutcheson KA, Glower DD and Kraus WE. Regenerating functional myocardium: Improved performance after skeletal myoblast transplantation. *Nat Med*. 1998;4:929-933.
47. Ghostine S, Carrion C, Souza LCG, Richard P, Bruneval P, Vilquin J-T, Pouzet B, Schwartz K, Menasché P and Hagège AA. Long-Term Efficacy of Myoblast Transplantation on Regional Structure and Function After Myocardial Infarction. *Circulation*. 2002;106:I-131-I-136.
48. Menasche P, Alfieri O, Janssens S, McKenna W, Reichenspurner H, Trinquart L, Vilquin JT, Marolleau JP, Seymour B, Larghero J, Lake S, Chatellier G, Solomon S, Desnos M and Hagege AA. The Myoblast Autologous Grafting in Ischemic Cardiomyopathy (MAGIC) trial: first randomized placebo-controlled study of myoblast transplantation. *Circulation*. 2008;117:1189-200.
49. Messina E, De Angelis L, Frati G, Morrone S, Chimenti S, Fiordaliso F, Salio M, Battaglia M, Latronico MVG, Coletta M, Vivarelli E, Frati L, Cossu G and Giacomello A. Isolation and Expansion of Adult Cardiac Stem Cells From Human and Murine Heart. *Circulation research*. 2004;95:911-921.
50. Bearzi C, Rota M, Hosoda T, Tillmanns J, Nascimbene A, De Angelis A, Yasuzawa-Amano S, Trofimova I, Siggins RW, LeCapitaine N, Cascapera S, Beltrami AP, D'Alessandro DA, Zias E, Quaini F, Urbanek K, Michler RE, Bolli R, Kajstura J, Leri A and Anversa P. Human cardiac stem cells. *Proceedings of the National Academy of Sciences of the United States of America*. 2007;104:14068-14073.

51. Beltrami AP, Barlucchi L, Torella D, Baker M, Limana F, Chimenti S, Kasahara H, Rota M, Musso E, Urbanek K, Leri A, Kajstura J, Nadal-Ginard B and Anversa P. Adult Cardiac Stem Cells Are Multipotent and Support Myocardial Regeneration. *Cell*. 2003;114:763-776.
52. Bolli R, Jneid H, Tang X-L, Dawn B, Rimoldi O, Mosna F, Loredi M, Gatti A, Kajstura J, Leri A, Bearzi C, Abdel-Latif A and Anversa P. Abstract 1267: Intracoronary Administration of Cardiac Stem Cells Improves Cardiac Function in Pigs with Old Infarction. *Circulation*. 2006;114:II\_239-II\_239.
53. Bolli R, Chugh AR, D'Amario D, Loughran JH, Stoddard MF, Ikram S, Beache GM, Wagner SG, Leri A, Hosoda T, Sanada F, Elmore JB, Goichberg P, Cappetta D, Solankhi NK, Fahsah I, Rokosh DG, Slaughter MS, Kajstura J and Anversa P. Cardiac stem cells in patients with ischaemic cardiomyopathy (SCIPIO): initial results of a randomised phase 1 trial. *The Lancet*. 2011;378:1847-1857.
54. Kajstura J, Rota M, Cappetta D, Ogórek B, Arranto C, Bai Y, Ferreira-Martins J, Signore S, Sanada F, Matsuda A, Kostyla J, Caballero M-V, Fiorini C, D'Alessandro DA, Michler RE, del Monte F, Hosoda T, Perrella MA, Leri A, Buchholz BA, Loscalzo J and Anversa P. Cardiomyogenesis in the Aging and Failing Human Heart. *Circulation*. 2012;126:1869-1881.
55. Sultana N, Zhang L, Yan J, Chen J, Cai W, Razzaque S, Jeong D, Sheng W, Bu L, Xu M, Huang G-Y, Hajjar RJ, Zhou B, Moon A and Cai C-L. Resident c-kit+ cells in the heart are not cardiac stem cells. *Nature Communications*. 2015;6:8701.
56. van Berlo JH, Kanisicak O, Maillet M, Vagnozzi RJ, Karch J, Lin S-CJ, Middleton RC, Marbán E and Molkentin JD. c-kit(+) Cells Minimally Contribute Cardiomyocytes to the Heart. *Nature*. 2014;509:337-341.
57. Young PP and Schäfer R. Cell-based therapies for cardiac disease: a cellular therapist's perspective. *Transfusion*. 2015;55:441-451.
58. Pittenger MF, Mackay AM, Beck SC, Jaiswal RK, Douglas R, Mosca JD, Moorman MA, Simonetti DW, Craig S and Marshak DR. Multilineage Potential of Adult Human Mesenchymal Stem Cells. *Science*. 1999;284:143-147.
59. Prockop DJ. Marrow Stromal Cells as Stem Cells for Nonhematopoietic Tissues. *Science*. 1997;276:71-74.
60. Caplan AL. Mesenchymal stem cells. *Journal of Orthopaedic Research*. 1991;9:641-650.
61. Abdi R, Fiorina P, Adra CN, Atkinson M and Sayegh MH. Immunomodulation by Mesenchymal Stem Cells : A Potential Therapeutic Strategy for Type 1 Diabetes. *Diabetes*. 2008;57:1759-1767.
62. Parekkadan B and Milwid JM. Mesenchymal Stem Cells as Therapeutics. *Annual review of biomedical engineering*. 2010;12:87-117.
63. Squillaro T, Peluso G and Galderisi U. Clinical Trials With Mesenchymal Stem Cells: An Update. *Cell Transplant*. 2016;25:829-48.
64. Galderisi U and Giordano A. The Gap Between the Physiological and Therapeutic Roles of Mesenchymal Stem Cells. *Medicinal Research Reviews*. 2014;34:1100-1126.
65. Bernardo Maria E and Fibbe Willem E. Mesenchymal Stromal Cells: Sensors and Switchers of Inflammation. *Cell Stem Cell*. 2013;13:392-402.
66. Kwak BR and Mach F. Paracrine action accounts for marked protection of ischemic heart by Akt-modified mesenchymal stem cells. *Nature medicine*. 2005;11:367.
67. Orlic D, Kajstura J, Chimenti S, Jakoniuk I, Anderson SM, Li B, Pickel J, McKay R, Nadal-Ginard B, Bodine DM, Leri A and Anversa P. Bone marrow cells regenerate infarcted myocardium. *Nature*. 2001;410:701-705.
68. Murry CE, Soonpaa MH, Reinecke H, Nakajima H, Nakajima HO, Rubart M, Pasumarthi KBS, Ismail Virag J, Bartelmez SH, Poppa V, Bradford G, Dowell JD, Williams DA and Field LJ. Haematopoietic stem cells do not transdifferentiate into cardiac myocytes in myocardial infarcts. *Nature*. 2004;428:664-668.
69. Balsam LB, Wagers AJ, Christensen JL, Kofidis T, Weissman IL and Robbins RC. Haematopoietic stem cells adopt mature haematopoietic fates in ischaemic myocardium. *Nature*. 2004;428:668-673.



70. Nygren JM, Jovinge S, Breitbach M, Sawen P, Roll W, Hescheler J, Taneera J, Fleischmann BK and Jacobsen SEW. Bone marrow-derived hematopoietic cells generate cardiomyocytes at a low frequency through cell fusion, but not transdifferentiation. *Nat Med*. 2004;10:494-501.
71. Dai W, Hale SL, Martin BJ, Kuang J-Q, Dow JS, Wold LE and Kloner RA. Allogeneic Mesenchymal Stem Cell Transplantation in Postinfarcted Rat Myocardium. *Short- and Long-Term Effects*. 2005;112:214-223.
72. Perin EC, Silva GV, Assad JA, Vela D, Buja LM, Sousa AL, Litovsky S, Lin J, Vaughn WK, Coulter S, Fernandes MR and Willerson JT. Comparison of intracoronary and transendocardial delivery of allogeneic mesenchymal cells in a canine model of acute myocardial infarction. *Journal of molecular and cellular cardiology*. 2008;44:486-95.
73. Shake JG, Gruber PJ, Baumgartner WA, Senechal G, Meyers J, Redmond JM, Pittenger MF and Martin BJ. Mesenchymal stem cell implantation in a swine myocardial infarct model engraftment and functional effects. *The Society of Thoracic Surgeons*. 2002;73:1919-26.
74. Wollert KC, Meyer GP, Lotz J, Ringes Lichtenberg S, Lippolt P, Breidenbach C, Fichtner S, Korte T, Hornig B, Messinger D, Arseniev L, Hertenstein B, Ganser A and Drexler H. Intracoronary autologous bone-marrow cell transfer after myocardial infarction: the BOOST randomised controlled clinical trial. *The Lancet*. 2004;364:141-148.
75. Hare JM, Traverse JH, Henry TD, Dib N, Strumpf RK, Schulman SP, Gerstenblith G, DeMaria AN, Denktas AE, Gammon RS, Hermiller JB, Jr., Reisman MA, Schaer GL and Sherman W. A randomized, double-blind, placebo-controlled, dose-escalation study of intravenous adult human mesenchymal stem cells (prochymal) after acute myocardial infarction. *Journal of the American College of Cardiology*. 2009;54:2277-86.
76. Schächinger V, Erbs S, Elsässer A, Haberbosch W, Hambrecht R, Hölschermann H, Yu J, Cort R, Mathey DG, Hamm CW, Süselbeck T, Assmus B, Tonn T, Dimmeler S and Zeiher AM. Intracoronary Bone Marrow-Derived Progenitor Cells in Acute Myocardial Infarction. *The New England journal of medicine*. 2006;355:1210-21.
77. Traverse JH, Henry TD, Pepine CJ and et al. Effect of the use and timing of bone marrow mononuclear cell delivery on left ventricular function after acute myocardial infarction: The time randomized trial. *JAMA : the journal of the American Medical Association*. 2012;308:2380-2389.
78. Hare JM, Fishman JE, Gerstenblith G and et al. Comparison of allogeneic vs autologous bone marrow-derived mesenchymal stem cells delivered by transendocardial injection in patients with ischemic cardiomyopathy: The poseidon randomized trial. *JAMA : the journal of the American Medical Association*. 2012;308:2369-2379.
79. Traverse JH, Henry TD, Ellis SG and et al. Effect of intracoronary delivery of autologous bone marrow mononuclear cells 2 to 3 weeks following acute myocardial infarction on left ventricular function: The latetime randomized trial. *JAMA : the journal of the American Medical Association*. 2011;306:2110-2119.
80. Sürder D, Manka R, Lo Cicero V, Moccetti T, Rufibach K, Soncin S, Turchetto L, Radrizzani M, Astori G, Schwitter J, Erne P, Zuber M, Auf der Maur C, Jamshidi P, Gaemperli O, Windecker S, Moschovitis A, Wahl A, Bühler I, Wyss C, Kozerke S, Landmesser U, Lüscher TF and Corti R. Intracoronary Injection of Bone Marrow-Derived Mononuclear Cells Early or Late After Acute Myocardial Infarction. *Effects on Global Left Ventricular Function*. 2013;127:1968-1979.
81. Traverse JH, Henry TD, Ellis SG, Pepine CJ, Willerson JT, Zhao DXM, Forder JR, Byrne BJ, Hatzopoulos AK, Penn MS, Perin EC, Baran KW, Chambers J, Lambert C, Raveendran G, Simon DI, Vaughan DE, Simpson LM, Gee AP, Taylor DA, Cogle CR, Thomas JD, Silva GV, Jorgenson BC, Olson RE, Bowman S, Francescon J, Geither C, Handberg E, Smith DX, Baraniuk S, Piller LB, Loghin C, Aguilar D, Richman S, Zierold C, Bettencourt J, Sayre SL, Vojvodic RW, Skarlatos SI, Gordon DJ, Ebert RF, Kwak M, Moyé LA, Simari RD and The Cardiovascular Cell Therapy Research N. Effect of Intracoronary Delivery of Autologous Bone

Marrow Mononuclear Cells Two to Three Weeks Following Acute Myocardial Infarction on Left-Ventricular Function: The LateTIME Randomized Trial. *JAMA : the journal of the American Medical Association*. 2011;306:2110-2119.

82. Thomson JA. Embryonic Stem Cell Lines Derived from Human Blastocysts. *Science*. 1998;282:1145-1147.
83. Takahashi K and Yamanaka S. Induction of pluripotent stem cells from mouse embryonic and adult fibroblast cultures by defined factors. *Cell*. 2006;126:663-76.
84. Freund C and Mummery CL. Prospects for pluripotent stem cell-derived cardiomyocytes in cardiac cell therapy and as disease models. *Journal of cellular biochemistry*. 2009;107:592-9.
85. Martins AM, Vunjak-Novakovic G and Reis RL. The Current Status of iPS Cells in Cardiac Research and Their Potential for Tissue Engineering and Regenerative Medicine. *Stem Cell Rev*. 2014;10:177-90.
86. Mummery C, Ward-van Oostwaard D, Doevendans P, Spijker R, van den Brink S, Hassink R, van der Heyden M, Opthof T, Pera M, de la Riviere AB, Passier R and Tertoolen L. Differentiation of human embryonic stem cells to cardiomyocytes: role of coculture with visceral endoderm-like cells. *Circulation*. 2003;107:2733-40.
87. Kehat I, Kenyagin-Karsenti D, Snir M, Segev H, Amit M, Gepstein A, Livne E, Binah O, Itskovitz-Eldor J and Gepstein L. Human embryonic stem cells can differentiate into myocytes with structural and functional properties of cardiomyocytes. *Journal of Clinical Investigation*. 2001;108:407-414.
88. Zhang J, Wilson GF, Soerens AG, Koonce CH, Yu J, Palecek SP, Thomson JA and Kamp TJ. Functional cardiomyocytes derived from human induced pluripotent stem cells. *Circ Res*. 2009;104:e30-41.
89. Lian X, Hsiao C, Wilson G, Zhu K, Hazeltine LB, Azarin SM, Raval KK, Zhang J, Kamp TJ and Palecek SP. Robust cardiomyocyte differentiation from human pluripotent stem cells via temporal modulation of canonical Wnt signaling. *Proc Natl Acad Sci U S A*. 2012;109:E1848-57.
90. Laflamme MA, Chen KY, Naumova AV, Muskheli V, Fugate JA, Dupras SK, Reinecke H, Xu C, Hassanipour M, Police S, O'Sullivan C, Collins L, Chen Y, Minami E, Gill EA, Ueno S, Yuan C, Gold J and Murry CE. Cardiomyocytes derived from human embryonic stem cells in pro-survival factors enhance function of infarcted rat hearts. *Nature biotechnology*. 2007;25:1015-24.
91. Graf S, Garipey J, Maddonneau M, Armentano R, Mansour S, Barra J, Simon A and Levenson J. Experimental and clinical validation of arterial diameter waveform and intimal media thickness obtained from B-mode ultrasound image processing. *Ultrasound in medicine ....* 1999;25:1353-1363.
92. He JQ, Ma Y, Lee Y, Thomson JA and Kamp TJ. Human embryonic stem cells develop into multiple types of cardiac myocytes: action potential characterization. *Circ Res*. 2003;93:32-9.
93. Mummery CL, Zhang J, Ng ES, Elliott DA, Elefanty AG and Kamp TJ. Differentiation of human embryonic stem cells and induced pluripotent stem cells to cardiomyocytes: a methods overview. *Circ Res*. 2012;111:344-58.
94. Sharma S, Jackson PG and Mangan J. Cardiac troponins. *Journal of clinical pathology*. 2004;57:1025-6.
95. Sjoblom B, Salmazo A and Djinnovic-Carugo K. Alpha-actinin structure and regulation. *Cellular and molecular life sciences : CMLS*. 2008;65:2688-701.
96. Lundy SD, Zhu WZ, Regnier M and Laflamme MA. Structural and functional maturation of cardiomyocytes derived from human pluripotent stem cells. *Stem Cells Dev*. 2013;22:1991-2002.
97. Yang X, Pabon L and Murry CE. Engineering adolescence: maturation of human pluripotent stem cell-derived cardiomyocytes. *Circ Res*. 2014;114:511-23.
98. Yang X, Rodriguez M, Pabon L, Fischer KA, Reinecke H, Regnier M, Sniadecki NJ, Ruohola-Baker H and Murry CE. Tri-iodo-L-thyronine Promotes the Maturation of Human Cardiomyocytes-Derived from Induced Pluripotent Stem Cells. *Journal of molecular and cellular cardiology*. 2014;72:296-304.

99. Huethorst E, Hortigon M, Zamora-Rodriguez V, Reynolds PM, Burton F, Smith G and Gadegaard N. Enhanced Human-Induced Pluripotent Stem Cell Derived Cardiomyocyte Maturation Using a Dual Microgradient Substrate. *ACS Biomaterials Science & Engineering*. 2016;2:2231-2239.
100. Mauritz C, Martens A, Rojas SV, Schnick T, Rathert C, Schecker N, Menke S, Glage S, Zweigerdt R, Haverich A, Martin U and Kutschka I. Induced pluripotent stem cell (iPSC)-derived Flk-1 progenitor cells engraft, differentiate, and improve heart function in a mouse model of acute myocardial infarction. *European heart journal*. 2011;32:2634-41.
101. Chong JJ, Yang X, Don CW, Minami E, Liu YW, Weyers JJ, Mahoney WM, Van Biber B, Cook SM, Palpant NJ, Gantz JA, Fugate JA, Muskheli V, Gough GM, Vogel KW, Astley CA, Hotchkiss CE, Baldessari A, Pabon L, Reinecke H, Gill EA, Nelson V, Kiem HP, Laflamme MA and Murry CE. Human embryonic-stem-cell-derived cardiomyocytes regenerate non-human primate hearts. *Nature*. 2014;510:273-7.
102. Carpenter L, Carr C, Yang CT, Stuckey DJ, Clarke K and Watt SM. Efficient differentiation of human induced pluripotent stem cells generates cardiac cells that provide protection following myocardial infarction in the rat. *Stem Cells Dev*. 2012;21:977-86.
103. Caspi O, Huber I, Kehat I, Habib M, Arbel G, Gepstein A, Yankelson L, Aronson D, Beyar R and Gepstein L. Transplantation of human embryonic stem cell-derived cardiomyocytes improves myocardial performance in infarcted rat hearts. *Journal of the American College of Cardiology*. 2007;50:1884-93.
104. van Laake LW, Passier R, Monshouwer-Kloots J, Verkleij AJ, Lips DJ, Freund C, den Ouden K, Ward-van Oostwaard D, Korving J, Tertoolen LG, van Echteld CJ, Doevendans PA and Mummery CL. Human embryonic stem cell-derived cardiomyocytes survive and mature in the mouse heart and transiently improve function after myocardial infarction. *Stem cell research*. 2007;1:9-24.
105. van Laake LW, Passier R, den Ouden K, Schreurs C, Monshouwer-Kloots J, Ward-van Oostwaard D, van Echteld CJ, Doevendans PA and Mummery CL. Improvement of mouse cardiac function by hESC-derived cardiomyocytes correlates with vascularity but not graft size. *Stem cell research*. 2009;3:106-12.
106. Miki K, Uenaka H, Saito A, Miyagawa S, Sakaguchi T, Higuchi T, Shimizu T, Okano T, Yamanaka S and Sawa Y. Bioengineered myocardium derived from induced pluripotent stem cells improves cardiac function and attenuates cardiac remodeling following chronic myocardial infarction in rats. *Stem cells translational medicine*. 2012;1:430-7.
107. Blin G, Nury D, Stefanovic S, Neri T, Guillevic O, Brinon B, Bellamy V, Rücker-Martin C, Barbry P, Bel A, Bruneval P, Cowan C, Pouly J, Mitalipov S, Gouadon E, Binder P, Hagege A, Desnos M, Renaud J-F, Menasché P and Pucéat M. A purified population of multipotent cardiovascular progenitors derived from primate pluripotent stem cells engrafts in postmyocardial infarcted nonhuman primates. *The Journal of clinical investigation*. 2010;120:1125-1139.
108. Templin C, Zweigerdt R, Schwanke K, Olmer R, Ghadri J-R, Emmert MY, Müller E, Küest SM, Cohrs S, Schibli R, Kronen P, Hilbe M, Reinisch A, Strunk D, Haverich A, Hoerstrup S, Lüscher TF, Kaufmann PA, Landmesser U and Martin U. Transplantation and Tracking of Human-Induced Pluripotent Stem Cells in a Pig Model of Myocardial Infarction. *Assessment of Cell Survival, Engraftment, and Distribution by Hybrid Single Photon Emission Computed Tomography/Computed Tomography of Sodium Iodide Symporter Transgene Expression*. 2012;126:430-439.
109. Hou D, Youssef EA, Brinton TJ, Zhang P, Rogers P, Price ET, Yeung AC, Johnstone BH, Yock PG and March KL. Radiolabeled cell distribution after intramyocardial, intracoronary, and interstitial retrograde coronary venous delivery: implications for current clinical trials. *Circulation*. 2005;112:1150-6.
110. Vrtovec B, Poglajen G, Lezaic L, Sever M, Socan A, Domanovic D, Cernelc P, Torre-Amione G, Haddad F and Wu JC. Comparison of transendocardial and intracoronary CD34+ cell transplantation in patients with nonischemic dilated cardiomyopathy. *Circulation*. 2013;128:S42-9.
111. Ratcliffe E, Glen KE, Naing MW and Williams DJ. Current status and perspectives on stem cell-based therapies undergoing clinical trials for regenerative medicine: case studies. *Br Med Bull*. 2013;108:73-94.

112. Osterberg K and Mattsson E. Intimal hyperplasia in mouse vein grafts is regulated by flow. *Journal of vascular research*. 2005;42:13-20.
113. Ahmed TA, Dare EV and Hincke M. Fibrin: a versatile scaffold for tissue engineering applications. *Tissue engineering Part B, Reviews*. 2008;14:199-215.
114. Li J, Liu Y, Zhang Y, Cai H-L and Xiong R-G. Molecular ferroelectrics: where electronics meet biology. *Phys Chem Chem Phys*. 2013;15:20786-96.
115. Thomson KS, Korte FS, Giachelli CM, Ratner BD, Regnier M and Scatena M. Prevascularized microtemplated fibrin scaffolds for cardiac tissue engineering applications. *Tissue engineering Part A*. 2013;19:967-77.
116. III LDB, Meyers JD, Weinbaum JS, Shvelidze YA and Tranquillo RT. Cell-Induced Alignment Augments Twitch Force in Fibrin Gel-Based Engineered Myocardium via Gap Junction Modification. *Tissue engineering Part A*. 2009;15:3099-3108.
117. Christoforou N, Liao B, Chakraborty S, Chellapan M, Bursac N and Leong KW. Induced pluripotent stem cell-derived cardiac progenitors differentiate to cardiomyocytes and form biosynthetic tissues. *PLoS One*. 2013;8:e65963.
118. Cornwell KG and Pins GD. Discrete crosslinked fibrin microthread scaffolds for tissue regeneration. *Journal of biomedical materials research Part A*. 2007;82:104-12.
119. Proulx MK, Carey SP, Ditroia LM, Jones CM, Fakhrazadeh M, Guyette JP, Clement AL, Orr RG, Rolle MW, Pins GD and Gaudette GR. Fibrin microthreads support mesenchymal stem cell growth while maintaining differentiation potential. *Journal of biomedical materials research Part A*. 2011;96:301-12.
120. Guyette JP, Fakhrazadeh M, Burford EJ, Tao ZW, Pins GD, Rolle MW and Gaudette GR. A novel suture-based method for efficient transplantation of stem cells. *Journal of biomedical materials research Part A*. 2013;101:809-18.

### 3 Objective 1a: Investigate cell seeding conditions to improve attachment of hMSCs onto fibrin microthread sutures.

The introduction (starting with section 3.1), methods, results, and discussion presented in this objective are published in BioResearch Open Access. These sections are published under the liberal CC-BY license and can be freely reused with the proper citation: Hansen et al. "Functional Effects of Delivering Human Mesenchymal Stem Cell-Seeded Biological Sutures to an Infarcted Heart." *BioResearch Open Access*. 2016; 5(1):249-260 (see Chapter 9: Appendix).

#### 3.1 Introduction

A limitation of MSC based cell therapy is the inefficient retention associated with most cell delivery methods<sup>1</sup>. Current delivery methods achieve a small and inefficient 10-20% retention rate. In addition, targeting cell delivery to a specific region is also challenging. Biomaterials have been proposed for MSC delivery to ischemic tissue; many focus on the development of injectable biomaterials as well as cardiac patch materials. Both natural and synthetic injectable biomaterials that have been explored include alginate<sup>2</sup>, chitosan<sup>3</sup>, collagen<sup>4</sup>, fibrin<sup>5, 6</sup>, and poly(ethylene glycol)<sup>7</sup> based biomaterials. All biomaterials, with the exception of collagen, were shown to support stem cell survival upon delivery and improve cell retention. Similar biomaterials, fibrin<sup>8</sup>, chitosan/alginate<sup>9</sup>, collagen<sup>10</sup>, and polyglycolic acid<sup>11</sup>, were used to create stem cell seeded cardiac patches. Consistent with injectable biomaterials, cardiac patches also improved cell survival *in vivo*, however, many studies have reported minimal migration of cells from the patch to the host tissue. Natural biomaterials have the added advantage of having innate biological activity, however, the material properties of synthetic biomaterials are more easily customizable to fit the application.

Fibrin has been used as a glue, a hydrogel, and a scaffold for applications in tissue engineering of bone<sup>12, 13</sup>, ocular<sup>14, 15</sup>, liver<sup>16, 17</sup>, muscle<sup>18, 19</sup>, cartilage<sup>20, 21</sup>, skin<sup>22-24</sup>, and cardiovascular tissue<sup>6, 25, 26</sup>. Many of these applications have incorporated mesenchymal stem cells into the fibrin either encapsulated within the substrate or seeded on top of the substrate. These studies have demonstrated fibrin to be capable of

supporting MSC attachment as well as growth and survival for extended culture duration. Fibrin provides a self-supporting, naturally biodegradable structure for MSC survival and will be investigated in this dissertation as a vehicle to deliver hMSCs.

To overcome issues of poor cell retention while simultaneously providing a delivery method that allows for targeted cell delivery, we developed fibrin based biological sutures. These sutures have been demonstrated to support hMSC attachment and survival and does not impact the potential of the hMSCs to differentiate<sup>27</sup>. Using this delivery method, previous studies have shown a 64% retention of hMSCs to cardiac tissue<sup>28</sup>. Herein, we use this delivery method to deliver of hMSCs to infarcted myocardium and determine if these cells lead to improved active mechanical function. In this objective we aim to understand and tune the seeding conditions to promote hMSC attachment onto the biological sutures. Previous work in our lab developed a seeding method to allow attachment of hMSCs to the biological sutures; however, how different seeding concentrations and seeding times affect hMSC attachment has not been examined.

## 3.2 Materials and methods

### 3.2.1 Fibrin microthread production

Discrete fibrin microthreads were produced as described previously<sup>27</sup>. Briefly, fibrinogen (70mg/mL; MP Biomedical) and thrombin (8U/mL; Sigma) were coextruded using a blending tip connector in a 10mM HEPES (Calbiochem) buffered bath (pH 7.4). A custom built extrusion system was used to extrude microthreads at a flow rate of 0.23 mL/min through 0.38 mm polyethylene tubing. After extrusion, the microthreads were allowed to polymerize before being removed and air dried.

To create biological sutures, 12 individual microthreads were arranged parallel to one another, hydrated with distilled water, and twisted together (Figure 3-1A, B). After drying, each bundle was cut to 4 cm lengths. The 4 cm bundles were threaded through the eye of a surgical needle (size 26, Havel's Inc.), hydrated with distilled water, and the free ends of the bundle were twisted together to form a 2cm long suture (Figure 3-1C, D). Once dried, each suture was placed in a 4cm long piece of silastic tubing (1.98mm

ID, Dow Corning) with a 27-gauge ½ inch needle (Becton Dickinson) and secured with a slide clamp across the needles (Figure 3-1E). Suture constructs were ethylene-oxide sterilized for a 12 hour period and stored in a desiccator before cell seeding.

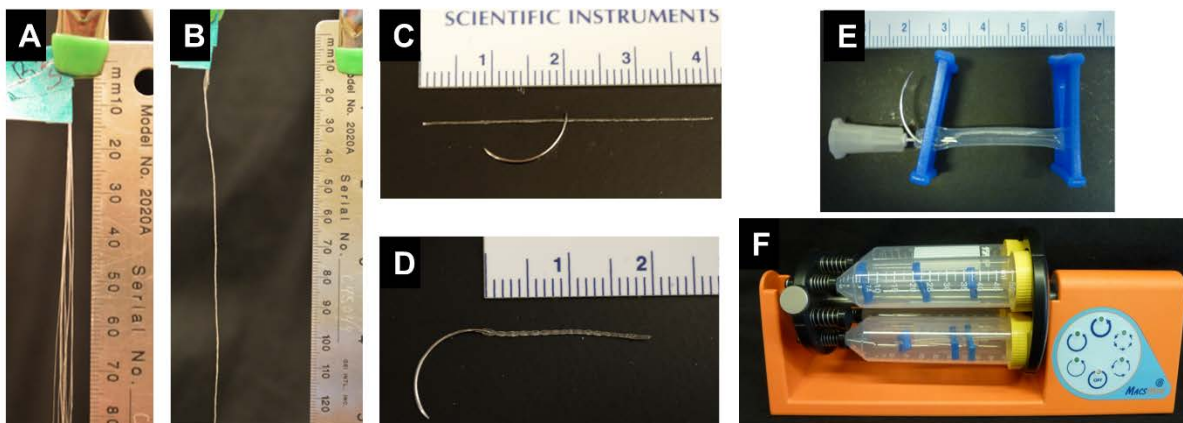


**Figure 3-1. Fibrin suture seeding.** 12 individual fibrin microthreads are placed together (A) and hydrated and twisted together to form a bundle (B). Each bundle is cut to 4 cm lengths and placed through the eye of a suture needle (C) and hydrated and twisted together form a suture (D). Each suture is placed into a piece of silastic tubing with a 27G needle to facilitate seeding (E). hMSCs in media are injected into the tubing and clamped off and then placed in a vented conical tube in a rotator in the incubator for seeding.

### 3.2.2 Human MSC culture

hMSCs (Lonza Inc.) were cultured in T75 flasks incubated at 37°C in 5% CO<sub>2</sub>. Passage 4-8 hMSCs were grown in monolayer culture in growth medium (MSCGM; Lonza Inc.) until cells reached 80-90% confluence. All implanted hMSCs were treated with MSCGM supplemented with 8.2 nM Qdot 655 ITK carboxyl quantum dots (Qdots; Invitrogen) to allow for cell tracking. Qdots were added to 70-80% confluent layers of hMSCs and were allowed to incubate for 24 hours at 37°C in 5% CO<sub>2</sub>. Quantum dot loading was verified using fluorescent microscopy. After 24 hours, Qdot media was replaced and cells were maintained until further use.

### 3.2.3 Biological suture seeding

Prior to cell seeding, sutures were hydrated with 100 µL of dPBS for 20 minutes within the seeding construct; dPBS is expelled before cells were introduced. For cell seeding, 100 µL of a 2.5x10<sup>5</sup>, 5x10<sup>5</sup>, 1x10<sup>6</sup> hMSC/mL solution was drawn into a 1ml syringe (Becton Dickinson). The syringe was attached to the 27-gauge needle and dispensed into the silastic tubing containing the suture. The 27-gauge needle and

syringe were removed and a slide clamp was added to the free end of the tubing to seal both ends. The seeding construct was placed in a vented 50mL conical tube and placed in a portable MACsmix rotator (Miltenyi Biotech, Figure 3-1F). The rotator was set to 4 rotations per minute and placed into a 37°C incubator in 5% CO<sub>2</sub>. To determine the role of incubation time, sutures were allowed to seed for 1, 3, 6, 12, and 24 hours.

#### 3.2.4 hMSC cell attachment quantification

After seeding, hMSC-seeded sutures were removed from the seeding construct and either fixed in 4% paraformaldehyde for staining or prepped for a CyQuant DNA assay. For CyQuant DNA assays, sutures were placed in a 1.5mL Eppendorf tube with 100uL of phosphate buffered saline (PBS) in a -80°C freezer for cell lysis. Sutures were allowed to freeze for 1 hour to 4 weeks before use in the CyQuant assay. The CyQuant assay was run according to manufacturer's specifications. Briefly, sutures were removed from freezer, allowed to thaw, and 400 µL of cell lysis buffer with GR dye was added to the Eppendorf tube. Four, 100 µL aliquots of the cell suspension were added to a 96 well plate along with an independent standard curve. Fluorescent measurements were taken using a plate reader (Victor 3, Perkin Elmer) at an excitation of 480nm and absorption of 520nm. Values are reported as mean±SEM cell count per linear centimeter of suture.

#### 3.2.5 Histological data

Sutures not prepared for CyQuant were fixed in 4% paraformaldehyde for 10 minutes and stained for F-actin. Briefly, sutures were washed in PBS, blocked for 30 minutes in 1% albumin from bovine serum, and stained with 488 phalloidin (Invitrogen) for 30 minutes. Sutures were washed in PBS and then counterstained with Hoechst 33342 (0.5ug/mL, Invitrogen) for 5 minutes at room temperature. Images were acquired at 200x with a Leica Upright DMLB2 or a Leica TCP SP5 confocal laser scanning microscope.

#### 3.2.6 Statistical analysis

Statistical analyses were performed using GraphPad Prism 6 (GraphPad Software, Inc., La Jolla, CA). Results are represented as mean±SEM. Comparisons between seeding conditions were analyzed using a



one-way analysis of variance (ANOVA), with a post-hoc Tukey test for multiple comparisons. All conditions were considered significant at a value of  $p < 0.05$ .

### 3.3 Results

#### 3.3.1 Effect of cell seeding concentration on hMSC attachment to biological sutures

Three different concentrations of hMSCs ( $2.5 \times 10^5$ ,  $5 \times 10^5$ ,  $1 \times 10^6$  hMSCs/mL solution) of human MSCs were seeded onto 2 cm long biological sutures. There were significantly more hMSCs attached to the sutures seeded with the higher concentrations ( $5 \times 10^5$ ,  $1 \times 10^6$  hMSC/mL) compared to a concentration of  $2.5 \times 10^5$  ( $n=10$ ;  $p < 0.05$ ) (Figure 3-2A), a finding which was further supported by F-actin staining (Figure 3-2B, C, and D).

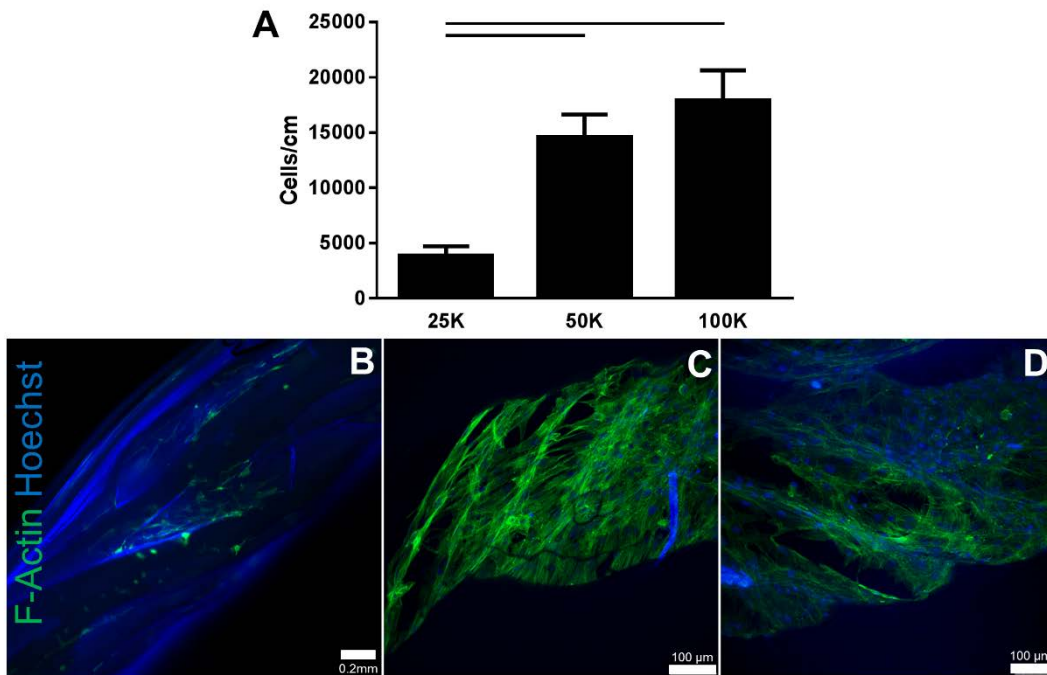


**Figure 3-2. Effect of cell seeding concentration on hMSC attachment to biological suture.** Biological sutures were seeded with three different concentrations of hMSCs: 25, 50, and 100K cells per suture. Highest attachment was found for the higher concentrations (A) with no statistical difference found between the 50 and 100K. F-actin staining for 25K (B), 50K (C), and 100K (D) revealed similar cell attachment for the 50 and 100K conditions. Some blue autofluorescence seen in B and D is due to the suture. Mean $\pm$ SEM, -  $p < 0.05$ ,  $n=10$  per group.

#### 3.3.2 Effect of incubation time on hMSC attachment to biological sutures

To determine the effect of incubation time of cell attachment on biological sutures, five different incubation times were examined (1, 3, 6, 12, and 24 hours). Seeding for 12 and 24 hours significantly increased cell attachment compared to 1 and 3 hours ( $p < 0.05$ ) (Figure 3-3A). There was no significant

difference in the number of hMSCs attached at 6, 12 or 24 hours. F-actin staining shows cell attachment beginning at 1 hour (Figure 3-3B), more cells attached at 6 and 12 hours (Figure 3-3C and D) with cells appearing to elongate along the length of the suture at 12 and 24 hours.

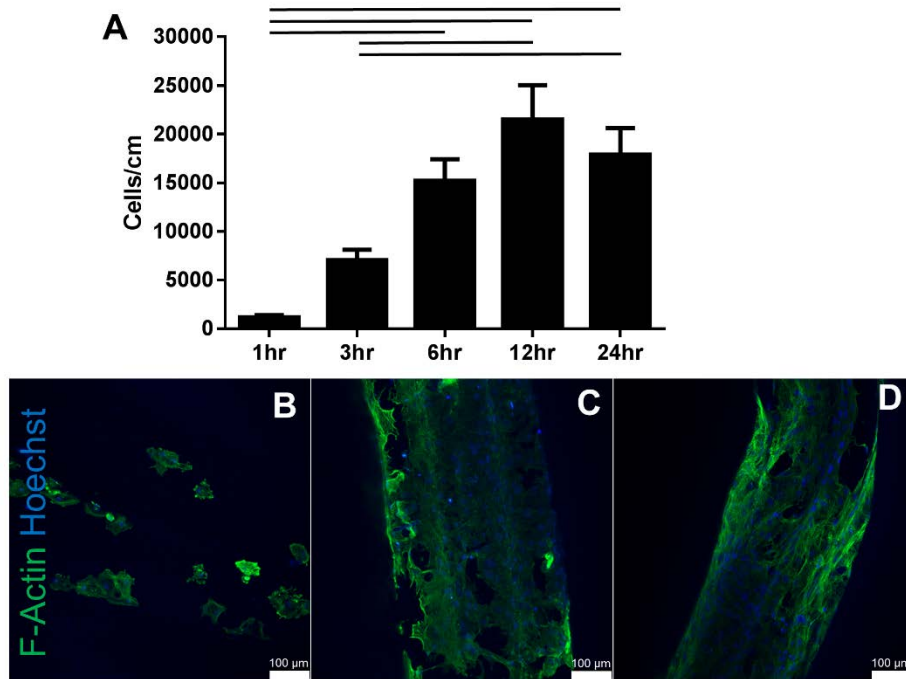


**Figure 3-3. Effect of seeding time on hMSC attachment to biological suture.** hMSC attachment for 5 different time points (1, 3, 6, 12, and 24 hours) was examined. Seeding times of 1 and 3 hours resulted in significantly fewer cells attached compared to 12 and 24 hours, where there was no significant differences in attachment at 6, 12 and 24 hours (A). F-actin staining shows cells attached at 1 hour (B), but with higher numbers of cells attached at 6 and 12 hours (C, D). Mean±SEM, -  $p < 0.05$ ,  $n = 10$  per group.

### 3.4 Discussion

Concerns remain when cells are delivered to the heart. Current delivery methods exhibit retention rates of only 10-20%, which are inefficient for delivering clinically relevant numbers of cells. Fibrin based biological sutures are able to efficiently (64% retention) deliver hMSCs to targeted areas of ischemic myocardium. While previous studies have developed methods to seed hMSCs onto biological sutures, no study has examined the effect of seeding concentration and seeding time on hMSC attachment.

In this study, we demonstrated the ability for cell seeding concentration and seeding times to affect the numbers of hMSCs seeded onto the biological suture. The highest hMSC attachment occurred using higher concentrations ( $5 \times 10^5$ ,  $1 \times 10^6$  hMSC/mL) compared to a concentration of  $2.5 \times 10^5$ . There was only a small

increase in cell attachment between the  $5 \times 10^5$  and  $1 \times 10^6$  hMSC/mL seeded groups, thus we do not believe that increasing the number of cells seeded beyond  $1 \times 10^6$  hMSC/mL would lead to improved cell attachment as the surface area available for cell attachment has been maximized. In regard to seeding time, there was no significant difference in hMSC attachment at 6, 12, or 24 hours. F-actin staining revealed cells beginning to attach a 1 hour, however at 12 and 24 hours cells were more elongated along the suture. As there was no significant difference in cell numbers attached at 6, 12, or 24 hour this suggests that a range of times could be used when delivering hMSCs on biological sutures which may be advantageous in a clinical setting. For consistency and due to time considerations, the 24 hour time point using a  $1 \times 10^6$  hMSC/mL seeding concentration was used in objective 1b.

### 3.5 References

1. Hou D, Youssef EA, Brinton TJ, Zhang P, Rogers P, Price ET, Yeung AC, Johnstone BH, Yock PG and March KL. Radiolabeled cell distribution after intramyocardial, intracoronary, and interstitial retrograde coronary venous delivery: implications for current clinical trials. *Circulation*. 2005;112:1150-6.
2. Yu J, Du KT, Fang Q, Gu Y, Mihardja SS, Sievers RE, Wu JC and Lee RJ. The use of human mesenchymal stem cells encapsulated in RGD modified alginate microspheres in the repair of myocardial infarction in the rat. *Biomaterials*. 2010;31:7012-7020.
3. Lu W-N, Lü S-H, Wang H-B, Li D-X, Duan C-M, Liu Z-Q, Hao T, He W-J, Xu B, Fu Q, Song YC, Xie X-H and Wang C-Y. Functional improvement of infarcted heart by co-injection of embryonic stem cells with temperature-responsive chitosan hydrogel. *Tissue engineering Part A*. 2009;15:1437-47.
4. Dai W, Hale SL, Kay GL, Jyrala AJ and Kloner RA. Delivering stem cells to the heart in a collagen matrix reduces relocation of cells to other organs as assessed by nanoparticle technology. *Regenerative medicine*. 2009;4:387-95.
5. Zhang G, Hu Q, Braunlin EA, Suggs LJ and Zhang J. Enhancing efficacy of stem cell transplantation to the heart with a PEGylated fibrin biomatrix. *Tissue engineering Part A*. 2008;14:1025-36.
6. Christman KL, Vardanian AJ, Fang Q, Sievers RE, Fok HH and Lee RJ. Injectable fibrin scaffold improves cell transplant survival, reduces infarct expansion, and induces neovasculature formation in ischemic myocardium. *Journal of the American College of Cardiology*. 2004;44:654-60.
7. Wang T, Jiang X-J, Tang Q-Z, Li X-Y, Lin T, Wu D-Q, Zhang X-Z and Okello E. Bone marrow stem cells implantation with  $\alpha$ -cyclodextrin/MPEG-PCL-MPEG hydrogel improves cardiac function after myocardial infarction. *Acta biomaterialia*. 2009;5:2939-2944.
8. Sun C-K, Zhen Y-Y, Leu S, Tsai T-H, Chang L-T, Sheu J-J, Chen Y-L, Chua S, Chai H-T, Lu H-I, Chang H-W, Lee F-Y and Yip H-K. Direct implantation versus platelet-rich fibrin-embedded adipose-derived mesenchymal stem cells in treating rat acute myocardial infarction. *International journal of cardiology*. 2014;173:410-423.
9. Ceccaldi C, Bushkalova R, Alfarano C, Lairez O, Calise D, Bourin P, Frugier C, Rouzaud-Laborde C, Cussac D, Parini A, Sallerin B and Fullana SG. Evaluation of polyelectrolyte complex-based scaffolds for mesenchymal stem cell therapy in cardiac ischemia treatment. *Acta biomaterialia*. 2014;10:901-11.
10. Roche ET, Hastings CL, Lewin SA, Shvartsman D, Brudno Y, Vasilyev NV, O'Brien FJ, Walsh CJ, Duffy GP and Mooney DJ. Comparison of biomaterial delivery vehicles for improving acute retention of stem cells in the infarcted heart. *Biomaterials*. 2014;35:6850-6858.
11. Fukuhara S, Tomita S, Nakatani T, Fujisato T, Ohtsu Y, Ishida M, Yutani C and Kitamura S. Bone marrow cell-seeded biodegradable polymeric scaffold enhances angiogenesis and improves function of the infarcted heart. *Circ J*. 2005;69:850-7.
12. Kim B-S, Kim J-S, Yang S-S, Kim H-W, Lim HJ and Lee J. Angiogenin-loaded fibrin/bone powder composite scaffold for vascularized bone regeneration. *Biomaterials Research*. 2015;19:18.
13. Jia L, Peng X, Jie T, Zhaojun J, Hong C and Zhongjun L. Enhanced angiogenesis and osteogenesis in critical bone defects by the controlled release of BMP-2 and VEGF: implantation of electron beam melting-fabricated porous Ti 6 Al 4 V scaffolds incorporating growth factor-doped fibrin glue. *Biomedical Materials*. 2015;10:035013.
14. Han B, Schwab IR, Madsen TK and Isseroff RR. A Fibrin-based Bioengineered Ocular Surface With Human Corneal Epithelial Stem Cells. *Cornea*. 2002;21:505-510.
15. Alaminos M, Sánchez-Quevedo MaDC, Muñoz-Ávila JI, Serrano D, Medialdea S, Carreras I and Campos A. Construction of a Complete Rabbit Cornea Substitute Using a Fibrin-Agarose Scaffold. *Investigative Ophthalmology & Visual Science*. 2006;47:3311-3317.
16. Bruns H, Kneser U, Holzhuter S, Roth B, Kluth J, Kaufman PM, Kluth D and Fiegel H, C. Injectable liver- a novel approach using fibrin as a matrix for culture FIBRIN SCAFFOLDS FOR TISSUE ENGINEERING 209 and intrahepatic transplantation of hepatocytes. *Tissue engineering Part A*. 2005;11.

17. Sun T, Chan MLH, Quek CH and Yu H. Improving mechanical stability and density distribution of hepatocyte microcapsules by fibrin clot and gold nano-particles. *Journal of Biotechnology*. 2004;111:169-177.
18. Beier JP, Stern-Straeter J, Foerster VT, Kneser U, Stark GB and Bach AD. Tissue Engineering of Injectable Muscle: Three-Dimensional Myoblast-Fibrin Injection in the Syngeneic Rat Animal Model. *Plastic and Reconstructive Surgery*. 2006;118:1113-1121.
19. Grasman JM, Do DM, Page RL and Pins GD. Rapid release of growth factors regenerates force output in volumetric muscle loss injuries. *Biomaterials*. 2015;72:49-60.
20. Snyder TN, Madhavan K, Intrator M, Dregalla RC and Park D. A fibrin/hyaluronic acid hydrogel for the delivery of mesenchymal stem cells and potential for articular cartilage repair. *Journal of Biological Engineering*. 2014;8:10-10.
21. Cakmak O, Babakurban ST, Akkuzu HG, Bilgi S, Ovalı E, Kongur M, Altintas H, Yilmaz B, Bilezikçi B, Y. Celik Z, Yakicier MC and Sahin FI. Injectable tissue-engineered cartilage using commercially available fibrin glue. *The Laryngoscope*. 2013;123:2986-2992.
22. Hojo M, Inokuchi S, Kidokoro M, Fukuyama N, Tanaka E, Tsuji C, Miyasaka M, Tanino R and Nakazawa H. Induction of Vascular Endothelial Growth Factor by Fibrin as a Dermal Substrate for Cultured Skin Substitute. *Plastic and Reconstructive Surgery*. 2003;111:1638-1646.
23. Idrus RH, Rameli MAbP, Low KC, Law JX, Chua KH, Latiff MBA and Saim AB. Full-Thickness Skin Wound Healing Using Autologous Keratinocytes and Dermal Fibroblasts with Fibrin: Bilayered Versus Single-Layered Substitute. *Advances in Skin & Wound Care*. 2014;27:171-180.
24. Bacakova M, Musilkova J, Riedel T, Stranska D, Brynda E, Zaloudkova M and Bacakova L. The potential applications of fibrin-coated electrospun polylactide nanofibers in skin tissue engineering. *International Journal of Nanomedicine*. 2016;11:771-789.
25. Wendel JS, Ye L, Tao R, Zhang J, Zhang J, Kamp TJ and Tranquillo RT. Functional Effects of a Tissue-Engineered Cardiac Patch From Human Induced Pluripotent Stem Cell-Derived Cardiomyocytes in a Rat Infarct Model. *Stem cells translational medicine*. 2015;4:1324-32.
26. Mol A, van Lieshout MI, Dam-de Veen CG, Neuenschwander S, Hoerstrup SP, Baaijens FPT and Bouten CVC. Fibrin as a cell carrier in cardiovascular tissue engineering applications. *Biomaterials*. 2005;26:3113-3121.
27. Proulx MK, Carey SP, Ditroia LM, Jones CM, Fakharzadeh M, Guyette JP, Clement AL, Orr RG, Rolle MW, Pins GD and Gaudette GR. Fibrin microthreads support mesenchymal stem cell growth while maintaining differentiation potential. *Journal of biomedical materials research Part A*. 2011;96:301-12.
28. Guyette JP, Fakharzadeh M, Burford EJ, Tao ZW, Pins GD, Rolle MW and Gaudette GR. A novel suture-based method for efficient transplantation of stem cells. *Journal of biomedical materials research Part A*. 2013;101:809-18.

#### 4 Objective 1b: Evaluate changes in mechanical function when hMSC seeded fibrin sutures are implanted in the infarct zone.

The introduction (starting with section 4.1), methods, results, and discussion presented in this objective are published in BioResearch Open Access. These sections are published under the liberal CC-BY license and can be freely reused with the proper citation: Hansen et al. "Functional Effects of Delivering Human Mesenchymal Stem Cell-Seeded Biological Sutures to an Infarcted Heart." *BioResearch Open Access*. 2016; 5(1):249-260 (see Chapter 9: Appendix).

##### 4.1 Introduction

Cell based therapies have been proposed as a treatment for MI. Multiple cell types have shown promising pre-clinical and clinical results<sup>1-4</sup>. Human mesenchymal stem cells (hMSCs) were initially shown to improve ejection fraction and regional function in pre-clinical animal models<sup>5, 6</sup>. Importantly for the clinical use of these cells, Hare and colleagues demonstrated no deleterious effects of hMSCs when delivered intravenously to patients<sup>7</sup>. While several clinical trials have demonstrated promising initial results with short term improvements in ejection fraction, longer term studies have shown that functional benefits dissipate within one year<sup>8</sup>. A limiting factor to the success of all studies was the method in which cells were delivered such that all studies fail to deliver cells in an efficient manner (<19% retention). Fibrin microthreads have previously demonstrated the ability to deliver hMSCs to cardiac tissue with a 64% delivery efficiency<sup>9</sup>. This objective seeks to build upon that work by using the fibrin suture to deliver hMSCs to an acute rat infarct model to examine changes in regional function.

##### 4.2 Materials and methods

hMSCs were cultured and seeded as done in objective 1a. All implanted sutures were seeded with 100uL of a  $1 \times 10^6$  hMSC/mL solution for 24 hours.

###### 4.2.1 Infarct model

Male nude rats (NIH nude, Taconic) were used for all procedures. Animals were anesthetized using 5% inhaled isoflurane in oxygen, intubated, and mechanically ventilated with anesthesia maintained with 3% isoflurane. A 2cm incision along the fourth intercostal space and subsequent blunt dissection of the

muscle was used to expose the heart. To induce an infarct, the left anterior descending (LAD) artery was ligated for 1 hour using 5-0 Prolene (Ethicon) suture. After 1 hour, the ligature was cut to restore blood flow and the chest was either closed or the suture was implanted and the chest was closed. The suture was implanted from the base of the heart towards the apex of the heart and excess suture was cut and removed from the entry and exit points (Figure 4-1). Sham operations underwent the same procedure described above without the ligation of the LAD and suture implantation. Animals were allowed to recover for 1 week.

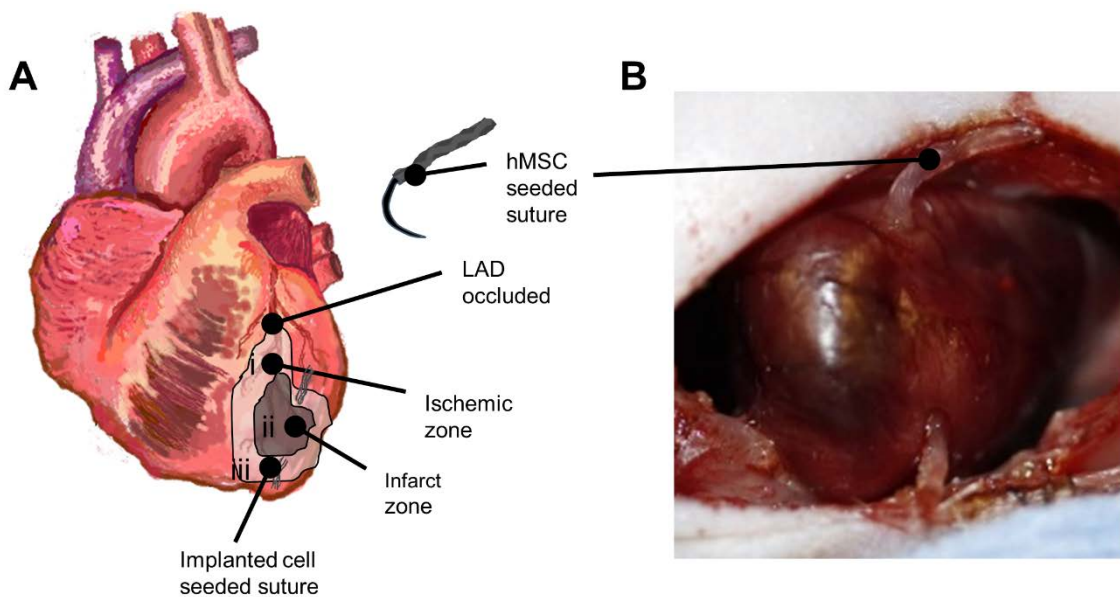


**Figure 4-1. Implanted hMSC seeded suture.** Male athymic rat heart was exposed and the LAD was ligated to induce infarct. 1 hour post ligation, ligature was cut and blood flow was resumed. The hMSC seeded fibrin suture was implanted from the base to the apex such that suture entered in the ischemic zone (i), passed through the infarcted myocardium (ii), and exited through the ischemic zone at the apex (iii) (A). Implantation of fibrin suture in rat heart (B). Excess suture was removed.

#### 4.2.2 Terminal surgery

One week post operation, animals were once again anesthetized, intubated and placed on a respirator as described above. The heart was exposed through the original suture lines and retractors were placed into the intercostal space to expose the left ventricle of the heart. The infarcted muscle tissue was identified based on the darkened color of infarcted heart tissue compared to bright red healthy heart tissue, as well as lack of contractility. A 3.5 French size micro tip catheter (Millar) was inserted into the left ventricle of the heart through the apex and sutured in place. A high speed video camera (Fastec

HiSpec4, Fastec Inc.) was used to record high speed videos (250 frames/second, 8 bit depth, 1696x1710 pixels) of the contracting ventricular muscle. Pressure data was synchronized to video frame acquisition via a DAQ board (National Instruments) and a LabVIEW-based controller. Videos were acquired from multiple different angles and video and pressure data were saved for offline data analysis. After video acquisition, a 0.3mg/kg dose of Beuthanasia-D (VetOne) was injected into the left atrium to arrest the heart. The heart tissue was then carefully removed for histological processing and analysis.

#### 4.2.3 Assessment of global and regional mechanical function

Global mechanical function was assessed using the collected pressure waveforms as described previously<sup>10</sup>. Maximum developed pressure was determined by averaging the difference between the maximum and minimum pressure for each beat. Minimum rate of pressure decline and maximum rate of pressure development were determined by applying a 5 point linear averaging filter to the pressure waveform and finding the maximum and minimum of the discrete derivative of the signal for each beat. Finally, the diastolic relaxation time constant was determined by applying a 3 parameter least squared fitting method to pressure data from its negative inflection point to its minimum for each beat<sup>11</sup>. All global function data are averaged over at least 5 beats per animal and reported as mean±SEM.

High density mapping (HDM) was used to assess regional mechanical function as previously described<sup>9, 10, 12</sup>. HDM is an image tracking algorithm based on Fourier domain phase correlation with the subpixel registration algorithm described by Foroosh *et al.*<sup>13</sup>. Using this method, a region of interest was defined on the rat heart over the thread and/or infarct region. The region was subsequently divided into small (32x32 pixel) windows. Individual windows were tracked from frame to frame across several cardiac cycles to yield a displacement field. Displacement fields were used to quantify systolic area of contraction (SAC) and regional stroke work (RSW), as described previously<sup>12</sup>.

#### 4.2.4 Histological data

After terminal surgery, hearts were removed and cut in half to produce cross-sections, bisecting the infarct and biological suture, and fixed in 4% paraformaldehyde overnight. After fixation, heart sections



were moved to a 30% sucrose solution for 24 hours. Each half was embedded in a Peel-a-Way disposable embedding mold (Polysciences, Inc.) with OCT and placed in a -20°C freezer. Once the OCT has solidified the heart block was removed from the block and placed in a Leica CM 3050 cryostat (Leica Microsystems) and cut into 10 µm thick sections and placed on charged glass microscope slides (Globe Scientific, Inc.) Sections were stained with Masson's Trichrome reagents according to manufacturer's instruction. Adjacent sections were used for immunofluorescence staining. Briefly, sections were fixed in acetone at -20°C for 10 minutes, and blocked with 5% goat serum for 45 minutes. The sections were incubated in mouse anti- $\alpha$ -actinin monoclonal antibody (1:100; Abcam) overnight at 4°C. Subsequently, sections were treated in goat anti-mouse secondary antibody (1:400; Alexa Fluor 488, Thermo Fisher Scientific) for 1 hour at room temperature. Sections were then counterstained with Hoechst 33342 (0.5 µg/mL) for 5 minutes at room temperature. Fluorescence images were obtained using a Leica Upright DMLB2 or Leica TCP SP5 confocal laser scanning microscope.

#### 4.2.5 Infarct region and suture area quantification

Images (taken at 50x magnification) from sections stained with Masson's Trichrome were stitched together using Microsoft Image Composite Editor to generate composite images of the full cross-sections. Images were uploaded into a custom MATLAB image analysis program (Mathworks) that evaluates color of individual pixels in the image, and from this information extrapolates the location of the lumen and outer boundary of the section. Image regions outside the boundary of the heart and within the lumen (white space) are removed, leaving the image region corresponding to heart tissue intact. As Masson's Trichrome stains viable cardiac muscle tissue red and fibrosis blue, blue regions of the image were programmatically identified and used to determine infarct size. The program approximates and outputs total section area and total area of the infarct. Sectional area was calculated by the sum of squared pixel lengths, and converted to microns. Total area of the infarct was calculated with the same method, and used to determine the percentage of the section that is infarcted.

For suture area measurement, images with Masson's Trichrome staining were uploaded to ImageJ (NIH). Manual tracings around the remaining suture in each cross-section were obtained to give the area of the suture. Every section containing a suture was used for the measurements to give an average area.

#### 4.2.6 Statistical analysis

Statistical analyses were performed using GraphPad Prism 6 (GraphPad Software, Inc., La Jolla, CA). Results are represented as mean±SEM. Comparisons between *in vivo* treatments were analyzed using a Kruskal-Wallis test with a Dunn's test for multiple comparisons. An unpaired t-test was used to determine significance between suture areas. All conditions were considered significant at a value of  $P < 0.05$ .

### 4.3 Results

#### 4.3.1 hMSC seeded biological sutures do not improve global function after infarction

After the model was successfully developed, five sham, two infarct, one unseeded, and three animals from the hMSC-seeded group died prior to successful completion of all data acquisition. These animals were not included in this study.

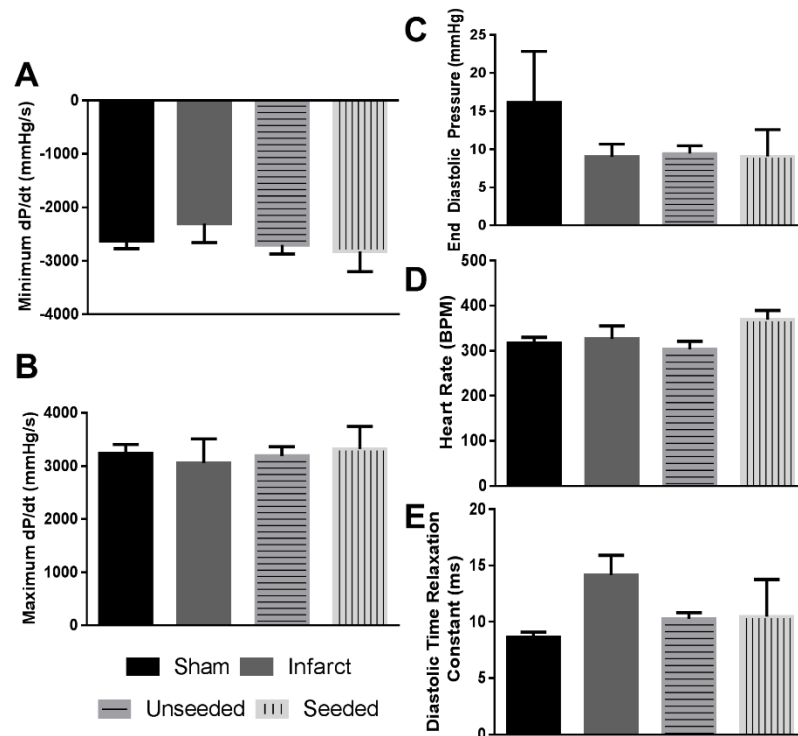


**Figure 4-2. Global function is not impacted by hMSC seeded biological suture treatment after infarct.** No significant changes were noted for any of the following measurements: minimum dP/dt (A), maximum dP/dt (B), end diastolic pressure (C), heart rate (D), or diastolic time relaxation constant (E). Mean±SEM. n=6 per group.

No differences were noted in the maximum or minimum rate of pressure development or end diastolic pressures between groups (sham, MI, MI with unseeded sutures, and MI with hMSC-seeded sutures, n=6 per group; Figure 4-2A-C). There were no significant differences in the heart rates in all groups at the time of terminal surgery (Figure 4-2D). Similarly, no significant differences were seen in diastolic relaxation time constant, although sham operated hearts had the shortest relaxation time ( $8.6 \pm 1.1$  ms) and infarcted hearts had the longest time ( $14.1 \pm 4.3$  ms) (Figure 4-2E).

#### 4.3.2 hMSC seeded biological sutures improve regional mechanical function after infarction

In order to assess regional mechanical function, a particle tracking algorithm, HDM, was used to determine epicardial displacement of multiple regions within the infarcted tissue. From the two-dimensional displacement, changes in regional area were determined, which when combined with left ventricular pressure, allowed for determination of regional stroke work (Figure 4-3A). The average region in which function was determined was similar in all groups. Creation of an MI resulted in significant decrease in RSW ( $0.026 \pm 0.011$ ) and SAC ( $0.022 \pm 0.015$ ) compared to sham operated animals (RSW 0.141

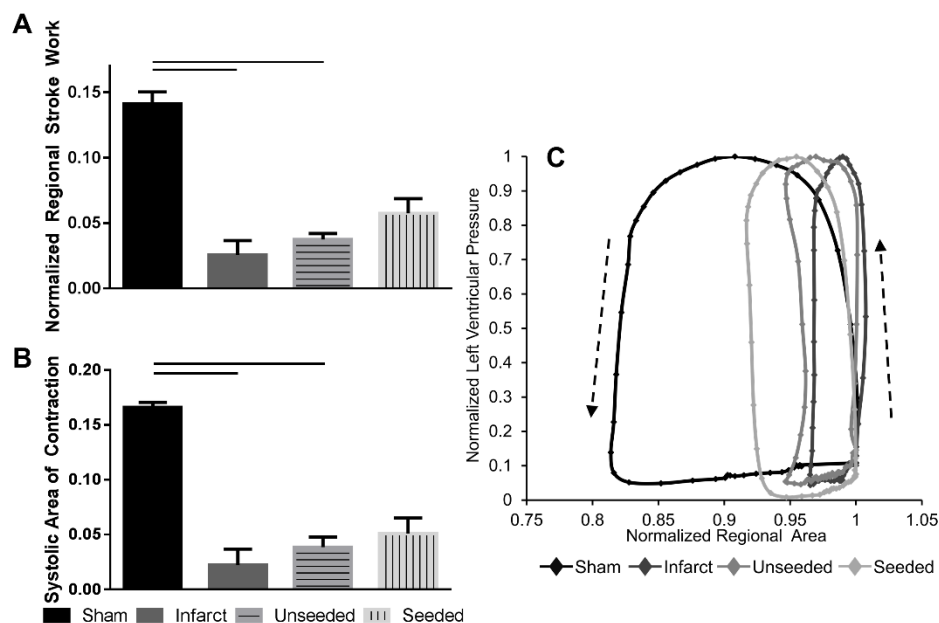


**Figure 4-3. hMSC seeded biological sutures improve regional mechanical function after infarct.** RSW and SAC were significantly decreased for infarct and unseeded suture groups compared to the sham group (A, B). Representative pressure area work loop (C) shows improved function for seeded group compared to infarct and unseeded groups. Arrows indicate direction of all work loops over time. Mean±SEM, - p<-0.05, n=6 per group.

$\pm 0.009$ ; SAC:  $0.166 \pm 0.005$ ) ( $n=6$ ,  $p=0.0027$  RSW and SAC) (Figure 4-3A and B). Delivery of unseeded sutures to the infarcted regions also resulted in statistically reduced RSW ( $0.037 \pm 0.005$ ) and SAC ( $0.039 \pm 0.009$ ) compared to sham operated animals ( $n=6$ ,  $p=0.012$  RSW;  $p=0.026$  SAC). hMSC-seeded sutures had a lower RSW ( $0.057 \pm 0.011$ ) and SAC ( $0.051 \pm 0.014$ ) than sham operated hearts, although statistical significance was not achieved ( $n=6$ ,  $p=0.165$  RSW;  $p=0.086$  SAC). There were no significant differences in regional mechanical function between infarct, unseeded and seeded groups, however infarcted hearts treated with cell-seeded sutures showed a trend toward increase of RSW when compared to infarcted hearts ( $p=0.07$ ). Pressure area work loops (Figure 4-3C) indicate improved function in hMSC seeded group over unseeded and infarcted groups.

#### 4.3.3 Cells delivered via the suture remain in the heart at least one week after delivery

Numerous Qdot-loaded cells were detected in the seeded group. Cells were found in regions close to the biological sutures (Figure 4-4), but not on the suture suggesting migration into surrounding tissue.

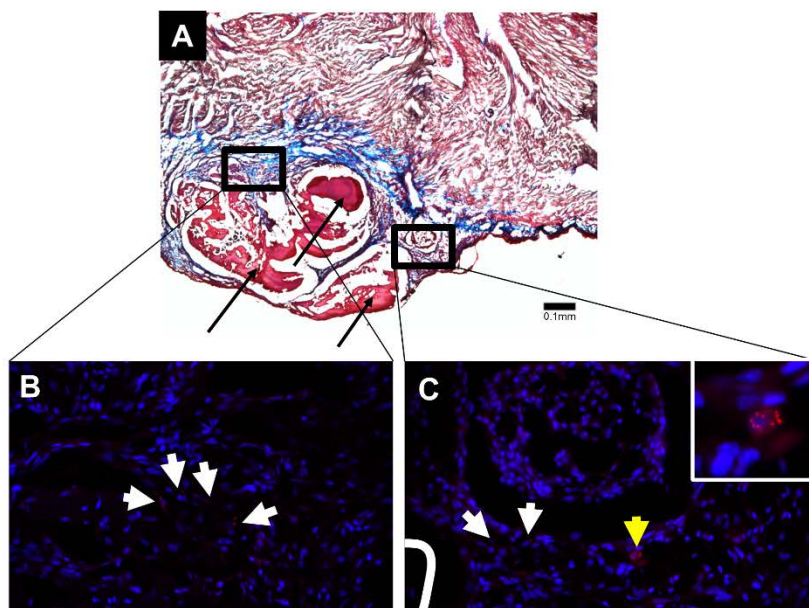


**Figure 4-4. hMSCs persist in myocardium 1 week after delivery.** Masson's Trichrome stained cross-sections show successful delivery of biological suture (pink; black arrows in A, white lines in B and C) to myocardium. The black boxes (B, C) show the location of serial sections stained for alpha-actinin and Hoechst relative to (A). The arrows in B and C indicate quantum dot positive hMSCs that have migrated off the suture into fibrotic tissue. The cell identified by the yellow arrow in C is shown in the insert.

When stained to visualize  $\alpha$ -actinin, no quantum dot loaded cells visualized exhibited positive  $\alpha$ -actinin expression.

#### 4.3.4 Infarct size is reduced using unseeded and hMSC seeded sutures

Serial sections of Masson's Trichrome stained sections were analyzed to determine infarct size, denoted as a percentage of the cross section. No infarcted tissue was detected by Masson's Trichrome staining in sham operated hearts, whereas the MI, unseeded suture, and seeded suture groups all appeared to have similarly sized infarct regions (Figure 4-5A). Infarcted hearts without suture delivery had the greatest infarct size of  $7.0 \pm 2.2\%$ . Unseeded and hMSC-seeded groups had comparable infarct sizes of  $3.8 \pm 0.6$  and  $3.7 \pm 0.8\%$ , respectively, but were not significantly different from MI alone ( $p > 0.05$ , Figure 4-5 B). Due to the automated method used to calculate infarct size, the sham group had a small infarct size of  $1.6 \pm 0.1\%$  (likely due to inherent collagen structure in the healthy heart).

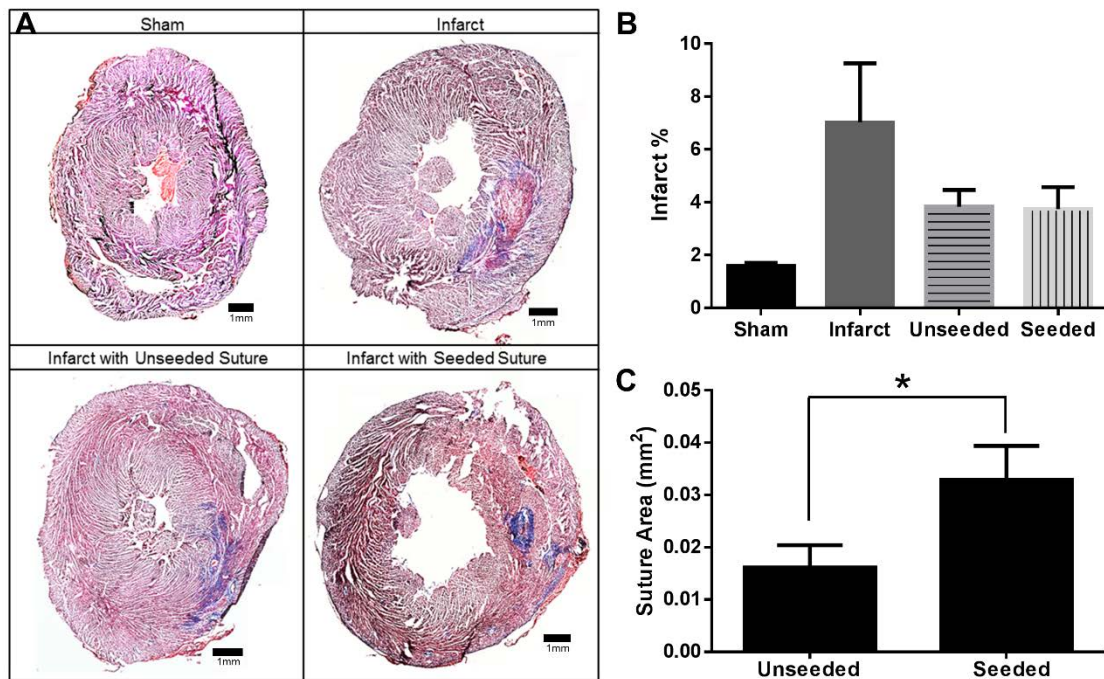


**Figure 4-5. Infarct size and suture area.** Masson's Trichrome staining shows infarcted area in blue and healthy muscle in red (A). Quantification of infarct size from serial trichrome stained sections indicates an increase in infarct size for infarct only group with a similar reduction in infarct size shown for seeded and unseeded groups ( $n=6$ ) (B). Quantification of persisting suture area after 1 week shows significantly smaller suture area for unseeded sutures ( $n=6$ ) (C). Mean $\pm$ SEM, \* $P < 0.05$ .

#### 4.3.5 hMSCs preserve suture area in infarct

Serial sections of Masson's trichrome stained sections were analyzed for suture area. An average suture area of  $0.027 \pm 0.01 \text{mm}^2$  and  $0.041 \pm 0.01 \text{mm}^2$  was found for unseeded and seeded groups, respectively (Figure 4-5C). The group with hMSCs had a significantly greater suture area ( $p < 0.05$ ) indicating that the hMSCs preserved suture area at 1 week after delivery in the infarcted heart.

#### 4.4 Discussion

Cell therapy continues to hold tremendous potential to treat millions of patients living with MIs and heart failure. However, the full benefits of cell therapy have yet to be realized. The past decade has seen the emergence of dozens of clinical trials aimed at improving cardiac output. These studies have examined different cell types including bone marrow mononuclear cells<sup>2</sup>, MSCs<sup>7,14</sup>, and cardiosphere derived cells<sup>4</sup>, effect of timing on cell delivery<sup>15-17</sup>, chronic<sup>18, 19</sup> and acute<sup>20</sup> MI, and cell delivery methods: intracoronary<sup>4,20</sup>, intravenous<sup>7</sup>, intramyocardial<sup>21</sup>, and transendocardial<sup>22, 23</sup>. Despite numerous trials investigating extensive variables, these clinical trials demonstrated only limited improvements in ejection fraction without restoring cardiovascular function to baseline values. All studies failed to efficiently deliver the chosen cell type to infarcted tissue, further underscoring the value of investigating new delivery methods that improve cell retention.

Current cell delivery methods to the heart exhibit retention rates of only 10-20%, which are inefficient for delivering clinically relevant numbers of cells<sup>23-25</sup>. Previously, we demonstrated cell-seeded biological sutures capable of efficiently delivering cells to a targeted area (64% retention)<sup>9</sup> Additionally, we reported that delivering unseeded sutures to a healthy heart demonstrated a small fibrotic reaction that was significantly reduced with hMSC-seeded sutures<sup>10</sup>. In terms of regional function, unseeded sutures decreased SAC, where hMSC-seeded sutures dampened the decrease in SAC<sup>10</sup>. Similar values for RSW and SAC were reported for sham animals in the previous study and our current study. In this study, we investigated the functional effects of delivering hMSCs via a biological suture to an infarcted heart. When combined with our method for evaluating regional mechanical function with high spatial resolution, we

are uniquely able to determine changes in regional mechanical function that occur directly in the region of cell delivery. This combination allows for targeted cell delivery followed by targeted evaluation of regional mechanical function.

No changes between conditions were found for global parameters including pressure changes, diastolic relaxation constant, or heart rate. The MI created in the rat may not have been large enough to result in a detectable change in global function. In addition, rat ventricular remodeling after an MI can take 4-8 weeks to manifest such that changes on a global level may not be seen at 1 week<sup>26</sup>. This finding further necessitates the use of HDM, which images the region of damage and cell delivery to determine on a regional level if improvements in mechanical function were found that may have been negated at a global level.

Using HDM to analyze myocardial function in infarcted rat hearts we demonstrated decreased regional mechanical function in animals with an induced MI, using metrics of RSW and SAC. Delivering unseeded-sutures demonstrated improvements in regional mechanical function over the MI group, the hMSC-seeded sutures demonstrated slightly higher function, however not statistically significant. This suggests that the biological suture alone has the ability to improve regional mechanical function in the infarct zone. Studies have demonstrated that acellular biomaterial delivery to an infarct can improve mechanical function by stabilizing the infarct, thickening the left ventricle, and decreasing infarct expansion<sup>27-29</sup>. As both the unseeded and hMSC-seeded suture groups had similar infarct sizes, the significantly increased suture area for the hMSC-seeded group may explain the improvement in regional mechanical function for the hMSC-seeded group, compared to the unseeded group. A similar trend of increased suture area for hMSC-seeded sutures was also found in studies in a healthy heart, suggesting the ability for the hMSCs to decrease the *in vivo* degradation time, by modulating the inflammatory response and decreasing the number of cells present that may contribute to fibrin degradation, of biological sutures compared to unseeded sutures<sup>10</sup>.

It has been established that MSCs act transiently and die off within days to weeks of being delivered to the infarct<sup>30</sup>. As such, we chose not to examine cell retention as hMSC retention may be altered by the infarct environment at 1 week independent of the method used for delivery. However, hMSCs were found to persist in the myocardium for 1 week and were found in regions away from the suture, suggesting their propensity to migrate from the suture into the damaged tissue. Delivered cells were tracked using Qdots, which have previously been shown to be taken up by hMSCs and remain in the cells for several passages *in vitro*<sup>31</sup>.

Despite the emergence of many clinical trials focused on the delivery of MSCs to injured cardiac tissue, none of these trials have found significant findings to suggest the robust ability for MSCs to improve contractile cardiac function. Many of these studies used delivery methods with low delivery efficiencies. In this study, we describe findings using a biological suture based method to efficiently deliver cells to infarcted tissue. While we did not see statistically improved function when seeded sutures were delivered over infarct alone, we do remain optimistic about the use of the biological suture for cell delivery. Many studies have demonstrated the immunomodulatory effects of delivered MSCs. While this cell type may not be the most appropriate cell to use in regeneration of contractile cardiomyocytes, they may still have beneficial effects in the infarcted heart<sup>32,33</sup>. Recent advances in induced pluripotent and embryonic stem cell technology have enabled the development of a cardiomyocyte that has demonstrated the *in vitro* contractile properties that may be ideal for cell replacement strategies<sup>34,35</sup>. Objectives 2 and 3 will focus on delivering cardiomyocytes differentiated from pluripotent stem cells using our fibrin based suture technology.



#### 4.5 References

1. Jakob P and Landmesser U. Current status of cell-based therapy for heart failure. *Current heart failure reports*. 2013;10:165-76.
2. Schächinger V, Erbs S, Elsässer A, Haberbosch W, Hambrecht R, Hölschermann H, Yu J, Cort R, Mathey DG, Hamm CW, Süselbeck T, Assmus B, Tonn T, Dimmeler S and Zeiher AM. Intracoronary Bone Marrow-Derived Progenitor Cells in Acute Myocardial Infarction. *The New England journal of medicine*. 2006;355:1210-21.
3. Hare JM, Fishman JE, Gerstenblith G and et al. Comparison of allogeneic vs autologous bone marrow-derived mesenchymal stem cells delivered by transendocardial injection in patients with ischemic cardiomyopathy: The poseidon randomized trial. *JAMA : the journal of the American Medical Association*. 2012;308:2369-2379.
4. Malliaras K, Makkar RR, Smith RR, Cheng K, Wu E, Bonow RO, Marban L, Mendizabal A, Cingolani E, Johnston PV, Gerstenblith G, Schuleri KH, Lardo AC and Marban E. Intracoronary cardiosphere-derived cells after myocardial infarction: evidence of therapeutic regeneration in the final 1-year results of the CADUCEUS trial (Cardiosphere-Derived autologous stem Cells to reverse ventricular dysfunction). *Journal of the American College of Cardiology*. 2014;63:110-22.
5. Tang J, Xie Q, Pan G, Wang J and Wang M. Mesenchymal stem cells participate in angiogenesis and improve heart function in rat model of myocardial ischemia with reperfusion. *European journal of cardio-thoracic surgery : official journal of the European Association for Cardio-thoracic Surgery*. 2006;30:353-61.
6. Shake JG, Gruber PJ, Baumgartner WA, Senechal G, Meyers J, Redmond JM, Pittenger MF and Martin BJ. Mesenchymal stem cell implantation in a swine myocardial infarct model engraftment and functional effects. *The Society of Thoracic Surgeons*. 2002;73:1919-26.
7. Hare JM, Traverse JH, Henry TD, Dib N, Strumpf RK, Schulman SP, Gerstenblith G, DeMaria AN, Denktas AE, Gammon RS, Hermiller JB, Jr., Reisman MA, Schaer GL and Sherman W. A randomized, double-blind, placebo-controlled, dose-escalation study of intravenous adult human mesenchymal stem cells (prochymal) after acute myocardial infarction. *Journal of the American College of Cardiology*. 2009;54:2277-86.
8. Meyer GP, Wollert KC, Lotz J, Steffens J, Lippolt P, Fichtner S, Hecker H, Schaefer A, Arseniev L, Hertenstein B, Ganser A and Drexler H. Intracoronary bone marrow cell transfer after myocardial infarction: eighteen months' follow-up data from the randomized, controlled BOOST (BOne marrOw transfer to enhance ST-elevation infarct regeneration) trial. *Circulation*. 2006;113:1287-94.
9. Guyette JP, Fakharzadeh M, Burford EJ, Tao ZW, Pins GD, Rolle MW and Gaudette GR. A novel suture-based method for efficient transplantation of stem cells. *Journal of biomedical materials research Part A*. 2013;101:809-18.
10. Tao ZW, Favreau JT, Guyette JP, Hansen KJ, Lessard J, Burford E, Pins GD and Gaudette GR. Delivering stem cells to the healthy heart on biological sutures: effects on regional mechanical function. *Journal of tissue engineering and regenerative medicine*. 2014.
11. De Mey S, De Sutter J, Vierendeels J and Verdonck P. Diastolic filling and pressure imaging: taking advantage of the information in a colour M-mode Doppler image. *Eur J Echocardiogr*. 2001;2:219-33.
12. Kelly DJ, Azeloglu EU, Kochupura PV, Sharma GS and Gaudette GR. Accuracy and reproducibility of a subpixel extended phase correlation method to determine micron level displacements in the heart. *Medical engineering & physics*. 2007;29:154-62.
13. Foroosh H, Zerubia JB and Berthod M. Extension of phase correlation to subpixel registration. *IEEE transactions on image processing : a publication of the IEEE Signal Processing Society*. 2002;11:188-200.
14. Chen SL, Fang WW, Ye F, Liu YH, Qian J, Shan SJ, Zhang JJ, Chunhua RZ, Liao LM, Lin S and Sun JP. Effect on left ventricular function of intracoronary transplantation of autologous bone marrow mesenchymal stem cell in patients with acute myocardial infarction. *Am J Cardiol*. 2004;94:92-5.

15. Traverse JH, Henry TD, Ellis SG and et al. Effect of intracoronary delivery of autologous bone marrow mononuclear cells 2 to 3 weeks following acute myocardial infarction on left ventricular function: The latetime randomized trial. *JAMA : the journal of the American Medical Association*. 2011;306:2110-2119.
16. Traverse JH, Henry TD, Pepine CJ and et al. Effect of the use and timing of bone marrow mononuclear cell delivery on left ventricular function after acute myocardial infarction: The time randomized trial. *JAMA : the journal of the American Medical Association*. 2012;308:2380-2389.
17. Surder D, Manka R, Lo Cicero V, Moccetti T, Rufibach K, Soncin S, Turchetto L, Radrizzani M, Astori G, Schwitter J, Erne P, Zuber M, Auf der Maur C, Jamshidi P, Gaemperli O, Windecker S, Moschovitis A, Wahl A, Buhler I, Wyss C, Kozerke S, Landmesser U, Luscher TF and Corti R. Intracoronary injection of bone marrow-derived mononuclear cells early or late after acute myocardial infarction: effects on global left ventricular function. *Circulation*. 2013;127:1968-79.
18. Mathiasen AB, Qayyum AA, Jørgensen E, Helqvist S, Fischer-Nielsen A, Kofoed KF, Haack-Sørensen M, Ekblond A and Kastrup J. Bone marrow-derived mesenchymal stromal cell treatment in patients with severe ischaemic heart failure: a randomized placebo-controlled trial (MSC-HF trial). *European heart journal*. 2015;36:1744-1753.
19. Bartunek J, Behfar A, Dolatabadi D, Vanderheyden M, Ostojic M, Dens J, El Nakadi B, Banovic M, Beleslin B, Vrolix M, Legrand V, Vrints C, Vanoverschelde JL, Crespo-Diaz R, Homsy C, Tendera M, Waldman S, Wijns W and Terzic A. Cardiopoietic Stem Cell Therapy in Heart Failure: The C-CURE (Cardiopoietic stem Cell therapy in heart failURE) Multicenter Randomized Trial With Lineage-Specified Biologics. *Journal of the American College of Cardiology*. 2013;61:2329-2338.
20. Wollert KC, Meyer GP, Lotz J, Ringes Lichtenberg S, Lippolt P, Breidenbach C, Fichtner S, Korte T, Hornig B, Messinger D, Arseniev L, Hertenstein B, Ganser A and Drexler H. Intracoronary autologous bone-marrow cell transfer after myocardial infarction: the BOOST randomised controlled clinical trial. *The Lancet*. 2004;364:141-148.
21. Hamano K, Nishida M, Hirata K, Mikamo A, Li T-S, Masahiko Harada M, Miura T, Matsuzaki M and Esato K. Local Implantation of Autologous Bone Marrow Cells for Therapeutic Angiogenesis in Patients with Ischemic Heart Disease. *Japanese Circulation Journal*. 2001;65:845-47.
22. Perin EC, Willerson JT, Pepine CJ and et al. Effect of transendocardial delivery of autologous bone marrow mononuclear cells on functional capacity, left ventricular function, and perfusion in chronic heart failure: The focus-cctrn trial. *JAMA : the journal of the American Medical Association*. 2012;307:1717-1726.
23. Vrtovec B, Poglajen G, Lezaic L, Sever M, Socan A, Domanovic D, Cernelc P, Torre-Amione G, Haddad F and Wu JC. Comparison of transendocardial and intracoronary CD34+ cell transplantation in patients with nonischemic dilated cardiomyopathy. *Circulation*. 2013;128:S42-9.
24. Laflamme MA and Murry CE. Regenerating the heart. *Nat Biotech*. 2005;23:845-856.
25. Hou D, Youssef EA, Brinton TJ, Zhang P, Rogers P, Price ET, Yeung AC, Johnstone BH, Yock PG and March KL. Radiolabeled cell distribution after intramyocardial, intracoronary, and interstitial retrograde coronary venous delivery: implications for current clinical trials. *Circulation*. 2005;112:I150-6.
26. Krzeminski TF, Nozynski JK, Grzyb J and Porc M. Wide-spread myocardial remodeling after acute myocardial infarction in rat. Features for heart failure progression. *Vascular pharmacology*. 2008;48:100-8.
27. Christman KL, Vardanian AJ, Fang Q, Sievers RE, Fok HH and Lee RJ. Injectable fibrin scaffold improves cell transplant survival, reduces infarct expansion, and induces neovasculature formation in ischemic myocardium. *Journal of the American College of Cardiology*. 2004;44:654-60.
28. Dai W, Wold LE, Dow JS and Kloner RA. Thickening of the Infarcted Wall by Collagen Injection Improves Left Ventricular Function in Rats: A Novel Approach to Preserve Cardiac Function After Myocardial Infarction. *Journal of the American College of Cardiology*. 2005;46:714-719.

29. Rane AA and Christman KL. Biomaterials for the Treatment of Myocardial Infarction A 5-Year Update. *Journal of the American College of Cardiology*. 2011;58:2615-2629.
30. Laflamme MA and Murry CE. Heart regeneration. *Nature*. 2011;473:326-35.
31. Rosen AB, Kelly DJ, Schuldt AJ, Lu J, Potapova IA, Doronin SV, Robichaud KJ, Robinson RB, Rosen MR, Brink PR, Gaudette GR and Cohen IS. Finding fluorescent needles in the cardiac haystack: tracking human mesenchymal stem cells labeled with quantum dots for quantitative in vivo three-dimensional fluorescence analysis. *Stem cells*. 2007;25:2128-38.
32. Behfar A, Yamada S, Crespo-Diaz R, Nesbitt JJ, Rowe LA, Perez-Terzic C, Gaussin V, Homsy C, Bartunek J and Terzic A. Guided Cardiopoiesis Enhances Therapeutic Benefit of Bone Marrow Human Mesenchymal Stem Cells in Chronic Myocardial Infarction. *Journal of the American College of Cardiology*. 2010;56:721-734.
33. Zhang M, Mal N, Kiedrowski M, Chacko M, Askari AT, Popovic ZB, Koc ON and Penn MS. SDF-1 expression by mesenchymal stem cells results in trophic support of cardiac myocytes after myocardial infarction. *FASEB journal : official publication of the Federation of American Societies for Experimental Biology*. 2007;21:3197-207.
34. Takahashi K and Yamanaka S. Induction of pluripotent stem cells from mouse embryonic and adult fibroblast cultures by defined factors. *Cell*. 2006;126:663-76.
35. Laflamme MA, Chen KY, Naumova AV, Muskheli V, Fugate JA, Dupras SK, Reinecke H, Xu C, Hassanipour M, Police S, O'Sullivan C, Collins L, Chen Y, Minami E, Gill EA, Ueno S, Yuan C, Gold J and Murry CE. Cardiomyocytes derived from human embryonic stem cells in pro-survival factors enhance function of infarcted rat hearts. *Nature biotechnology*. 2007;25:1015-24.

## 5 Objective 2a: Develop a method to characterize the contractile behavior of hPS-CM

The introduction (starting with section 5.1), methods, results, and discussion presented in this objective are reprinted with permission from *TISSUE ENGINEERING: Part C, Volume 23*[8], pp. 445-454, published by Mary Ann Liebert, Inc., New Rochelle, NY (see Chapter 9: Appendix).

### 5.1 Introduction

Investigation within the past decade has yielded the ability to reprogram somatic cells into induced pluripotent stem cells (iPS)<sup>1,2</sup>. iPS cells can be differentiated into a multitude of cellular phenotypes while maintaining the original genetic blueprint from the donor<sup>3</sup>. Maintaining the donor's genetic information within these reprogrammable cells allows investigators to model disease states<sup>4</sup>, many of which focus on cardiac specific pathologies<sup>5</sup>. Generation of cardiomyocytes from iPS and embryonic stem cells (ESC)<sup>1,6-8</sup> presents great promise for the generation of patient-specific cardiac disease models, myocardial regeneration therapies, and drug discovery<sup>9-11</sup>. However, human pluripotent stem cell-derived cardiomyocytes (hPS-CMs) are most phenotypically similar to fetal cardiomyocytes in terms of force production, adrenergic response, and sarcomere organization<sup>12</sup>, which may not be ideal for drug development or regenerative therapies. Therefore, recent research has focused on improving the maturation of hPS-CM to yield a more adult-like phenotype<sup>13-15</sup>. However, there are limited tools available to effectively measure the cellular physiological response to different stimuli over time, which would significantly aid investigations seeking to mature hPS-CM and utilize them in disease modeling and regenerative therapies.

Many cardiac diseases manifest themselves as changes in cardiac tissue which directly affect mechanical strain, electrical propagation, beat frequency, beat consistency (arrhythmia), and delays between calcium flux and initiation of mechanical contraction<sup>16</sup>. Current techniques to monitor these changes in single cells or clusters of hPS-CM include integrating microelectrode arrays (MEA), flexible posts, force transducers, incorporation of fluorescent beads into the culture platform, patch-clamping techniques, and calcium sensitive dyes<sup>17-21</sup>. However, the incorporation of these devices into a culture platform is costly, low-

throughput, time consuming, and may have secondary effects on cell performance, such as changes in beat frequency or magnitude of contraction<sup>22, 23</sup>. Thereby, the development of cost-effective and less-invasive modalities able to concurrently measure mechanical and electrical components of contraction are needed for long-term experimentation.

In this study, we describe a method to study the physiology of cardiomyocyte contractility with high spatial and temporal resolution using an image capture system. The system works by rapidly alternating between brightfield and epifluorescent illumination for each frame, to record mechanical contraction and calcium transients of contracting cardiomyocytes, respectively. A speckle tracking algorithm<sup>24</sup> applied to the sequence of brightfield images determines the deformation of sub-pixel regions of cells and clusters in the field of view. From this information, the contractile strain and beat frequency can be calculated for the cell or cluster of interest that corresponds to the calcium transient frame that lies in between. As a result, the temporal relationship between the calcium transients and mechanical components leading to the contraction of a cardiomyocyte can be investigated. This technique can be applied aseptically and without the need to alter the culture platform, allowing for determination of cardiomyocyte behavior over time for use in drug discovery and functional tissues for myocardial regeneration strategies.

## 5.2 Materials and methods

### 5.2.1 Generation and culture of pluripotent stem cell derived cardiomyocytes

Human induced pluripotent (iPS-CM) and embryonic (hES-CM) stem cells were differentiated into cardiomyocytes using a previously described guided differentiation protocol involving the serial application of activin-A and bone morphogenetic protein-4<sup>7, 9, 25</sup> and were cryopreserved as previously reported<sup>26</sup>. hES-CMs modified to express the genetically encoded protein calcium sensor, GCaMP, were used<sup>27</sup>. All employed cell preparations were confirmed to contain >70% cardiac troponin T+ cardiomyocytes by flow cytometry. hPS-CM cells were thawed and seeded at a density of 150,000 cells/cm<sup>2</sup> onto collagen IV coated 96 well plates (Sigma, 10 µg/mL). Cells were cultured at 37°C at 5% CO<sub>2</sub> and media (RPMI-B27, Pen Strep, L-Glutamine) was changed every 2-3 days. Upon thawing, cells adhered

to the coated plates within 24 hours. After three days in culture, regions within the monolayer of cells appeared to form clusters of cells, which began to spontaneously contract. Over the next 18 days, clusters did not appear to change in size, although some of the clusters detached from the surface of the culture plate.

#### 5.2.2 High density mapping analysis of cardiomyocyte contraction

A high speed camera (HiSpec4, Fastec Inc.) attached to an inverted microscope (Leica, DMIL) was used to record contracting myocytes at 60 frames per second. HDM (high density mapping), a speckle tracking algorithm previously developed to measure strains on cardiac tissues<sup>24</sup> was applied to the raw images to calculate strain fields and beat frequency (Figure 5-1). Briefly, HDM divides a selected region of interest (ROI) into variable window sizes (e.g. 16x16 pixel windows) (Figure 5-1B) and tracks displacements of each window between two sequential frames over a series of images. Displacement calculations are based on the phase correlation algorithm with subpixel accuracy first described by Foroosh *et al.*<sup>28</sup> and are theoretically accurate to within 0.2 pixels<sup>24</sup>. Briefly, a hamming window is applied to the pixel windows, which are then transformed to the Fourier domain and combined via a cross power spectrum function (Figure 5-1C, D). Computation of the inverse Fourier transform of the cross power spectrum yields an impulse function marking the x and y displacement of the region between the two frames (Figure 5-1D,E). This process is repeated across the entire ROI with windows overlapping in both directions by a spacing equal to half the window size (e.g., 8 pixels for a 16x16 window, see Figure 5-1B) for each pair of frames yielding displacement fields over time. From displacement fields, regional strain tensors were computed via the Green-Lagrange definition<sup>29</sup> using the start of contraction as a reference state. All strain fields reported herein are the maximum contractile strain (minimum E2) from the initiation of contraction to peak contraction. To isolate regions with significant contraction from noise, only regions contracting with greater than 0.5% strain were analyzed. Overlapping windows were applied to obtain a spatial map of contractile strain across the cardiomyocyte cluster for each contraction cycle. From these data, heatmaps were generated to indicate the location and magnitude of contractile strain spatially within a cluster at

peak contraction (Figure 5-3A). From this map, the spatial average (reported as contractile strain) and maximum contractile strains were calculated across a cluster, and plotted over time (Figure 5-5, Figure 5-6). Finally, to compare effects of culture duration on cardiomyocyte contractility, these spatial average and maximum strains were temporally averaged over three contraction cycles (Figure 5-5). For display of strain waveforms, baseline drift (due to frame-to-frame error propagation in the HDM algorithm) was removed by subtracting a spline curve fit to the minimum (spatial average) strain just prior to each contraction beat. Average principal strain across the entire ROI over time was used to determine beat frequency via Fourier analysis. To determine the parameters to be used for HDM analysis, different window sizes (8x8, 16x16, and 32x32 pixels), each with a spacing equal to half of the window width, and different number of averaging windows (3 - 9) were examined.

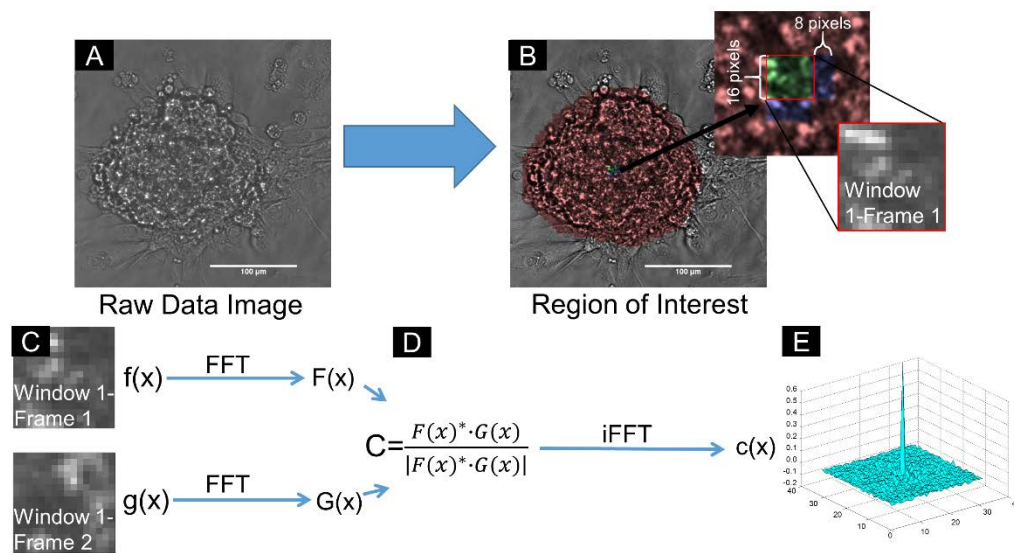


**Figure 5-1 Use of High Density Mapping to determine displacement fields of contracting hPS-CM.** HDM was applied by acquiring a high speed video of contracting hPS-CM to obtain a stack of images (A) from which a region of interest could be selected (B) and subdivided into 16x16 pixel windows. Each 16x16 pixel window is transformed to the Fourier domain (C) where phase correlation between frames is applied (D) and an inverse Fourier transform is taken resulting in the peak displacement between the two frames (E).

### 5.2.3 Brightfield and fluorescent imaging acquisition

Dual brightfield and fluorescent cardiomyocyte imaging was performed using a Zeiss AxioObserver.A1 inverted microscope with Zeiss Fluor objective lens (20x, Numerical Aperture: 0.5) and a Hamamatsu Orca Flash 4.0 sCMOS camera with CameraLink board mounted with a 1.0x c-Mount adapter. A digital

illumination controller (Nobska Imaging) synchronized image capture with alternating pulses of either (1) epifluorescence excitation illumination from a 50W blue LED (Mightex) coupled to the microscope by a liquid light guide, or (2) brightfield illumination from a green 3W LED (Luxeon Rebel with Spot optics, LEDsupply) mounted above the stage in place of the condenser. MicroManager software controlled image

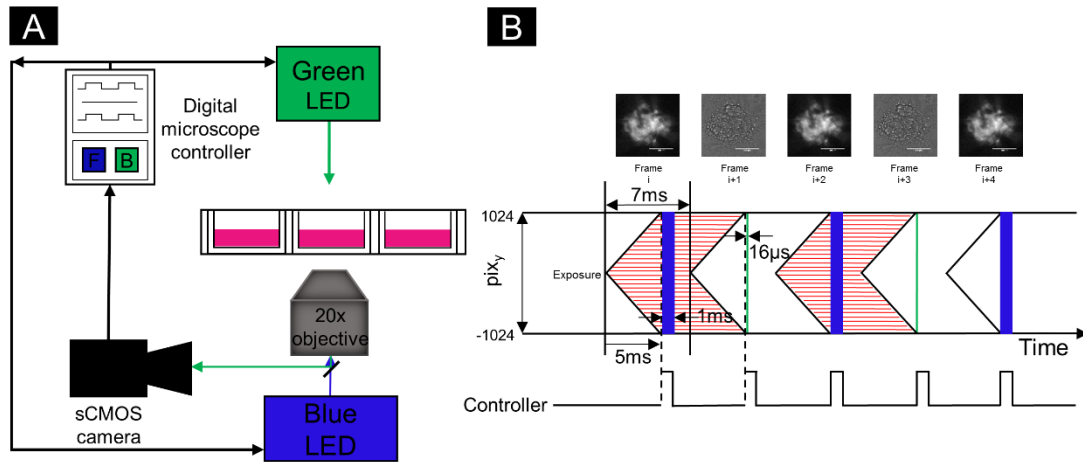


**Figure 5-2. Image acquisition schematic with temporal control of fluorescence or brightfield illumination.** Microscope schematic, a digital microscope controller for image capture of contracting cardiomyocytes using an Orca Flash 4.0 sCMOS camera with alternating pulses of fluorescence and brightfield illumination (A). Timing chart indicating sensor readout and the start of pixel exposure; when all lines are exposed the controller initiates a pulse of fluorescent (blue) or brightfield (green) illumination (B). The cycle is started over after the total exposure time (7ms) with alternating brightfield and fluorescent illuminations.

streaming parameters and illumination timing (pulse duration and delay relative to start of frame capture) via programmable TTL logic from the camera (Figure 5-2A). The controller activated either the epifluorescence LED (blue), for a pulse duration as specified by the user in MicroManager, or the brightfield LED (green) for a fixed 16 μs pulse (Figure 5-2B). Time-series videos were acquired in free-running streaming mode with a minimum exposure time defined by:

$$t_{\text{exp}} \geq t_{\text{pulse}} + \frac{N_v}{2} t_{\text{readout}}$$

where  $t_{\text{pulse}}$  is the excitation pulse duration,  $N_v$  is the vertical images size (pixels), and  $t_{\text{readout}}$  is the readout time per vertical line = 9.744 μs. For a typical 2048(h) x 1024(v) pixel image, the readout time is ~5 ms, limiting total framerate to ~200 fps and rate of brightfield/fluorescent frame pairs to ~100 fps. Reducing



		Typical	High Speed
<b>Camera</b>	pixels H	2048	2048
	pixels V	1024	96
<b>Objective</b>	x	20	5
<b>FOV</b>	mm H	0.665	2.660
	mm V	0.333	0.125
<b>Readout time</b>	ms	4.99	0.47
<b>FL excitation</b>	ms	1.00	0.50
<b>Min. exposure time</b>	ms	5.99	0.97
<b>Exposure time</b>	ms	6.99	0.97
<b>Max. framerate (per FL/BF)</b>	fps	143.1	1033.4
<b>Net framerate</b>	fps	71.5	516.7
<b>Binning</b>	x	2	1
<b>Resolution</b>	um	0.649	1.299
<b>Data</b>	MB/frame	1	0.375
<b>Data rate</b>	MB/s	143	388

**Table 5-1.** Table showing possible combinations of optical system parameters and each resultant frame rate. Column labeled “typical” shows the parameters chosen for this study.

vertical pixel number proportionally increases framerate, with 1000 fps possible with a narrowed vertical image size (Table 5-1). Image stacks were de-interlaced using ImageJ.

to de-esterify inside the cells. All fluorescence imaging of calcium transients were recorded at 71 frames per second within 2 hours of dye addition. After recording, cells were rinsed in RPMI-B27 medium and returned to incubator for continued culture in RPMI-B27 medium. To assess if the calcium signal occurred independently of the mechanical contraction, cells were treated with 10 $\mu$ M Cytochalasin-D (Sigma) for 10 minutes prior to imaging.

#### 5.2.5 Calcium transient analysis

Intracellular calcium levels were quantified using a custom MATLAB code that determined average fluorescent intensity change with respect to baseline intensity values across a selected ROI and reported as  $\Delta F/F_0$ .  $F_0$ , the baseline fluorescent value, was defined as the minimum intensity value in the region, while  $\Delta F$  is the average change in intensity for the selected region at each given time point. A deconvolution algorithm was implemented in MATLAB (‘deconv’ function with exponential decay kernel) to correct for the dynamics of the fluorescent calcium reporters, using time constants of 4 ms for the fluo-4 AM indicator<sup>30</sup> and 50 ms for GCaMP (representing the ‘on’-kinetics)<sup>31</sup>.

fresh pre-warmed RPMI-B27 medium was added and cells were allowed to sit for 20 minutes to allow the dye

#### 5.2.4 Loading iPS-CM with fluo-4 AM

Fluo-4 AM dye (Invitrogen) was loaded into iPS-CM for calcium transient analysis. Cells were incubated with Fluo-4 AM (5 $\mu$ M dissolved in Pluronic F-127 (20% solution in DMSO; Invitrogen) in RPMI-B27 medium) for 10 minutes at 37°C. Before recordings were obtained,

#### 5.2.6 Infusion of chemical stimulation via epinephrine

Isoproterenol hydrochloride (Sigma) was used to examine the cardiomyocytes response to an adrenergic stimulant. Baseline recordings were taken with cells cultured in normal medium, medium was then removed and a recording was obtained with cells incubated in medium supplemented with isoproterenol at 0.1, 1, and 10 $\mu$ M. The same contracting region was analyzed for each increasing drug addition with a total of 5 regions analyzed.

#### 5.2.7 Statistical analysis

Statistical analyses were performed using GraphPad Prism 6 (GraphPad Software, Inc., La Jolla, CA). Comparisons for contractile parameters of hPS-CM between time points were done using a one-way ANOVA with a Tukey post-hoc analysis for multiple comparisons. All measurements were averaged over the entire selected region and then averaged over three contraction cycles. All data is reported as mean $\pm$ SEM, with the exception of strain data (Figure 5-3B), and frequency data (Figure 5-5A and Figure 5-6B) reported as mean $\pm$ SD. Significance was considered at  $p < 0.05$ .

### 5.3 Results

#### 5.3.1 Effect of spatial resolution on determining contraction in hPS-CM

Using the dual image acquisition system, high-speed videos were captured of regions of beating hPS-CMs at 142 fps (71 frame pairs/s). A computational algorithm based on Fourier transforms (HDM) was applied to the recorded image sequences to determine contractile strain. Different window sizes (8 - 32 pixels), window spacing (half of window size), and number of windows (3 - 9; used to obtain an averaged contractile strain) were examined to determine how these parameters affected contractile strain quantification across a cluster of contracting hPS-CM (Figure 5-3). The smallest window size (8x8 pixels) gave the widest range of contractile strains (4.5 - 11.3%) and highest standard deviation using 3 or 5 averaging windows (Figure 5-3B), and the finest spatial resolution and largest strain map (Figure 5-3C), but also the longest computation time (Figure 5-3D). The largest window size (32x32 pixels), resulted in a coarser and smaller map of the strain distribution due to overlapping window regions, showed no difference in the contractile strain output when averaged over a range of windows, and was computed 5

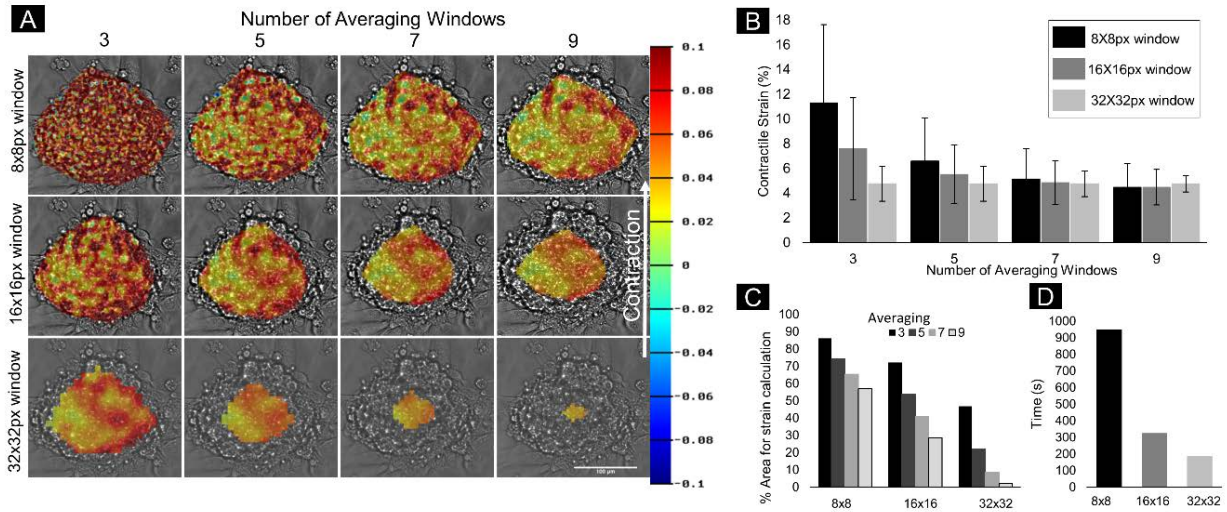


**Figure 5-3. The effect of window size and window spacing on reported contractile strain values.** The resulting strain magnitude and location was used to generate heatmaps (A) with increasing average spatial contractile strain at peak contraction in red. Pixel width for boxes in (A) was 325 wide and 272 pixels in height. Using different window sizes and spacings (1/2 window size) can affect reported contractile strain values (B), area used for contractile strain calculations reported as a change from the original selected ROI (C), and computing times (D). A 16x16 pixel window spacing with an 8 pixel window shift and an average contractile strain calculated over 5 windows was used to report contractile strain (A, B). Mean $\pm$ SD.

times faster than an 8x8 window for the same region. Overall, the number of windows used to calculate strain did not have a significant effect on computational time. A 16x16 pixel window with 8 pixel window spacing and 5-window averaging was chosen for further applications of HDM, based on its narrower range of contractile strain values (4.5 - 7.6%), subcellular spatial resolution, and reasonable computation time.

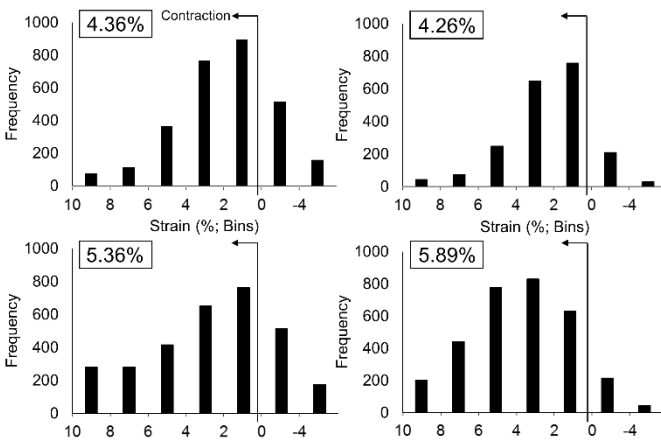


**Figure 5-4. Representative distribution of strain within clusters.** Spatial distribution of strain for four independent contracting clusters was examined. Strain values were placed in 2-4% bins from -4 to 10% strain and plotted as a histogram with the average value in the upper left. Black arrow indicates values used for average strain calculation. All histograms followed a normal distribution.

Additionally, spatial distribution of strain for four independent contracting clusters was examined and was found to follow a normal distribution (Figure 5-4).

### 5.3.2 Contractile mechanics of hPS-CM can be monitored over 21 days

In order to test the ability for the HDM algorithm to evaluate cardiac contractile mechanics over time, hPS-CMs were cultured on collagen type IV coated plates and high

speed videos of contracting hPS-CM were taken on days 7, 14, and 21. Three clusters of contracting cells within two wells were analyzed for contraction over three contraction cycles per cluster (n=6). HDM was applied to the cluster using a window size of 16x16 pixels, an 8 pixel window spacing, and 5 averaging windows. Beat frequency, contractile strain, and maximum strain were computed for each time point. hPS-CMs showed increased beating frequency over-time, where cells exhibited a significantly higher (p<0.001) beat frequency on day 21 (1.52±0.09 Hz) when compared to day 7 (1.06±0.09 Hz; Figure 5-5A). Cells seeded on collagen IV coated plates had a contractile strain on day 7 of 4.5±0.4%, which significantly decreased (p<0.05) to 2.9±0.3% strain at day 21 (Figure 5-5B). Maximum contractile strain calculated on day 7 for hPS-CMs was found to be 19.9±1.4%, which decreased significantly (p<0.001) to 10.8±1.5% strain at day 21 (Figure 5-5C). These results indicate the ability for the HDM algorithm to detect and quantify changes in cardiomyocyte contractility over 21 days.

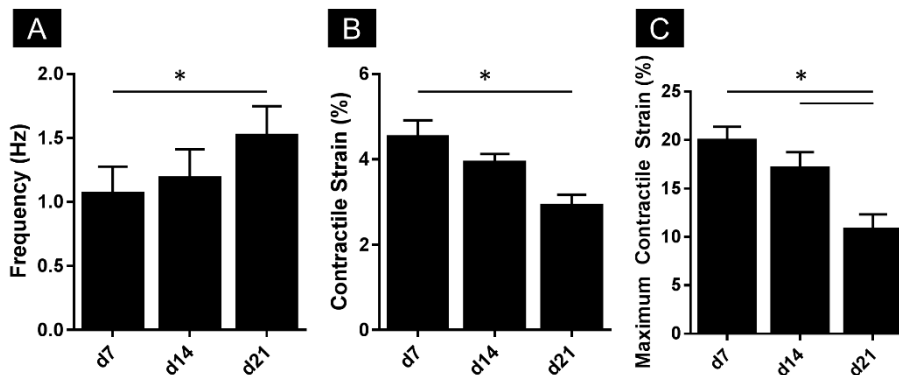


**Figure 5-5. HDM can be used to quantify contraction of hPS-CM seeded on collagen IV coated plates over 21 days.** hPS-CM significantly increased beat frequency by 1.5x between day 7 and day 21(A). A significant decrease between day 7 and day 21 was observed for contractile strain (B) and maximum contractile strain (C). Mean±SD for frequency, Mean±SEM for contractile and maximum strain, n=6, \*p<0.05.

### 5.3.3 Measurements of calcium transients and mechanical contraction in hPS-CM

iPS-CM calcium transients were visualized by loading the cells with 5µM Fluo-4 AM, a calcium indicator dye that changes fluorescence in proportion to intracellular free calcium. In addition, calcium transients were observed in ES-derived cardiomyocytes (ES-CMs) differentiated from a reporter line expressing the

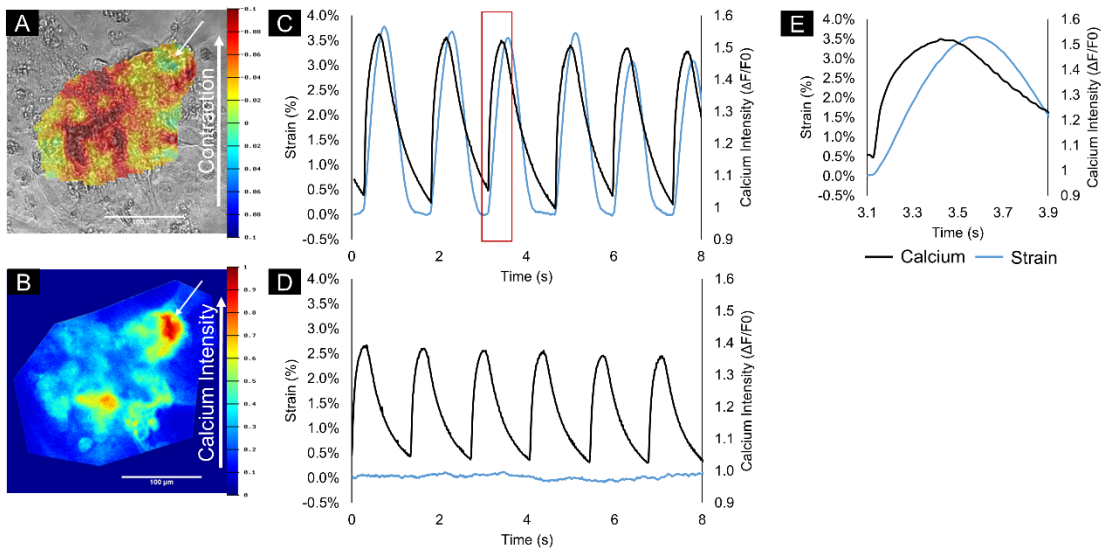


**Figure 5-6. Overlay of mechanical contraction and calcium transients in iPS-CM.** Alternating brightfield and fluorescent images of contracting iPS-CM loaded with fluo-4 AM at day 21 resulted in spatial heatmaps for peak mechanical contraction (A) and peak calcium flux (B). The location of peak calcium intensity did not correspond with location of peak contractile strains. (A, B white arrows) The resulting cyclic contractile strain and calcium signal is presented over 8 seconds (C) with an isolated cycle indicated by the red box in C (E). Cells treated with Cytochalasin-D exhibit loss of mechanical contraction while calcium transients are maintained (D).

genetically-encoded calcium indicator GCaMP<sup>9</sup>. The same image acquisition system was able to detect calcium changes over the contractile cycle via Fluo-4 AM in iPS-CMs (Figure 5-6) and GCaMP in ES-CMs (Figure 5-7). A 1ms fluorescent light pulse with 2x2 binning allowed for recordings at a frame rate of 142fps

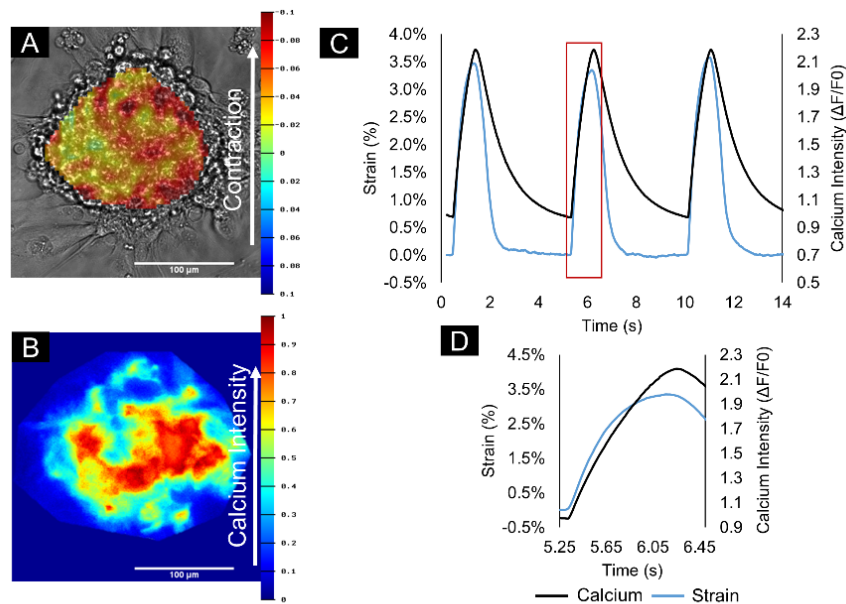


**Figure 5-7. Overlay of mechanical contraction and calcium transients in ES-CM.** Alternating brightfield and fluorescent images of contracting GCaMP3 ES-CM resulted in spatial heatmaps for peak mechanical contraction (A) and peak calcium flux (B). The resulting cyclic contractile strain and calcium signal is presented over 14 seconds (C) with an isolated cycle indicated by the red box in C (D).

(71fps for each channel, brightfield and fluorescent), spatial resolution of 0.65  $\mu\text{m}/\text{pixel}$ , and field of view of 1024 x 512 pixels or 665 x 333  $\mu\text{m}$  (Table 1). These settings yielded a calcium signal-to-noise ratio of 21 dB as determined using MATLAB. Fluorescent traces were deconvolved to remove the effects of slow optical calcium sensor dynamics, using the “on”-kinetics of the Fluo-4 and GCaMP sensors. Whereas no difference was seen before and after deconvolution for the faster Fluo-4 sensor (data not shown), the deconvolved GCaMP trace rose faster than the original trace, however both traces began at the same time (Figure 5-8).

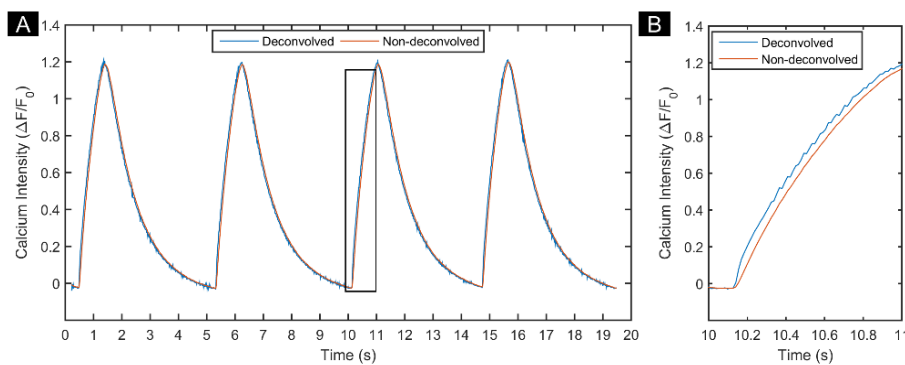


**Figure 5-8. Deconvolved GCaMP calcium transient traces.** Deconvolved (blue) and non-deconvolved (orange) GCaMP calcium traces (A). Expanded portion of the traces from A, black box indicates region shown (B).

Brightfield and fluorescent images were alternatively acquired to examine the spatial and temporal relationships between mechanical contraction and calcium transients of contracting hPS-CMs. Regions of peak contractile strain (Figure 5-6A) and peak calcium intensity change (Figure 5-6B) during the contractile beat cycle were not well correlated across the iPS-CM cluster. The mechanical contraction and calcium transient tracings across were plotted together in order to examine their temporal relationship (Figure 5-6C). Calcium levels rose before the onset of mechanical contraction for Fluo-4 AM loaded iPS-CM (Figure 5-6) and GCaMP-expressing ES-CM (Figure 5-7), following expectations for cardiomyocyte physiology. Fluo-4 calcium traces peaked before peak strain in iPS-CM, whereas GCaMP calcium traces peaked after peak ES-CM strain, reflecting differences in calcium sensor or cardiomyocyte dynamics. Cells treated with Cytochalasin-D, which eliminate mechanical function by inhibiting actin polymerization, retained similar

calcium signal cycles (Figure 5-6D), demonstrating that the calcium signal was due to calcium transients and not mechanical interferences.

#### 5.3.4 Isoproterenol stimulation increases contractile strain and beat frequency

Adrenergic stimulation (isoproterenol) was applied to Fluo-4 AM loaded iPS-CM to evaluate the ability of the algorithm to detect simultaneous changes in contractility in terms of contractile strain, beat frequency, and calcium transients. Isoproterenol, a  $\beta$ -adrenergic agonist, was chosen as it has been shown to increase beat frequency for adult cardiomyocytes<sup>32</sup>. Isoproterenol was applied at concentrations of 0.1, 1, and 10 $\mu$ M with recordings taken immediately after each addition (n=5). Beat frequency was found to be  $0.66\pm 0.13$ Hz with cells cultured in RPMI-B27 media without isoproterenol (Figure 5-9A, B). The addition of isoproterenol at concentrations up to 10 $\mu$ M significantly increased beat frequency to  $0.88\pm 0.09$ Hz (Figure 5-9A, B,  $p < 0.05$ ). Contractile strain began at  $3.1\pm 0.45\%$  with RPMI-B27 media (Figure 5-9). The addition of isoproterenol did not significantly change strain levels as all strain levels for stimulated cells were between 3.2-3.6% (Figure 5-9C,  $p > 0.05$ ). These results indicate that this system is capable of

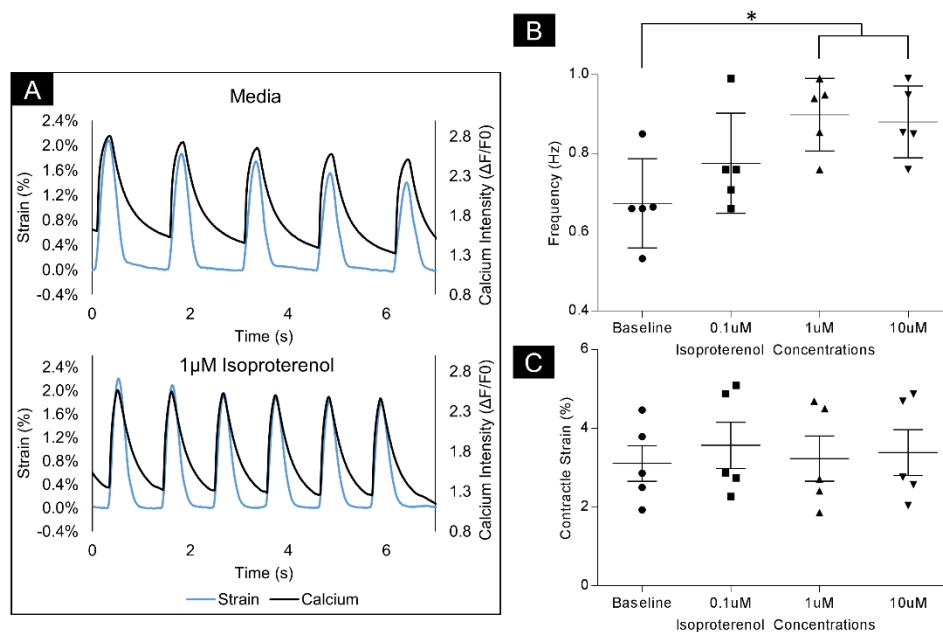


**Figure 5-9. Isoproterenol stimulation of hPS-CM.** Adding isoproterenol to hPS-CM increased beat frequency (A,B) up to the addition of 10 $\mu$ M isoproterenol, with representative traces of Fluo-4 AM loaded contracting hPS-CM (A) and frequency data averaged in (B). Addition of isoproterenol did not affect contractile strain for any condition compared to baseline (C). Mean $\pm$ SD for frequency, Mean $\pm$ SEM for contractile strain, n=3, \* $p < 0.05$ .

detecting changes in the contractile properties of cells when isoproterenol is applied, which may be helpful for drug screening studies.

#### 5.4 Discussion

Recent advances in stem cell technology have yielded high purity (>90%) populations of contracting cardiomyocytes derived from both ES and iPS cells<sup>7,8</sup>. These cardiomyocytes have the potential to be used in a wide variety of applications including myocardial regeneration therapies, disease modeling, drug screening, and development. To fulfill the potential of these applications, cost-effective, high-throughput techniques to concurrently monitor contractile and calcium transient changes in single cells or clusters of hPS-CM are needed. By concurrently monitoring the relationship between contractile and ionic changes overtime, physiological relationships can be better understood, which is valuable for applications such as drug screening for off target changes in cardiomyocyte contractility.

Current techniques to monitor cardiomyocyte electrophysiological function include the use of microelectrode arrays, patch clamping, and voltage or ion sensitive fluorescent dyes. Microelectrode arrays give measurements of beat frequency and field potential, but require cells to be cultured on a specific surface connected to the appropriate data acquisition system<sup>33</sup>. Patch clamping records action potential and ion channel information of single cells, and is low-throughput, time consuming, and requires expertise<sup>34</sup>. Voltage and ionic dyes, such as di-8-ANEPPS and Fluo-4 AM, or their genetically-encoded counterparts, such as ArcLight and GCaMP, are good for non-invasive measurements of cardiomyocyte electrophysiology or intracellular calcium concentrations at the single-cell level or in multicellular preparations<sup>35, 36</sup>.

Contractile force can be evaluated using force transducers or traction force microscopy (TFM)<sup>37-39</sup>. Both of these techniques require known substrate mechanical properties and necessitate changes to the culture platform that may have secondary effects on cell function<sup>22, 23</sup>. Force transducers are best suited for measurements on the macro tissue scale, which is not appropriate for studies investigating cellular



contractility. TFM can measure contractility on the cellular level, but requires cells to be cultured on a substrate with incorporated microbeads. Bead displacement is used to quantify cell contraction; however, microbead incorporation can severely limit measurements by having random bead distributions and densities that might not accurately depict cellular contractility.

Optical methods can be used to overcome the challenges of integrative culture platforms for monitoring cardiomyocyte function. Current image processing techniques focus on edge detection techniques, such as with laser diffraction and microscopic cell images to obtain information about cell contractility<sup>40, 41</sup>. However, these methods are limited to the spatial resolution of the imaging systems, as well as to changes in cardiomyocyte contraction from unexpected movement, asynchronous contraction, or cardiomyocyte rotation, which would result in an inaccurate contractile output. Imaging methods that focus on changes in sarcomere striations<sup>42</sup> are limited to single isolated cardiomyocytes with well-defined striated patterns. However, hPS-CM are comparatively immature<sup>43</sup>, exhibit less defined sarcomere patterns, and are cultured in monolayers instead of single cells; thus, these imaging techniques may not be sufficient to measure contractile mechanics of hPS-CM.

More recent techniques to monitor contraction apply an optical flow algorithm with macroblocks to estimate motion of a set of images of contracting cardiomyocytes<sup>22</sup>, or particle image velocimetry (PIV), a cross-correlation procedure to determine displacement fields of cardiomyocytes visualized using video microscopy<sup>23</sup>. Both methods quantify beating speed, beating velocity and beat pattern, but not the magnitude of contraction. Neither technique gives quantitative information about cardiomyocyte contraction combined with information about calcium signaling. While calcium signaling alone has been shown to predict *in vitro* cardiotoxicity<sup>19</sup>, the combination of calcium signaling and mechanical contraction provides a more robust method to detect cardiotoxicities that may affect mechanical contraction apart from calcium signaling.

Here, we describe a technique for concurrent monitoring of mechanical contraction and calcium transients of hPS-CM over several weeks using a system that alternates high speed imaging of brightfield and fluorescence. The system allows frames to be captured at >60fps over a 1024x512pixel region of interest (ROI), or up to 1000fps by decreasing the ROI to 96 vertical pixels. Our results demonstrate the ability to characterize mechanical contraction by applying HDM, a speckle tracking algorithm, to brightfield images to calculate beat frequency as well as quantitative information about the magnitude of contraction (contractile strain). Calcium transients were calculated by analyzing the acquired fluorescent signals from Fluo-4 AM or GCaMP calcium reporters. Calcium transients and contractile strain waveforms were plotted together; for Fluo-4 AM loaded iPS-CM, the calcium waveform was initiated and peaked before strain, as expected for cardiomyocyte physiology<sup>44</sup>. For GCaMP ES-CM, the calcium signal began before the strain signal, but the calcium signal peaked after strain began to decline, highlighting the differences between the cardiomyocyte sources and kinetics of the calcium reporters<sup>36, 45</sup>. Deconvolution was performed on both Fluo-4 and GCaMP fluorescent traces to attempt to remove any sensor-induced delays. At the frame rates used (14 ms interval), deconvolution had little effect on Fluo-4 traces (time constant 4 ms), but resulted in GCaMP traces that rose faster than the original traces (“on” time constant 50 ms). However, “off” kinetics of GCaMP sensors are often much slower than “on” kinetics<sup>31</sup>. Deconvolution algorithms that address different on- and off-kinetics can better correct for these effects.

Due to the aseptic nature of this analysis technique, recordings were obtained for several time points over a period of 21 days. Mechanical contraction of hPS-CM clusters was quantified using HDM in terms of beat frequency, contractile strain, and maximum contractile strain. Over 21 days, hPS-CM exhibited a significant increase in beat frequency, similar to reports from other groups<sup>46, 47</sup>, accompanied by a significant decrease in contractile strain. Isoproterenol stimulation demonstrated the system’s ability to capture chemically induced changes in mechanical contraction, which may be valuable for drug screening studies. With the addition of isoproterenol, we demonstrated a significant increase in beat frequency

along a similar order reported by others<sup>14, 20, 48</sup>, but no significant changes in contractile strain. While isoproterenol has been shown to increase twitch forces in mature adult cardiomyocytes, predicting an increase in contractile strain levels, studies have shown that immature cardiomyocytes, such as the hPS-CM used in this study, have different responses to drug additions than adult cardiomyocytes. For example, immature hPS-CMs produce less force in response to isoproterenol compared with adult cardiomyocytes<sup>49</sup>, this may describe why no significant change in strain was demonstrated with isoproterenol addition.

Another application of this system could be to measure functional differentiation of cultures over time. Although cardiac differentiation is a well-established technique, purity remains a major issue. Our system may be able to elucidate changes due to differentiation protocols or batch variability. In a computational model of fibroblasts and cardiomyocytes, Zhan and colleagues demonstrated changes in deformation resulting from changes in the ratio of fibroblasts to cardiomyocytes<sup>50</sup>. A lower purity of cardiomyocytes may result in decreased contraction. Additionally, the whole-field property of our system could be used to determine if regions of cells are not contracting under whole field stimulation, suggesting undifferentiated or dysfunctional cells. Together, this information may continuously inform investigators on the functional differentiation of their cultures.

The system developed here allows brightfield and fluorescent images to be acquired in rapid succession, for concurrent measurements of strain and intracellular calcium. Strain data is generated by analyzing the displacement between two brightfield images, which span each fluorescent image used to quantify calcium levels. Thus, the calcium information is obtained temporally at the midpoint of strain information, and the temporal relationship between calcium activity and the corresponding mechanical contraction can be obtained by overlaying the two waveforms. Additionally, by alternating image acquisition this system avoids the expense and alignment required by dual-view or dual-camera setups, which spectrally split fluorescence (blue-green) and brightfield (red or infrared), but capture both images simultaneously.

Another advantage of this system is that as it uses a 96 well cell culture plate, with the appropriate alterations the system could be automated to provide for real time information which would be ideal for high throughput screening.

Different window sizes and spacings were used to compute contractile strain to determine if the calculated strain reached an optimum point, suggesting a minimum number of pixels needed for calculating strain. A 16x16 pixel window with an 8 pixel spacing averaged over 5 windows was used for strain calculations as these parameters maintained spatial information with less strain variance and decreased computation time. By averaging over 5 windows, strain calculations are likely not overestimated, as regions of strain artifacts are removed, or underestimated, as using 5 windows maintains spatial information. The 8x8 pixel window with a 4 pixel spacing maintained the most spatial information, but had the highest computation time and the largest degree of strain variance when fewer averaging windows were used (3 and 5) due to the small regions being analyzed. A 32x32 pixel window with a 16 pixel spacing had the fastest computation time; however spatial information was lost due to large regions being analyzed. One of the advantages of this method is spatial resolution, as the smaller pixel window sizes allow the regions analyzed to be on the size of a cell. The larger spacing results in displacement being determined in fewer locations, while the larger window size may miss inhomogeneous deformation that may occur within the window. A key benefit to this technique is that HDM enables different combinations of window sizes, window spacings, and number of windows averaged, which can be tailored to the desired application.

The use of HDM provides high temporal resolution of quantitative information about cardiomyocyte contraction at a sub-pixel resolution. Here, this technique was demonstrated at a cellular level, but can also be applied at a tissue level as demonstrated on hPS-CM seeded myocardium fibers<sup>51</sup>. As this technique can be easily applied to high speed videos it is a powerful tool to examine cardiomyocyte contractility over time. This technique can be used to obtain information about how different drug

compounds affect cardiomyocyte contractility, both mechanically and at the intracellular calcium level, which would enhance the quality of current drug testing systems. Herein, we demonstrated the ability of the system to determine increased contractile frequencies with the administration of isoproterenol. Additionally, for hPS-CM potential to be realized for cell replacement strategies, hPS-CM should exhibit a more adult like phenotype in order to couple and contract with human myocardium. The use of this optical system to monitor contraction as an indicator for maturity, for example through adrenergic stimulation, would provide a convenient and economic solution to examine cell maturation without having to sacrifice cells for use in terminal analysis techniques.

## 5.5 References

1. Takahashi K and Yamanaka S. Induction of pluripotent stem cells from mouse embryonic and adult fibroblast cultures by defined factors. *Cell*. 2006;126:663-76.
2. Yu J, Vodyanik MA, Smuga-Otto K, Antosiewicz-Bourget J, Frane JL, Tian S, Nie J, Jonsdottir GA, Ruotti V, Stewart R, Slukvin II and Thomson JA. Induced Pluripotent Stem Cell Lines Derived from Human Somatic Cells. *Science*. 2007;318:1917-1920.
3. Bellin M, Marchetto MC, Gage FH and Mummery CL. Induced pluripotent stem cells: the new patient? *Nat Rev Mol Cell Biol*. 2012;13:713-726.
4. Soldner F and Jaenisch R. iPSC Disease Modeling. *Science*. 2012;338:1155-1156.
5. Moretti A, Bellin M, Welling A, Jung CB, Lam JT, Bott-Flügel L, Dorn T, Goedel A, Höhnke C, Hofmann F, Seyfarth M, Sinnecker D, Schömig A and Laugwitz K-L. Patient-Specific Induced Pluripotent Stem-Cell Models for Long-QT Syndrome. *New England Journal of Medicine*. 2010;363:1397-1409.
6. Thomson JA. Embryonic Stem Cell Lines Derived from Human Blastocysts. *Science*. 1998;282:1145-1147.
7. Laflamme MA, Chen KY, Naumova AV, Muskheli V, Fugate JA, Dupras SK, Reinecke H, Xu C, Hassanipour M, Police S, O'Sullivan C, Collins L, Chen Y, Minami E, Gill EA, Ueno S, Yuan C, Gold J and Murry CE. Cardiomyocytes derived from human embryonic stem cells in pro-survival factors enhance function of infarcted rat hearts. *Nature biotechnology*. 2007;25:1015-24.
8. Lian X, Hsiao C, Wilson G, Zhu K, Hazeltine LB, Azarin SM, Raval KK, Zhang J, Kamp TJ and Palecek SP. Robust cardiomyocyte differentiation from human pluripotent stem cells via temporal modulation of canonical Wnt signaling. *Proc Natl Acad Sci U S A*. 2012;109:E1848-57.
9. Shiba Y, Fernandes S, Zhu WZ, Filice D, Muskheli V, Kim J, Palpant NJ, Gantz J, Moyes KW, Reinecke H, Van Biber B, Dardas T, Mignone JL, Izawa A, Hanna R, Viswanathan M, Gold JD, Kotlikoff MI, Sarvazyan N, Kay MW, Murry CE and Laflamme MA. Human ES-cell-derived cardiomyocytes electrically couple and suppress arrhythmias in injured hearts. *Nature*. 2012;489:322-5.
10. Hansen A, Eder A, Bonstrup M, Flato M, Mewe M, Schaaf S, Aksehirlioglu B, Schwoerer AP, Uebeler J and Eschenhagen T. Development of a drug screening platform based on engineered heart tissue. *Circ Res*. 2010;107:35-44.
11. Godier-Furnemont AF, Tiburcy M, Wagner E, Dewenter M, Lammle S, El-Armouche A, Lehnart SE, Vunjak-Novakovic G and Zimmermann WH. Physiologic force-frequency response in engineered heart muscle by electromechanical stimulation. *Biomaterials*. 2015;60:82-91.
12. Snir M, Kehat I, Gepstein A, Coleman R, Itskovitz-Eldor J, Livne E and Gepstein L. Assessment of the ultrastructural and proliferative properties of human embryonic stem cell-derived cardiomyocytes. *American Journal of Physiology - Heart and Circulatory Physiology*. 2003;285:H2355-H2363.
13. Lundy SD, Zhu WZ, Regnier M and Laflamme MA. Structural and functional maturation of cardiomyocytes derived from human pluripotent stem cells. *Stem Cells Dev*. 2013;22:1991-2002.
14. Zhang D, Shadrin IY, Lam J, Xian HQ, Snodgrass HR and Bursac N. Tissue-engineered cardiac patch for advanced functional maturation of human ESC-derived cardiomyocytes. *Biomaterials*. 2013;34:5813-20.
15. Thavandiran N, Dubois N, Mikryukov A, Masse S, Beca B, Simmons CA, Deshpande VS, McGarry JP, Chen CS, Nanthakumar K, Keller GM, Radisic M and Zandstra PW. Design and formulation of functional pluripotent stem cell-derived cardiac microtissues. *PNAS*. 2013;49:E4698-707.
16. Lan F, Lee AS, Liang P, Sanchez-Freire V, Nguyen PK, Wang L, Han L, Yen M, Wang Y, Sun N, Abilez OJ, Hu S, Ebert AD, Navarrete EG, Simmons CS, Wheeler M, Pruitt B, Lewis R, Yamaguchi Y, Ashley EA, Bers DM, Robbins RC, Longaker MT and Wu JC. Abnormal calcium handling properties underlie familial hypertrophic cardiomyopathy pathology in patient-specific induced pluripotent stem cells. *Cell Stem Cell*. 2013;12:101-13.

17. Nunes SS, Miklas JW, Liu J, Aschar-Sobbi R, Xiao Y, Zhang B, Jiang J, Masse S, Gagliardi M, Hsieh A, Thavandiran N, Laflamme ML, Nanthakumar K, Gross GJ, Backx PH, Keller G and Radisic M. Biowire: a platform for maturation of human pluripotent stem cell-derived cardiomyocytes. *Nat Methods*. 2013;10:781-786.
18. Asakura K, Hayashi S, Ojima A, Taniguchi T, Miyamoto N, Nakamori C, Nagasawa C, Kitamura T, Osada T, Honda Y, Kasai C, Ando H, Kanda Y, Sekino Y and Sawada K. Improvement of acquisition and analysis methods in multi-electrode array experiments with iPS cell-derived cardiomyocytes. *Journal of pharmacological and toxicological methods*. 2015;75:17-26.
19. Sirenko O, Cromwell EF, Crittenden C, Wignall JA, Wright FA and Rusyn I. Assessment of Beating Parameters in Human Induced Pluripotent Stem Cells Enables Quantitative In Vitro Screening for Cardiotoxicity. *Toxicology and applied pharmacology*. 2013;273:500-507.
20. Bielawski KS, Leonard A, Bhandari S, Murry CE and Sniadecki N. Real-Time Force and Frequency Analysis of Engineered Human Heart Tissue Derived from Induced Pluripotent Stem Cells Using Magnetic Sensing. *Tissue Eng Part C Methods*. 2016.
21. Grespan E, Martewicz S, Serena E, Le Houérou V, Rühle J and Elvassore N. Analysis of calcium transients and uni-axial contraction force in single human embryonic stem cell derived-cardiomyocytes on microstructured elastic substrate with spatially controlled surface chemistries. *Langmuir*. 2016.
22. Huebsch N, Loskill P, Mandegar MA, Marks NC, Sheehan AS, Ma Z, Mathur A, Nguyen TN, Yoo JC, Judge LM, Spencer CI, Chukka AC, Russell CR, So PL, Conklin BR and Healy KE. Automated Video-Based Analysis of Contractility and Calcium Flux in Human-Induced Pluripotent Stem Cell-Derived Cardiomyocytes Cultured over Different Spatial Scales. *Tissue Eng Part C Methods*. 2015;21:467-79.
23. Rajasingh S, Thangavel J, Czirok A, Samanta S, Roby KF, Dawn B and Rajasingh J. Generation of Functional Cardiomyocytes from Efficiently Generated Human iPSCs and a Novel Method of Measuring Contractility. *PLoS One*. 2015;10:e0134093.
24. Kelly DJ, Azeloglu EU, Kochupura PV, Sharma GS and Gaudette GR. Accuracy and reproducibility of a subpixel extended phase correlation method to determine micron level displacements in the heart. *Medical engineering & physics*. 2007;29:154-62.
25. Zhu WZ, Van Biber B and Laflamme MA. Methods for the derivation and use of cardiomyocytes from human pluripotent stem cells. *Methods in molecular biology*. 2011;767:419-31.
26. Xu C, Police S, Hassanipour M, Li Y, Chen Y, Priest C, O'Sullivan C, Laflamme MA, Zhu WZ, Van Biber B, Hegerova L, Yang J, Delavan-Boorsma K, Davies A, Lebkowski J and Gold JD. Efficient generation and cryopreservation of cardiomyocytes derived from human embryonic stem cells. *Regenerative medicine*. 2011;6:53-66.
27. Zhu W-Z, Filice D, Palpant NJ and Laflamme MA. Methods for Assessing the Electromechanical Integration of Human Pluripotent Stem Cell-Derived Cardiomyocyte Grafts. *Methods in molecular biology (Clifton, NJ)*. 2014;1181:229-247.
28. Foroosh H, Zerubia JB and Berthod M. Extension of phase correlation to subpixel registration. *IEEE transactions on image processing : a publication of the IEEE Signal Processing Society*. 2002;11:188-200.
29. Fung YC. *A first course in continuum mechanics*. 3rd edition ed. Englewood Cliffs, NJ: Prentice Hall; 1993.
30. Zahradníková A, Poláková E, Zahradník I and Zahradníková A. Kinetics of calcium spikes in rat cardiac myocytes. *The Journal of Physiology*. 2007;578:677-691.
31. Helassa N, Zhang X-h, Conte I, Scaringi J, Esposito E, Bradley J, Carter T, Ogden D, Morad M and Török K. Fast-Response Calmodulin-Based Fluorescent Indicators Reveal Rapid Intracellular Calcium Dynamics. *Scientific Reports*. 2015;5:15978.
32. Endoh M. The effects of various drugs on the myocardial inotropic response. *General Pharmacology: The Vascular System*. 1995;26:1-31.

33. Navarrete EG, Liang P, Lan F, Sanchez-Freire V, Simmons C, Gong T, Sharma A, Burridge PW, Patlolla B, Lee AS, Wu H, Beygui RE, Wu SM, Robbins RC, Bers DM and Wu JC. Screening Drug-Induced Arrhythmia Using Human Induced Pluripotent Stem Cell-Derived Cardiomyocytes and Low-Impedance Microelectrode Arrays. *Circulation*. 2013;128:S3-S13.
34. Honda M, Kiyokawa J, Tabo M and Inoue T. Electrophysiological Characterization of Cardiomyocytes Derived From Human Induced Pluripotent Stem Cells. *Journal of Pharmacological Sciences*. 2011;117:149-159.
35. Herron TJ, Lee P and Jalife J. Optical imaging of voltage and calcium in cardiac cells & tissues. *Circ Res*. 2012;110:609-23.
36. Guatimosim S, Guatimosim C and Song L-S. Imaging Calcium Sparks in Cardiac Myocytes. *Methods in molecular biology (Clifton, NJ)*. 2011;689:205-214.
37. Zimmermann WH, Fink C, Kralisch D, Remmers U, Weil J and Eschenhagen T. Three-dimensional engineered heart tissue from neonatal rat cardiac myocytes. *Biotechnology and bioengineering*. 2000;68:106-114.
38. Jacot JG, McCulloch AD and Omens JH. Substrate stiffness affects the functional maturation of neonatal rat ventricular myocytes. *Biophys J*. 2008;95:3479-87.
39. Engler AJ, Carag-Krieger C, Johnson CP, Raab M, Tang HY, Speicher DW, Sanger JW, Sanger JM and Discher DE. Embryonic cardiomyocytes beat best on a matrix with heart-like elasticity: scar-like rigidity inhibits beating. *J Cell Sci*. 2008;121:3794-802.
40. Delbridge LMD and Roos KP. Optical Methods to Evaluate the contractile function of unloaded isolated cardiac myocytes. *Journal of molecular and cellular cardiology*. 1997;29:11-25.
41. Bazan C, Barba DT, Blomgren P and Paolini P. Image processing techniques for assessing contractility in isolated adult cardiac myocytes. *Int J Biomed Imaging*. 2009;2009:352954.
42. Bub G, Camelliti P, Bollensdorff C, Stuckey DJ, Picton G, Burton RAB, Clarke K and Kohl P. Measurement and analysis of sarcomere length in rat cardiomyocytes in situ and in vitro. *American Journal of Physiology - Heart and Circulatory Physiology*. 2010;298:H1616-H1625.
43. Yang X, Pabon L and Murry CE. Engineering adolescence: maturation of human pluripotent stem cell-derived cardiomyocytes. *Circ Res*. 2014;114:511-23.
44. Bers DM. Cardiac excitation-contraction coupling. *Nature*. 2002;415:198-205.
45. Tallini YN, Ohkura M, Choi B-R, Ji G, Imoto K, Doran R, Lee J, Plan P, Wilson J, Xin H-B, Sanbe A, Gulick J, Mathai J, Robbins J, Salama G, Nakai J and Kotlikoff MI. Imaging cellular signals in the heart in vivo: Cardiac expression of the high-signal Ca<sup>2+</sup> indicator GCaMP2. *Proceedings of the National Academy of Sciences of the United States of America*. 2006;103:4753-4758.
46. Hescheler J, Halbach M, Egert U, Lu ZJ, Bohlen H, Fleischmann BK and Reppel M. Determination of electrical properties of ES cell-derived cardiomyocytes using MEAs. *Journal of electrocardiology*. 2004;37, Supplement:110-116.
47. Eng G, Lee BW, Protas L, Gagliardi M, Brown K, Kass RS, Keller G, Robinson RB and Vunjak-Novakovic G. Autonomous beating rate adaptation in human stem cell-derived cardiomyocytes. *Nat Commun*. 2016;7.
48. Hayakawa T, Kunihiro T, Ando T, Kobayashi S, Matsui E, Yada H, Kanda Y, Kurokawa J and Furukawa T. Image-based evaluation of contraction-relaxation kinetics of human-induced pluripotent stem cell-derived cardiomyocytes: Correlation and complementarity with extracellular electrophysiology. *Journal of molecular and cellular cardiology*. 2014;77:178-191.
49. Pillekamp F, Haustein M, Khalil M, Emmelheinz M, Nazzal R, Adelmann R, Nguemo F, Rubenchyk O, Pfannkuche K, Matzkies M, Reppel M, Bloch W, Brockmeier K and Hescheler J. Contractile properties of early human embryonic stem cell-derived cardiomyocytes: beta-adrenergic stimulation induces positive chronotropy and lusitropy but not inotropy. *Stem Cells Dev*. 2012;21:2111-21.



50. Zhan H-q, Xia L, Shou G-f, Zang Y-l, Liu F and Crozier S. Fibroblast proliferation alters cardiac excitation conduction and contraction: a computational study. *Journal of Zhejiang University Science B*. 2014;15:225-242.
51. Guyette JP, Charest JM, Mills RW, Jank BJ, Moser PT, Gilpin SE, Gershlak JR, Okamoto T, Gonzalez G, Milan DJ, Gaudette GR and Ott HC. Bioengineering Human Myocardium on Native Extracellular Matrix. *Circ Res*. 2016;118:56-72.

## 6 Objective 2b: Produce and characterize contractile hPS-CM seeded microthreads.

In this objective we will use the method developed in objective 2b to determine contractile behavior of hPS-CM seeded along the scaffold in terms of contractile strain, beat frequency, and conduction velocity from calcium transient waveforms. The same cell type from objective 2a will be used and all microthreads used in this objective were produced as described in objective 1a.

### 6.1 Introduction

Our fibrin suture has been shown to be an effective delivery vehicle for hMSCs<sup>1</sup>, we hypothesize that we will be able to similarly deliver hPS-CM to healthy cardiac tissue. The aim of objective 2b is to identify and implement strategies to seed hPS-CM onto fibrin microthreads and characterize how these cells function on the microthreads and understand how their contractile properties may change over time in culture.

Fibrin microthreads have been previously shown to support hMSC attachment<sup>2</sup>, however it is unknown whether fibrin microthreads can support hPS-CM attachment. The ability of cells to bind to substrates is dependent on integrins, a family of cell surface receptors. Integrin's are  $\alpha\beta$  heterodimeric transmembrane glycoproteins on a cells surface that can bind ligands found on ECM proteins. While hPS-CM can be maintained on tissue culture polystyrene they are better supported on an ECM that more closely resembles in vivo conditions<sup>3, 4</sup>. Cardiac muscle is comprised of collagen type I and III in the interstitium, collagen type IV and glycoproteins fibronectin and laminin in the basement membrane<sup>5</sup>. hMSCs have shown the ability to bind to fibrin as well as ECM proteins vitronectin and fibronectin, among others<sup>2, 4, 6</sup>. hMSCs and hPS-CM share some integrins namely  $\alpha3$ ,  $\alpha5$ ,  $\alpha V$ , and  $\beta1$ <sup>4, 7-9</sup>, which may suggest that hPS-CM can bind to fibrin; however, hPS-CM express many other integrins that may preferentially bind to other ECM proteins. Mummery *et al.* described the integrin expression profile for hESC-CM to be comprised of  $\alpha3$ ,  $\alpha5$ ,  $\alpha6$ ,  $\alpha7$ ,  $\alpha11$ ,  $\alpha V$ , and  $\beta1$  which bind laminins ( $\alpha1\beta1$ ,  $\alpha3\beta1$ ,  $\alpha6\beta1$ , and  $\alpha7\beta1$ ) collagens (collagen IV;  $\alpha1\beta1$ ,  $\alpha3\beta1$ ,  $\alpha10\beta1$ ,  $\alpha11\beta1$ ), and fibronectin ( $\alpha3\beta1$ ,  $\alpha5\beta1$ ,  $\alpha V\beta1$ ) with unknown specificity<sup>7, 10, 11</sup>. In adult cardiomyocytes, the same integrin expression with the addition of  $\alpha1$  (collagen IV, laminin),  $\alpha9$

(fibronectin) and  $\alpha$ 10 (collagen IV), has been reported<sup>12, 13</sup>. Additionally, studies have shown that ESC and iPS derived cardiomyocytes preferentially bind to substrates coated with fibronectin and collagen type IV over uncoated substrates<sup>11, 13</sup>. Based on the above evidence, in this objective we will investigate the effect of ECM coatings of fibronectin and collagen type IV on fibrin microthreads on hPS-CM attachment.

hPS-CMs have the ability to spontaneously contract in a 2D environment *in vitro* after differentiation<sup>14</sup>. Previous studies have indicated that fibrin is a suitable biomaterial to support hPS-CM contraction<sup>15, 16</sup>. Various groups have used fibrin based hydrogels to create cardiac patches for myocardial regeneration strategies as well as engineered heart tissue for initial screening of the cardiac effects of drugs<sup>15, 17, 18</sup>. Both patches and engineered heart tissue incorporate hPS-CM and been shown to assemble into a functional 3D syncytium with measurable contractility. While these fibrin patches have been shown to be a competent scaffold for supporting hPS-CM contraction many studies implanting these patches onto the epicardial surface have found a collagen interface between the host myocardium and the graft limiting cell migration into the host myocardium<sup>15, 19</sup>. The use of a fibrin microthread suture may help over some these engraftment issues by delivering cells directly into the myocardium instead of on the epicardial surface, however, we must first examine if fibrin microthreads can also support hPS-CM attachment and contraction.

Previous studies have indicated that fibrin microthreads are capable of supporting C2C12 myoblast attachment and survival as well as direct cellular alignment for myoblasts<sup>20</sup>. As cardiomyocytes exist in a highly aligned environment, improved alignment *in vitro* may provide enhanced functional contraction and improvement in integration when implanted in native myocardium. Several groups have used various techniques to examine how improved alignment of cardiomyocytes affects cell function<sup>21-24</sup>. These studies demonstrated that improved alignment using micropatterning or engineered tissues results in a greater degree of electrical anisotropy and higher production of contractile forces. Given the results of these studies it will be important to determine if the fibrin microthreads are capable of guiding hPS-CM

alignment along the threads and if improved alignment results in increased function in terms of higher contractile strains.

As cardiovascular tissue is a highly aligned, contractile organ it will be important to determine if fibrin microthreads are capable of supporting hPS-CM attachment and cell contraction, and directing cellular alignment in a manner that will be beneficial for cell delivery via fibrin microthreads to cardiac tissue. To examine these properties, this objective will utilize different ECM proteins to examine cell attachment. Then, using the method developed and described in objective 2a, we will measure contractile strains, contractile orientation, beat frequency, and conduction velocity using calcium transients of hPS-CM seeded microthreads over three weeks in culture. Additionally, cell alignment will be examined using immunohistochemistry techniques and contractile orientation data. The results of this objective will define the ideal hPS-CM attachment conditions to fibrin microthread and will characterize hPS-CM alignment and mechanical contraction properties when seeded on fibrin microthreads over three weeks in culture.

## 6.2 Materials and methods

### 6.2.1 Seeding platform for hPS-CM attachment to fibrin microthreads

To facilitate hPS-CM seeding individual fibrin microthreads were used and adhered in groups of three to custom polydimethylsiloxane (PDMS) washers (inner diameter: 1.2cm) using medical grade silicone

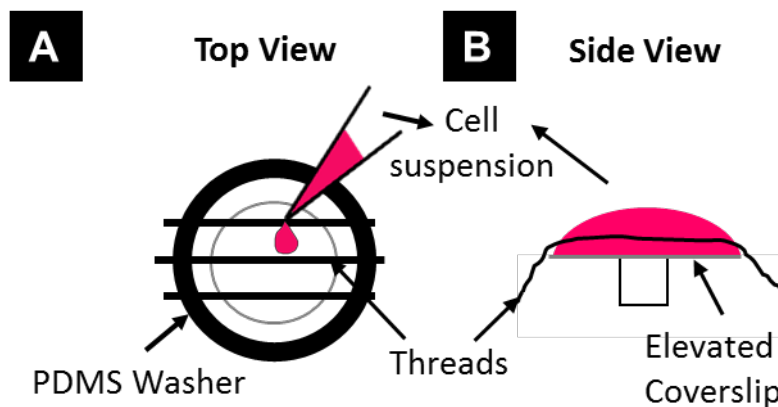


**Figure 6-1. Seeding schematic to seed hPS-CM onto fibrin microthreads.** Individual fibrin microthreads are glued to a PDMS washer (A) and then placed over an elevated 12mm coverslip (B). A 150 $\mu$ L suspension of cells is pipetted onto the coverslip with the threads for cell seeding.

adhesive (Figure 6-1). PDMS constructs with microthreads were placed in a six well plate for ethylene oxide (EtO) sterilization. Constructs were allowed to de-gas for 24 hours after EtO sterilization. Immediately before seeding, microthreads were allowed to rehydrate for 20 minutes in dPBS. Thread constructs were then placed over an elevated 12mm glass coverslip and coated with ECM protein (fibronectin or collagen IV, 10 $\mu$ g/mL) for 2 hours. For hPS-CM seeding, constructs were moved to new 12mm glass coverslip platforms and a 150 $\mu$ L cell suspension (1.33x10<sup>6</sup> cells/mL) in aprotinin (50 $\mu$ g/mL) supplemented RPMI-B27 medium was added to the coverslip (Figure 6-1). Control TCP plates were coated with 0.1% gelatin, collagen IV, or fibronectin and were seeded with hPS-CM at a density of 150,000 cells/cm<sup>2</sup>. Cells were allowed to attach for 18 hours in an incubator at 37°C, after which cell seeded microthreads were moved to a six well plate with fresh RPMI-B27 medium supplemented with aprotinin, medium was changed every 2-3 days.

#### 6.2.2 Effect of ECM surface coatings on hPS-CM attachment

To examine the effect of different surface coatings on hPS-CM attachment to fibrin microthreads, ECM proteins collagen IV and fibronectin were used. The seeding methods from section 6.2.2 was adapted to allow for ECM coatings. After the threads were hydrated and moved to an elevated 12mm coverslip, threads were coated as described in 6.2.2. ECM coatings were allowed to adhere for 2 hours after which constructs were moved to another elevated 12mm coverslip for final cell seeding. Cells were seeded as done in section 6.2.2. 48 hours after seeding, constructs were moved to new wells with fresh medium for continued culture, or microthreads were prepared for a CyQuant assay. All threads from one construct were cut and placed in an eppendorf tube containing 1mL of dPBS. The remaining steps in the CyQuant assay were run as described in section 3.2.4.

#### 6.2.3 Viability of hPS-CM attachment on fibrin microthreads

To characterize cell viability a LIVE/DEAD assay (Life Technologies) was conducted, according to manufactures recommendations, 48 hours after hPS-CM constructs were seeded. Briefly, medium was aspirated and replaced with 1mL of sterile RPMI containing a 4 $\mu$ M ethidium homodimer-1 and 2 $\mu$ M

calcein-AM working solution and plates were incubated at 37C for 15 minutes. The RPMI solution was aspirated and replaced with a 4 $\mu$ M ethidium homodimer-1 and 2 $\mu$ M calcein-AM working solution with Hoechst 33342 (0.5 $\mu$ g/mL; Life Technologies) and plates were incubated for an additional 15 minutes at 37C. Calcein-AM (green Ex/em 495nm/515nm) is retained within the cytoplasm of living cells, while ethidium homodimer-1 (red, Ex/em 495nm/635nm) enters dead cells and binds nuclear DNA, but is excluded from living cells with intact plasma membrane activity. Microthreads were imaged using a Leica DMIL inverted microscope.

#### 6.2.4 Capturing contraction of hPS-CM seeded microthreads

To record the contraction produced by seeded sutures a LEICA DMIL inverted microscope with a Fastec HiSpec4 camera mounted to record video at high magnifications. Video was recorded at 60 frames per second for 25 seconds at a magnification level of 200x at 4 different locations along the length of the thread. To determine the time course of contraction, microthreads were recorded at days 7, 14, and 21 post seeding. Collagen IV, fibronectin, and fibrin only hPS-CM seeded sutures were analyzed. Parallel control experiments were run with hPS-CM plated on fibronectin (10 $\mu$ g/mL) and collagen IV (10 $\mu$ g/mL) coated TCP at a density of 150,000cells/cm<sup>2</sup>. The data was analyzed using HDM as described in chapter 5. For contractility alignment, the angle of the principal strain (E2) was calculated in MATLAB utilizing the following formula where Exx, Eyy, and Exy are the x, y, and shear components of strain:

```
E1_angle (radians)=0.5*atan2(2*(Exy),Exx-Eyy)
E1_angle (degrees)=E1_angle (radians)*180/pi()
E2_angle (degrees)=E1_angle (degrees)-90
```

The values of the E2 angle were calculated for zero to peak of E2, for each contraction cycle, and were compared to the angle of the microthread and the difference between the two was determined. The percent of total angle differences between 0-13 degrees were reported for days 7, 14, and 21. 0-13 degrees was chosen as cardiomyocytes within human myocardium are aligned within 13 degrees<sup>25</sup>.

### 6.2.5 Immunocytochemistry

At day 1, 4, 7, 14, and 21 hPS-CM seeded microthreads were fixed in 4% paraformaldehyde for 10 minutes, rinsed with PBS and blocked in 5% goat serum or 1.5% rabbit serum in PBS for 45 minutes. Primary antibodies were applied at a dilution of 1:100 (mouse-anti-alpha actinin, Abcam; rabbit-anti-connexin-43, Cell Signaling Technologies) at 4°C overnight. Cells were incubated for an hour in the appropriate secondary antibodies (AF488 anti-mouse 1:400, AF568 anti-rabbit, Invitrogen). Cells were counterstained using Hoechst 33342 (0.5ug/mL, Life Technologies) for 5 minutes. Images were obtained using a Leica laser scanning confocal microscope.

### 6.2.6 Conduction velocity measurements

hPS-CM seeded sutures were loaded with Fluo-4 AM and recorded at days 7, 14, and 21 as described in chapter 5 in sections 5.2.3 and 5.2.4. Calcium transient analysis was done as described in 5.2.5 with the exception that 2-3 regions along the thread were analyzed. Calcium transients for each region were then plotted together and the frame difference between the start frames of each calcium transient cycle for the different regions was recorded and the time delay was calculated. Next, the distance between the center points of each region was calculated using ImageJ. Conduction velocity was then calculated by dividing the distance between the regions by the time delay between the initiations of the calcium transients and is reported in cm/s.

### 6.2.7 Alpha-actinin fiber alignment

Confocal images of alpha-actinin stained hPS-CM seed on microthreads and TCP were uploaded to ImageJ (NIH) for actinin fiber alignment using OrientationJ. Briefly, each image was split into its green channel and each section of fibers were outlined and analyzed. Output angle data for each image was averaged and compared to the angle of the thread and reported as the difference between the thread angle and the average fiber angle.

### 6.2.8 Statistical analysis

Statistical analyses were performed using GraphPad Prism 6 (GraphPad Software, Inc.). Comparisons between seeding conditions, alignment data, and conduction velocities were analyzed using a one-way

analysis of variance (ANOVA), with a post-hoc Tukey test for multiple comparisons. Comparisons for contractile parameters of hPS-CM seeded on different surface coatings (threads and TCP) between time points were done using a two-way ANOVA with a Tukey post-hoc analysis for multiple comparisons. Comparisons were done including all data from threads and TCP, and separately with data from just plates groups and just threads groups to elucidate differences washed out when all groups across time and culture substrates were compared. A Pearson linear correlation coefficient was calculated in excel using the PEARSON function to assess the strength of correlation between contractile alignment and contractile strain. Cell attachment number, contractile strain, maximum strain, actinin alignment, and conduction velocity are reported as mean±SEM, frequency data is reported as mean±SD. Significance was considered at p<0.05.

### 6.3 Results

#### 6.3.1 Collagen IV coating improves hPS-CM attachment to fibrin microthreads

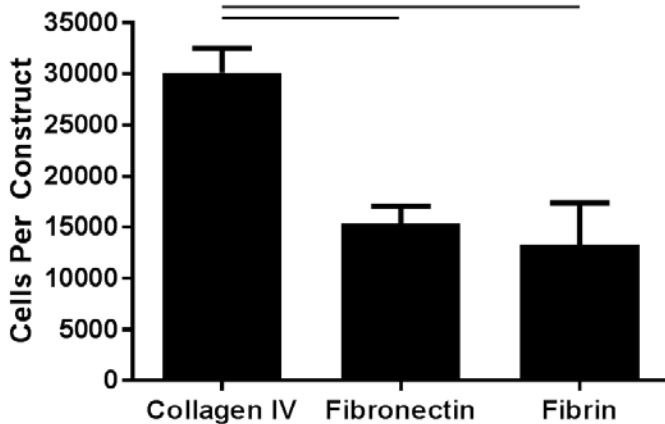


**Figure 6-2. Collagen IV ECM coating enhances hPS-CM attachment to fibrin microthreads.** Fibrin sutures were coated with collagen IV, fibronectin or no coating (fibrin) and were seeded with hPS-CM. A CyQuant DNA assay was used to quantify cell attachment per construct of three threads two days post seeding. Fibrin microthreads coated with collagen IV significantly improved hPS-CM attachment over fibronectin coated or non-coated fibrin microthreads. Mean±SEM. n=3-4, -p<0.05.

Fibronectin and collagen IV ECM protein coatings were evaluated against fibrin only to determine how ECM protein coating would affect hPS-CM attachment. Immunohistochemistry confirmed that both fibronectin and collagen IV proteins coatings resulted in positive expression of fibronectin and collagen IV on the surface of the microthread. Cell attachment was measured and quantified two days post seeding using a CyQuant DNA assay. hPS-

CM attachment was observed for all conditions, with significantly higher cells attached on the collagen IV coated microthreads (n=3-4, p<0.05, Figure 6-2). Increases in cell attachment and using different protein



coatings did not appear to affect cell viability as indicated qualitatively by a LIVE/DEAD stain completed 2 days post seeding (Figure 6-3).

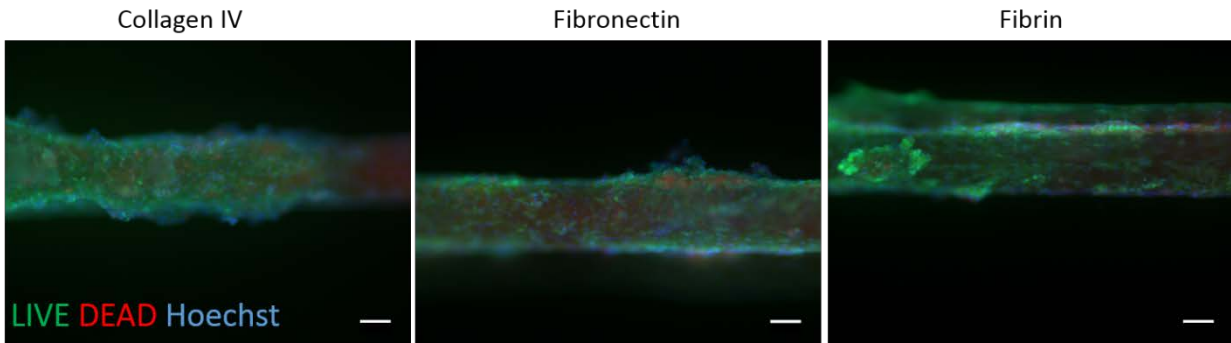


**Figure 6-3. hPS-CM seeded onto fibrin microthreads remain viable.** hPS-CM were seeded onto Collagen IV, fibronectin, and non-coated fibrin microthreads (fibrin). A LIVE/DEAD (live in green, dead in red) staining assay qualitatively confirmed cell viability 2 days after seeding. Scale bar=0.1mm

### 6.3.2 hPS-CM exhibit opposite temporal trends in contractile and maximum strains when cultured on TCP and fibrin microthreads

To examine contractile behavior, contractile and maximum contractile strains were evaluated from hPS-CM seeded TCP (0.1% gelatin, collagen IV, and fibronectin coated) and microthreads (fibrin, fibronectin and collagen IV coated) at days 7, 14, and 21 post seeding. On TCP both contractile strains and maximum contractile strains followed similar trends such that cells cultured on TCP produced decreased strains over 21 days. Cells on TCP exhibit a significantly different decrease in contractile strain beginning at  $4.23 \pm 0.23\%$  on day 7 and ending at  $3.08 \pm 0.19\%$  on day 21 (Figure 6-4A,  $n=18$ ,  $p < 0.05$ ). Maximum strain followed a similar trend; cells on TCP had a maximum strain of

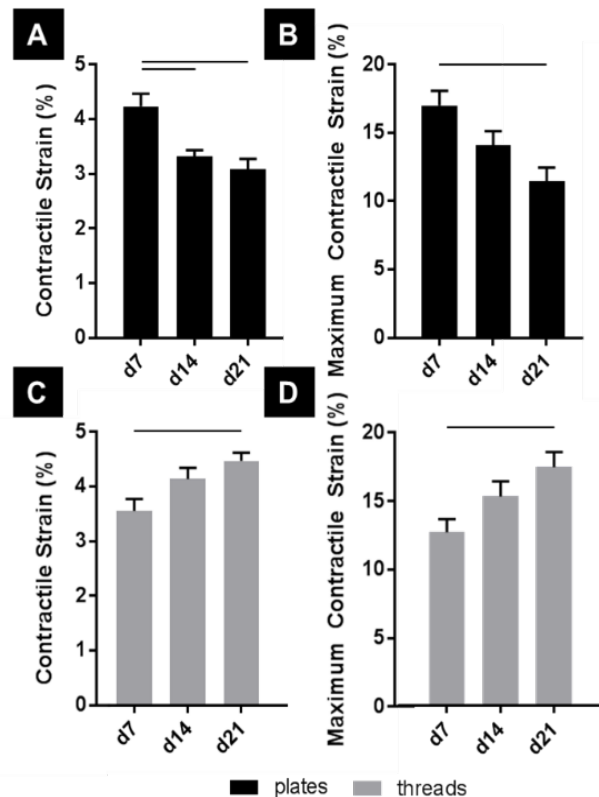


**Figure 6-4. hPS-CM exhibit opposite trends in contractile and maximum strains when cultured on TCP and fibrin microthreads over 21 days.** Contractile strain (A, C) and maximum contractile strain (B, D) was determined using HDM at days 7 (d7), 14 (d14), and 21 (d21). HPS-CM exhibit a significant decrease in contractile (A) and maximum strains (B) when cultured on TCP over 21 days. Conversely, hPS-CM cultured on fibrin microthreads exhibit an increase contractile (C) and maximum strains (D) over 21 days. Mean $\pm$ SEM for contractile and maximum strain,  $n=18$ ,  $p < 0.05$ .

17.01±1.07% on day 7, which significantly decreased to 11.48±0.99% on day 21 (Figure 6-4B, n=18, p<0.05). hPS-CM seeded on microthreads increased contractile and maximum contractile strains over 21 days. At day 7, hPS-CM seeded on microthreads begin at a contractile strain of 3.56±0.22% and increased contractile strain to 4.47±0.29% on day 21 (Figure 6-4C, n=18, p<0.05). In terms of maximum contractile strain, hPS-CM seeded on microthreads produced a maximum strain on day 7 of 12.70±0.94% which significantly increased to a maximum strain of 17.44±1.09% on day 21 (Figure 6-4D, n=18, p<0.05).

Looking between culture substrate and over time, cells cultured on TCP and microthreads exhibited significantly different contractile strains on days 7, 14, and 21, and significantly different maximum strains on days 7 and 21 (Figure 6-5, n=18, p<0.05). Both contractile and maximum strains ended at higher values at day 21 for hPS-CM cultured on fibrin microthreads than the strains produced by hPS-CM cultured on TCP began at on day 7. Contractile and maximum strains followed similar trends between coating groups, on TCP and on microthreads over 21 days, with no significant differences between groups.

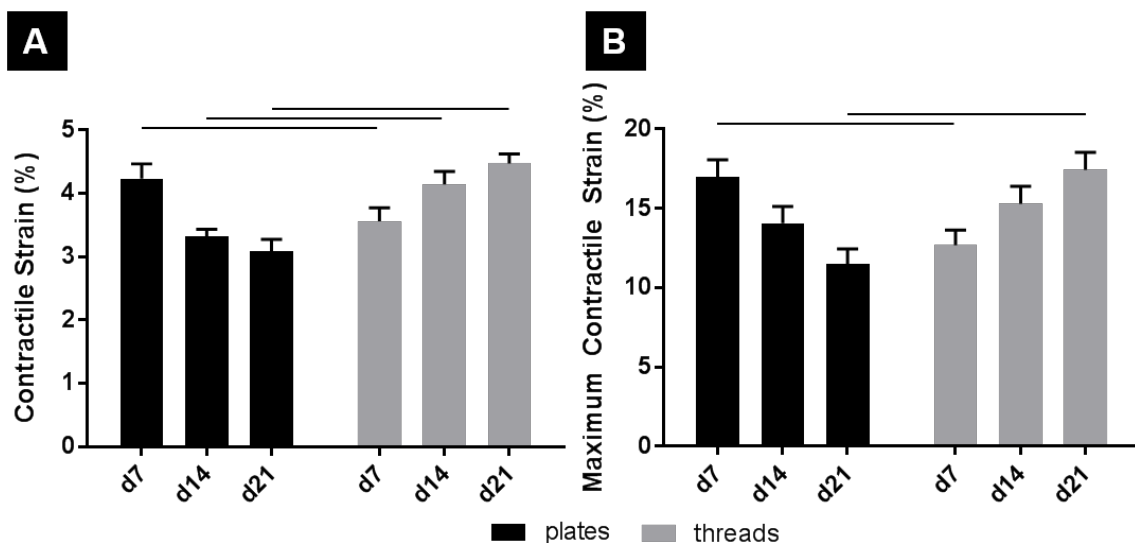


**Figure 6-5. hPS-CM exhibit significantly higher contractile and maximum strains when cultured on fibrin microthread compared to TCP by 21 days.** Contractile strain (A) and maximum contractile strain (B) was determined using HDM at days 7 (d7), 14 (d14), and 21 (d21). hPS-CM cultured on fibrin microthreads exhibit significantly different contractile strains, at all-time points, and maximum strains, at days 7 and 21, than cells cultured on TCP. Mean±SEM, n=18, p<0.05.

### 6.3.3 Contractile frequency increases over 21 days for hPS-CM cultured on TCP and microthreads

Beat frequency was examined to determine if there were any changes in beat rate for hPS-CM seeded on microthreads or TCP over 21 days (Figure 6-6). Frequency significantly increased from day 7 to day 21 for both TCP and microthread groups; from  $0.83 \pm 0.25 \text{ Hz}$  to  $1.11 \pm 0.45 \text{ Hz}$  for the TCP group and from  $0.84 \pm 0.15 \text{ Hz}$  to  $1.03 \pm 0.19 \text{ Hz}$  for the

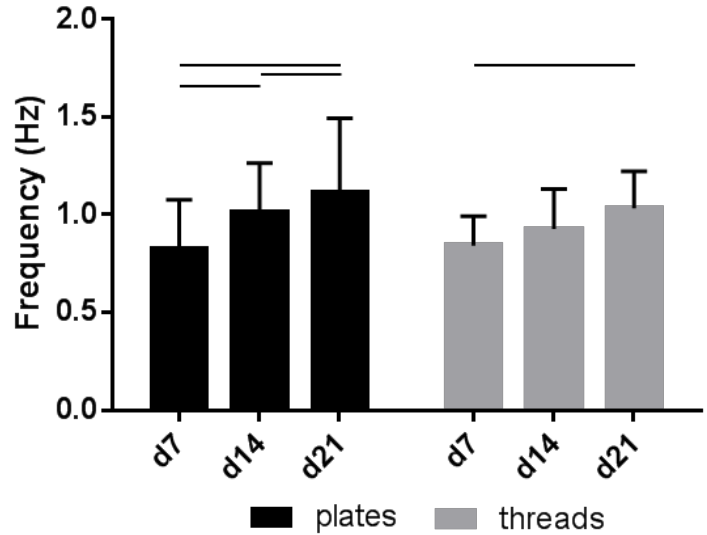


**Figure 6-6. Contractile frequency increased over 21 days for hPS-CM cultured on TCP and fibrin microthreads.** Contractile frequency was determined on days 7 (d7), 14 (d14), and 21 (d21). hPS-CM significantly increased beat frequency between day 7 and day 21 for both culture conditions. Mean $\pm$ SD, n=18,  $-p < 0.05$ .

microthread group (n=18,  $p < 0.05$ ). No differences were found between TCP and microthread groups for any time points. Frequency was found to increase over time for all surface coatings, on microthreads and TCP, with no differences between groups.

#### 6.3.4 hPS-CM contraction direction becomes more aligned with the thread over 21 days in culture

hPS-CM seeded on non-coated, collagen IV and fibronectin coated fibrin microthreads were used to examine changes in cellular alignment to the fibrin microthreads in terms of direction of principal contraction (n=17-18, Figure 6-7). Values reported are the percentage of cells that contracted within 0-13

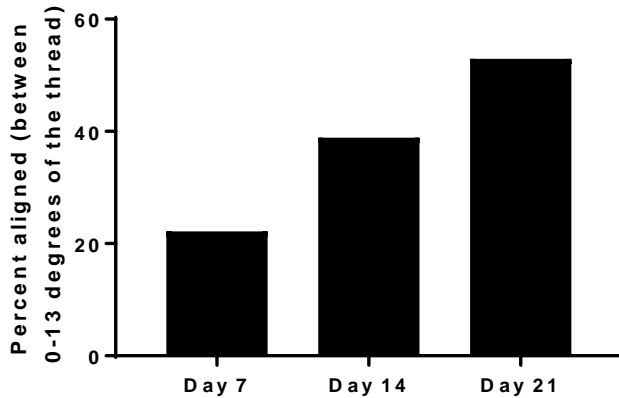


**Figure 6-7. hPS-CM contract with higher alignment to the microthread at later timepoints.** The angle of contraction was determined for days 7, 14, and 21 and was calculated as the difference between the contraction angle and the angle of the thread. A histogram was plotted and the percentage aligned between 0-13 degrees is represented here. Over 21 days in culture a higher percentage of hPS-CM contract in the same direction (within 13 degrees) as the microthread. n=17-18.

degrees of the direction of the fibrin microthread. At day 7 only 22% of cells contracted within 13 degrees of the direction the fibrin microthread, this increased to 53% by day 21. Additionally, hPS-CM seeded on TCP did not exhibit the same trend over 21 days in culture as cells had wide ranges of principal contraction angles at all-time points indicating that they remained unaligned over 21 days.

When contractile alignment was plotted together with changes in contractile strain over 21 days there was a linear relationship between contractile alignment and contractile strain for hPS-CM seeded on sutures (Figure 6-8). A Pearson linear correlation coefficient of 0.99 between variables was found indicating a strong correlation between increases in contractile alignment and contractile strain. For hPS-CM cultured on TCP contractile strain decreased over 21 days with no major change in alignment as indicated by the flat orange trendline in Figure 6-8 and a Pearson linear correlation coefficient of -0.20.

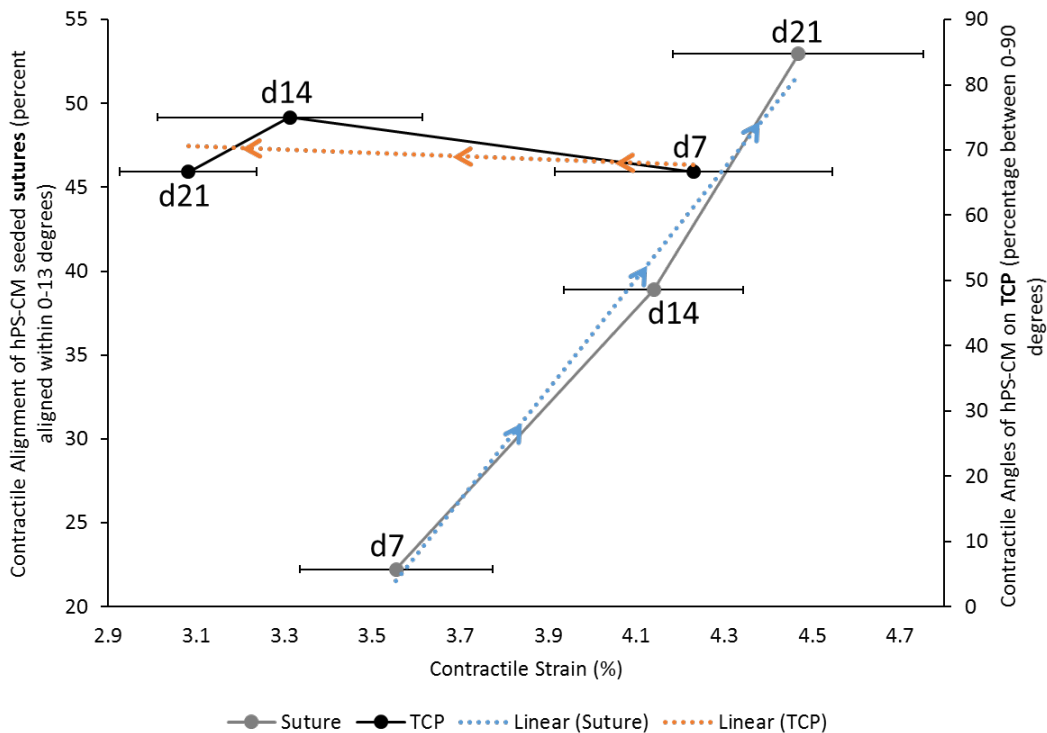


**Figure 6-8 A linear relationship exists between contractile alignment and contractile strain for hPS-CM seeded on fibrin sutures, not on TCP.** Over 21 days in culture hPS-CM seeded on fibrin microthreads (grey line) increased both alignment and contractile strain in a linear fashion with a Pearson correlation coefficient of 0.99. hPS-CM on TCP (black line) decreased contractile strain with no major change in alignment over 21 days. The grey dots with a blue trendline is representative of the suture group and follows the left y-axis. The black line with an orange trendline is representative of the TCP group and follows the right y-axis. Mean±SEM, n=18. Arrows indicate the direction of strain increase or decrease over time.

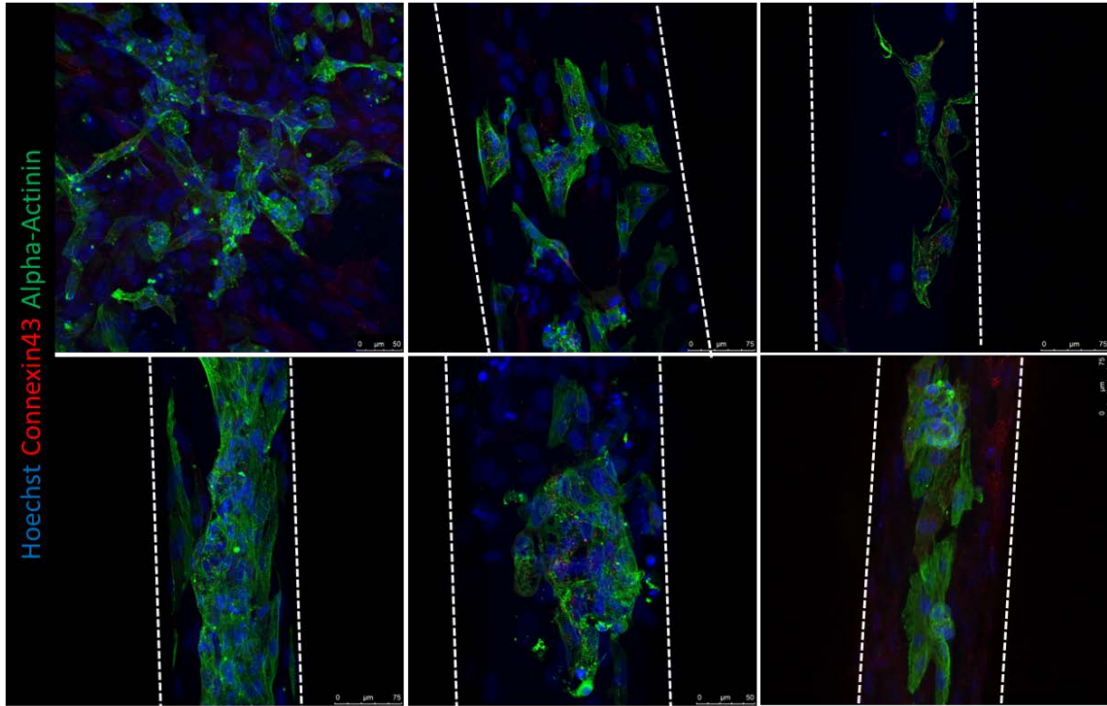


**Figure 6-9. hPS-CM seeded onto fibrin microthreads express alpha-actinin and connexin 43.** hPS-CM seeded onto Collagen IV coated fibrin microthreads express alpha-actinin and connexin 43 proteins at days 1, 4, 7, 14, and 21 in culture. Cells at later time points appeared more aligned along the length of the fibrin microthread with no major differences in alpha-actinin or connexin 43 expression patterns at any time point.

### 6.3.5 hPS-CM become more aligned along the microthread over 21 days in culture

Alpha-actinin and connexin 43 staining were utilized to determine hPS-CM morphology up to 21 days in culture. hPS-CM were readily attached to microthreads at all-time points and exhibited positive alpha-

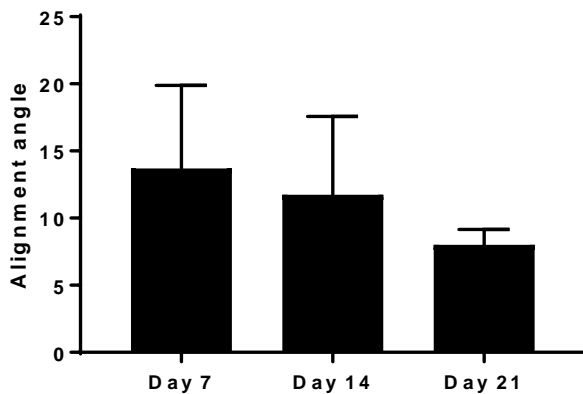


**Figure 6-10. hPS-CM demonstrate better alignment to the microthread at later timepoints.** Alpha-actinin staining at days 7, 14, and 21 was used to calculate the angle of the cells and was compared to the angle of the microthread. A lower alignment angle indicated a better alignment to the thread. Over 21 days in culture alpha-actinin staining indicated hPS-CM were aligned more closely with the microthread direction. Average difference in fiber angle and thread angle is reported. Mean±SEM, n=4-28, NS.

actinin and connexin 43 staining (Figure 6-9).

Cells were less elongated at the earlier time points, 1 and 4 days. By day 7 cells had begun to elongate along the direction of the microthread and exhibited more organized sarcomere structure. Quantifying alignment demonstrated that hPS-CM at day 7 were aligned within 13.7±6.2 degrees to the thread, compared to 11.7±5.8 and 8.0±1.1 degrees on days 14 and 21, respectively

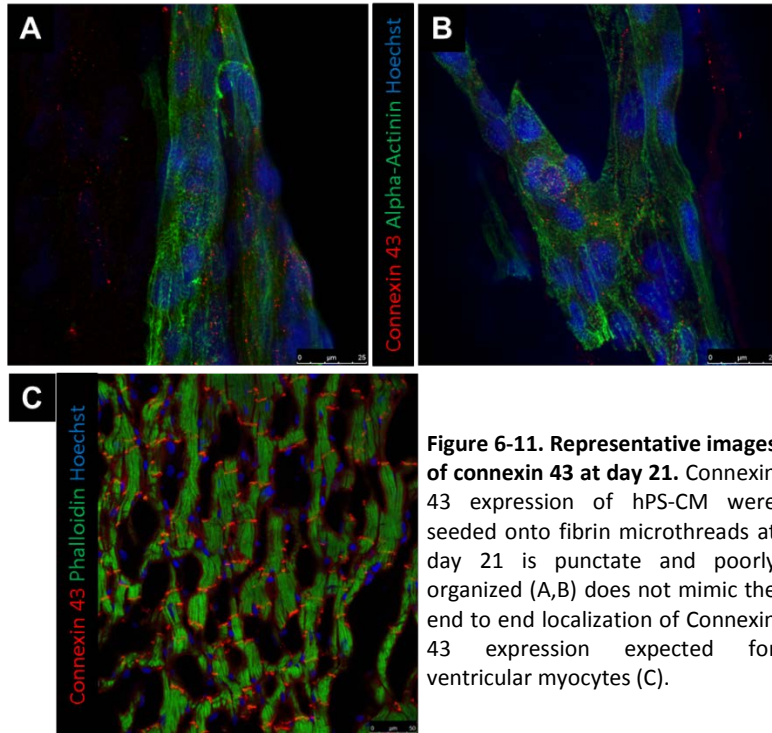


**Figure 6-11. Representative images of connexin 43 at day 21.** Connexin 43 expression of hPS-CM seeded onto fibrin microthreads at day 21 is punctate and poorly organized (A,B) does not mimic the end to end localization of Connexin 43 expression expected for ventricular myocytes (C).

(n=4-28 images, NS, Figure 6-10). Cells on TCP exhibited no dominate fiber alignment as indicated by a range of fiber angles from -86.6 to 86.4 degrees (n=43 cell regions) Cells demonstrated positive connexin 43 staining, however at all-time points the staining was diffuse through the cells with no evidence of organization and polarization to the intercalated disks (Figure 6-9 and Figure 6-11).

### 6.3.6 hPS-CM seeded on microthreads increase conduction velocity over 21 days in culture

Using the system developed in objective 2A we examined calcium transients in terms of conduction velocity of hPS-CM seeded on fibrin microthreads. High speed videos of hPS-CM seeded on microthreads loaded with fluo-4 dye were analyzed for calcium transient intensity over 2-3 regions along the microthread to determine conduction velocity at days 7, 14, and 21. Conduction velocities significantly increased from  $3.69 \pm 1.76 \text{ cm/s}$  at day 7 to  $24.26 \pm 8.42 \text{ cm/s}$  at day 21 (Figure 6-12, n=5-6,  $p < 0.05$ ).

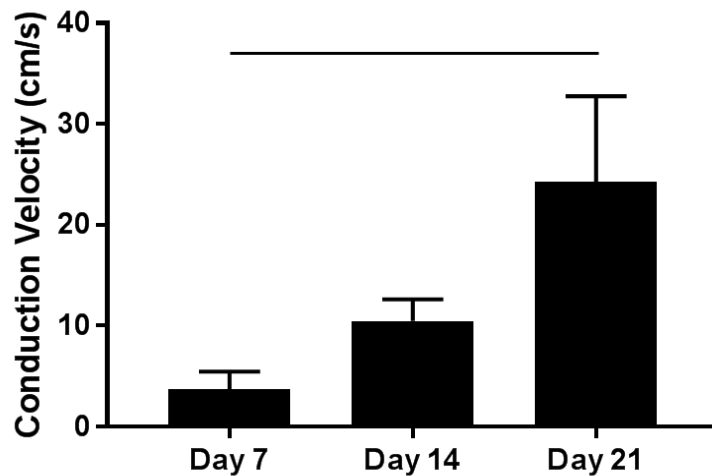


**Figure 6-12. Conduction velocity of hPS-CM seeded sutures.** High speed videos of Fluo-4 loaded hPS-CM seeded on fibrin microthreads were analyzed for calcium transient intensity over different regions along the microthread and the time difference between regions was used to calculate conduction velocity. Conduction velocities were found to significantly increase from  $3.7 \text{ cm/s}$  to  $24.3 \text{ cm/s}$  over 21 days in culture. Mean  $\pm$  SEM, n=5-6,  $p < 0.05$ .

#### 6.4 Discussion

The goals of this objective were to define the seeding conditions and time to obtain a contractile hPS-CM seeded microthread and characterize the cells contractile behavior when seeded on the microthreads. Different ECM surface coatings were used to improve cell attachment. Fibronectin and collagen IV were chosen due to their presence in cardiac basement membrane. Additionally, other studies seeding hPS-CM on various substrates have demonstrated successful hPS-CM attachment using fibronectin and collagen IV coatings<sup>11, 13</sup>. hPS-CM attached with higher quantities to collagen IV coated microthreads two days after seeding. All conditions did allow hPS-CM attachment, suggesting that hPS-CM preferentially attached to collagen IV coated microthreads, but a protein coating is not necessary to obtain hPS-CM attachment on fibrin microthreads. Qualitatively, protein coatings did not affect cell viability as the majority of cells attached were found to be viable for all conditions.

In regards to contractility, hPS-CM seeded on microthreads began to contract within 7 days after seeding and cell contraction was observed for all conditions. Beat frequency increased over 21 days for hPS-CM seeded on microthreads and on TCP to above 1Hz, a similar finding to other groups<sup>26, 27</sup>. Contractile strain and maximum strain was found to increase over 21 days for hPS-CM seeded on microthreads. These values, at all-time points, were significantly different than the contractile strain and maximum strains produced by hPS-CM on TCP, which were found to decrease over 21 days. Maximum contractile strains produced by hPS-CM on the microthreads near the 19% strain that is produced by adult human myocardium<sup>28</sup>. Other tissue engineered constructs, such as the engineered heart tissue created by Eng *et al.* have demonstrated strains upwards of 17%, however these tissues needed to be electrically stimulated to produce higher strains where the unstimulated controls only produced strains of 10%<sup>27</sup>.

Cardiomyocytes exist in an environment that requires them to be highly aligned and organized to produce efficient contractions. In order to investigate the relationship of alignment with strain changes over time we sought to quantify cell alignment to determine the effect cell alignment may have had on



changes in strain. Within a given layer of healthy myocardium, cardiomyocytes are aligned within 13 degrees of each other<sup>25</sup>. The same would be expected of hPS derived cardiomyocytes. Additionally, previous studies have suggested the ability for fibrin microthreads to direct cell orientation along the microthread<sup>20</sup>. We demonstrated that over 21 days in culture the direction of cell contraction was more aligned along thread. Additionally, alignment was confirmed by immunohistochemical stains as cells aligned more closely to the thread over 21 days with a final alignment within 8 degrees of the thread. Studies in two and three dimensions have demonstrated the importance of cardiomyocyte alignment on improving contractility compared to unaligned controls<sup>24, 29</sup>. As contractile strains and maximum strains increased over 21 days for hPS-CM seeded on microthreads, this would suggest that these cells are able to produce higher strains because they are contract in a direction more aligned with the microthreads. No principal contraction alignment was found for cells cultured on TCP, which may explain the decrease in strains produced by these cells over time.

Conduction velocity in a ventricular myocardial tissue is around to 50cm/s<sup>30, 31</sup>. Here, using calcium transient analysis we demonstrated conduction velocities that began at 3.7cm/s on day 7 and increased by day 21 to a mean of 24.2cm/s with some reaching 46.3cm/s. Not only do these conduction velocities near that of human myocardium, but increasing conduction velocities over time would suggest that this increase may be due to the higher alignment of hPS-CM over time. Other studies have indicated a similar trend in conduction velocities where aligned cultures of cardiomyocytes demonstrated a 1.6 increase in conduction velocity<sup>32</sup>.

Alignment may not be the only contribution to changes in strain over time, substrate stiffness may also play a role in how much strain the cells can produce. We demonstrated that the hPS-CM seeded on the fibrin microthreads aligned along the thread and increased their contractile strains over 21 days whereas cells on tissue culture plastic had no dominate alignment and decreased contractile strains over time. While alignment may be driving this increase in contractile strain it is possible that substrate stiffness

plays a role. Hydrated fibrin microthreads have a modulus value around 2.2MPa<sup>20</sup> whereas tissue culture plastic has a modulus value on the gigapascal range<sup>33</sup> which is significantly stiffer than human myocardial tissue, which can range in stiffness from 20-500kPa<sup>34</sup>. It has been demonstrated that increased cell functionality may be a function of both substrate stiffness and alignment<sup>35-38</sup>. McDevitt *et al.* demonstrated that cardiomyocytes patterned on glass coverslips lost their alignment over 10 days in culture suggesting that the stiff glass substrate is unfavorable to cardiomyocytes even though they had originally been patterned in an aligned manner<sup>37</sup>. Ribeiro *et al.* used matrigel micropatterns on physiologically relevant degrees of stiffness to constrain hPS-CMs into rectangular shapes that follow a physiological 7:1 aspect ratio<sup>24</sup>. These patterned hPS-CM were capable of producing higher contractile forces and improved myofibril alignment. The studies by McDevitt and Ribeiro were done on glass coverslips, however cardiomyocytes exist in a 3D environment and thus it is important to consider the effects of alignment and stiffness in an environment that better mimics myocardium. Chrobak *et al.* examined cardiomyocyte function using an unaligned fibrin gel with a modulus of approximately 0.25kPa<sup>39</sup>. She demonstrated contractile strains that decreased over time suggesting that in a soft unaligned environment cardiomyocytes are unable to increase strains over time. Black *et al.* demonstrated that an aligned cardiomyocyte populated fibrin gel was capable of increased twitch forces at 2 weeks in culture over unaligned controls<sup>40</sup>. These results, in conjunction with the data presented here, suggest that neither an unaligned soft substrate or an aligned stiff substrate are enough to improve cardiomyocyte function, but that a soft substrate that promotes alignment may be ideal for cardiomyocyte function.

When hPS-CM were seeded onto collagen IV coated tissue TCP, cells retained their contractile nature, but lacked a rod like phenotype with the organized sarcomere structure expected of mature cardiomyocyte. Connexin 43 is a protein found in cardiac connexons, which make up gap junctions that connect cardiomyocytes. To facilitate cardiac conduction, gap junctions are organized end-to-end at the

intercalated disks within cardiac tissue. Qualitatively, no organizational differences in connexin 43 staining was found for hPS-CM seeded on TCP or fibrin microthreads at any time points. However, we demonstrated that conduction velocity increased over 21 days, yet Connexin 43 expression did not appear to be more localized by 21 days. Studies have shown that increases in conduction velocity may not be solely Connexin 43 dependent. Cardiac conduction can be determined by several factors including membrane excitability, intercellular coupling, as well as the size, shape and orientation of the cardiomyocytes<sup>41, 42</sup>. de Boer *et al.* utilized a geometrically defined culture of immature cardiomyocytes and demonstrated that  $\beta$ -adrenergic induced increases in conduction velocity were due to changes in the intrinsic excitability of the cardiomyocytes and not alterations in gap junctional coupling. In adult mice with induced deletion of Connexin 43 a 50% decrease in the Connexin 43 protein did not have any impact on conduction velocity<sup>43</sup>. In a similar study, a 50% decrease in *Scn5a*, a gene that encodes sodium channel Nav1.5, demonstrated reduction in conduction velocity<sup>44</sup>. To examine this phenomenon at the cellular level strands of neonatal cardiac myocytes with a 43% reduction in Connexin 43 levels demonstrated no significant decrease in conduction velocity, but did demonstrate a significant increase in the action potential upstroke suggesting an increase in sodium channels. The data presented in these studies suggest that an increase in membrane excitability, plays an important role in conduction velocity. While not directly explored here, it is possible that Connexin 43 localization was not the main driver for the increase in conduction velocity and that increases in membrane excitability and alignment have a role.

However, it is still important to note that many of these differences in alpha-actinin and Connexin 43 organization and localization can be attributed to the immature phenotype of hPS-CM<sup>45</sup>. This suggests that further steps will be necessary for enhanced maturation of Connexin 43 localization and sarcomere organization of hPS-CM even given a substrate that promotes cell alignment. Others have shown that extended culture, as well incorporating electrical and mechanical stimulation can provide the cues necessary to impart maturation leading to improvements in cardiomyocytes functionality<sup>45-48</sup>.

The findings in this chapter suggest that hPS-CM are capable of attaching to fibrin microthreads, however a collagen IV protein coating improves hPS-CM attachment to fibrin microthreads. Additionally, hPS-CM were able to contract and align to the microthreads over 21 days in culture. By day 14 cells seeded sutures were contracting at a frequency of a human heart and were producing strains nearing those produced by human myocardium. These findings suggest that cell seeded sutures should be cultured on the microthreads beyond 7 days in order to deliver a more aligned, higher functioning contractile bundle for *in vivo* delivery.

## 6.5 References

1. Guyette JP, Fakharzadeh M, Burford EJ, Tao ZW, Pins GD, Rolle MW and Gaudette GR. A novel suture-based method for efficient transplantation of stem cells. *Journal of biomedical materials research Part A*. 2013;101:809-18.
2. Proulx MK, Carey SP, Ditroia LM, Jones CM, Fakharzadeh M, Guyette JP, Clement AL, Orr RG, Rolle MW, Pins GD and Gaudette GR. Fibrin microthreads support mesenchymal stem cell growth while maintaining differentiation potential. *Journal of biomedical materials research Part A*. 2011;96:301-12.
3. Baharvand H, Azarnia M, Parivar K and Ashtiani SK. The effect of extracellular matrix on embryonic stem cell-derived cardiomyocytes. *Journal of molecular and cellular cardiology*. 2005;38:495-503.
4. Tsuchiya K, Chen G, Ushida T, Matsuno T and Tateishi T. Effects of cell adhesion molecules on adhesion of chondrocytes, ligament cells and mesenchymal stem cells. *Materials Science and Engineering: C*. 2001;17:79-82.
5. Lundgren E, Terracio L and Borg TK. Adhesion of cardiac myocytes to extracellular matrix components. *Basic research in cardiology*. 1985;80 Suppl 1:69-74.
6. Ogura N, Kawada M, Chang W-J, Zhang Q, Lee S-Y, Kondoh T and Abiko Y. Differentiation of the human mesenchymal stem cells derived from bone marrow and enhancement of cell attachment by fibronectin. *J Oral Sci*. 2004;46:207-13.
7. van Laake LW, van Donselaar EG, Monshouwer-Kloots J, Schreurs C, Passier R, Humbel BM, Doevendans PA, Sonnenberg A, Verkleij AJ and Mummery CL. Extracellular matrix formation after transplantation of human embryonic stem cell-derived cardiomyocytes. *Cellular and molecular life sciences : CMLS*. 2010;67:277-90.
8. Docheva D, Popov C, Mutschler W and Schieker M. Human mesenchymal stem cells in contact with their environment: surface characteristics and the integrin system. *Journal of cellular and molecular medicine*. 2007;11:21-38.
9. Prowse AB, Chong F, Gray PP and Munro TP. Stem cell integrins: implications for ex-vivo culture and cellular therapies. *Stem cell research*. 2011;6:1-12.
10. Ross RS and Borg TK. Integrins and the Myocardium. *Circ Res*. 2001;88:1112-1119.
11. Moyes KW, Sip CG, Obenza W, Yang E, Horst C, Welikson RE, Hauschka SD, Folch A and Laflamme MA. Human embryonic stem cell-derived cardiomyocytes migrate in response to gradients of fibronectin and Wnt5a. *Stem Cells Dev*. 2013;22:2315-25.
12. Ross RS. The extracellular connections: the role of integrins in myocardial remodeling. *Journal of cardiac failure*. 2002;8:S326-31.
13. Rodriguez M, Graham BT, Pabon LM, Han SJ, Murry CE and Sniadecki N. Measuring the Contractile Forces of Human Induced Pluripotent Stem Cell-Derived Cardiomyocytes with Arrays of Microposts. *J Biomech Eng*. 2014.
14. Uosaki H. Efficient and Scalable Purification of Cardiomyocytes from Human Embryonic and Induced Pluripotent Stem Cells by VCAM1 Surface Expression. *PLoS One*. 2011;6.
15. Wendel JS, Ye L, Tao R, Zhang J, Zhang J, Kamp TJ and Tranquillo RT. Functional Effects of a Tissue-Engineered Cardiac Patch From Human Induced Pluripotent Stem Cell-Derived Cardiomyocytes in a Rat Infarct Model. *Stem Cells Transl Med*. 2015;4:1324-32.
16. Christoforou N, Liao B, Chakraborty S, Chellapan M, Bursac N and Leong KW. Induced pluripotent stem cell-derived cardiac progenitors differentiate to cardiomyocytes and form biosynthetic tissues. *PLoS One*. 2013;8:e65963.
17. Liao B, Christoforou N, Leong KW and Bursac N. Pluripotent stem cell-derived cardiac tissue patch with advanced structure and function. *Biomaterials*. 2011;32:9180-7.
18. Mannhardt I, Breckwoldt K, Letuffe-Brenière D, Schaaf S, Schulz H, Neuber C, Benzin A, Werner T, Eder A, Schulze T, Klampe B, Christ T, Hirt Marc N, Huebner N, Moretti A, Eschenhagen T and Hansen A. Human Engineered Heart Tissue: Analysis of Contractile Force. *Stem Cell Reports*. 2016;7:29-42.

19. Ye L, Chang Y-H, Xiong Q, Zhang P, Zhang L, Somasundaram P, Lepley M, Swingen C, Su L, Wendel JS, Guo J, Jang A, Rosenbush D, Greder L, Dutton JR, Zhang J, Kamp TJ, Kaufman DS, Ge Y and Zhang J. Cardiac repair in a porcine model of acute myocardial infarction with human induced pluripotent stem cell-derived cardiovascular cell populations. *Cell stem cell*. 2014;15:750-761.
20. Grasman JM, Pumphrey L, Dunphy M, Perez-Rogers J and Pins GD. Static Axial Stretching Enhances the Mechanical Properties and Cellular Responses of Fibrin Microthreads. *Acta biomaterialia*. 2014;10:4367-4376.
21. Bian W, Jackman CP and Bursac N. Controlling the Structural and Functional Anisotropy of Engineered Cardiac Tissues. *Biofabrication*. 2014;6:024109-024109.
22. Ma Z, Koo S, Finnegan MA, Loskill P, Huebsch N, Marks NC, Conklin BR, Grigoropoulos CP and Healy KE. Three Dimension Filamentous Human Cardiac Tissue Model. *Biomaterials*. 2014;35:1367-1377.
23. Pong T, Adams WJ, Bray M-A, Feinberg AW, Sheehy SP, Werdich AA and Parker KK. Hierarchical architecture influences calcium dynamics in engineered cardiac muscle. *Experimental biology and medicine (Maywood, NJ)*. 2011;236:366-373.
24. Ribeiro AJS, Ang Y-S, Fu J-D, Rivas RN, Mohamed TMA, Higgs GC, Srivastava D and Pruitt BL. Contractility of single cardiomyocytes differentiated from pluripotent stem cells depends on physiological shape and substrate stiffness. *Proc Natl Acad Sci U S A*. 2015;112:12705-10.
25. Lee WN, Pernot M, Couade M, Messas E, Bruneval P, Bel A, Hagege AA, Fink M and Tanter M. Mapping Myocardial Fiber Orientation Using Echocardiography-Based Shear Wave Imaging. *IEEE Transactions on Medical Imaging*. 2012;31:554-562.
26. Hescheler J, Halbach M, Egert U, Lu ZJ, Bohlen H, Fleischmann BK and Reppel M. Determination of electrical properties of ES cell-derived cardiomyocytes using MEAs. *Journal of electrocardiology*. 2004;37, Supplement:110-116.
27. Eng G, Lee BW, Protas L, Gagliardi M, Brown K, Kass RS, Keller G, Robinson RB and Vunjak-Novakovic G. Autonomous beating rate adaptation in human stem cell-derived cardiomyocytes. *Nat Commun*. 2016;7.
28. Taylor RJ, Moody WE, Umar F, Edwards NC, Taylor TJ, Stegemann B, Townend JN, Hor KN, Steeds RP, Mazur W and Leyva F. Myocardial strain measurement with feature-tracking cardiovascular magnetic resonance: normal values. *European Heart Journal - Cardiovascular Imaging*. 2015;16:871-881.
29. Bian W, Jackman CP and Bursac N. Controlling the structural and functional anisotropy of engineered cardiac tissues. *Biofabrication*. 2014;6:024109.
30. Dhillon PS, Gray R, Kojodjojo P, Jabr R, Chowdhury R, Fry CH and Peters NS. Relationship Between Gap-Junctional Conductance and Conduction Velocity in Mammalian Myocardium. *Circulation: Arrhythmia and Electrophysiology*. 2013;6:1208-1214.
31. DURRER D, VAN DAM RT, FREUD GE, JANSE MJ, MEIJLER FL and ARZBAECHER RC. Total Excitation of the Isolated Human Heart. *Circulation*. 1970;41:899-912.
32. Bursac N, Parker KK, Iravanian S and Tung L. Cardiomyocyte Cultures With Controlled Macroscopic Anisotropy. *A Model for Functional Electrophysiological Studies of Cardiac Muscle*. 2002;91:e45-e54.
33. Wells RG. The role of matrix stiffness in regulating cell behavior. *Hepatology*. 2008;47:1394-1400.
34. Radisic M and Christman KL. Materials Science and Tissue Engineering: Repairing the Heart. *Mayo Clinic proceedings Mayo Clinic*. 2013;88:884-898.
35. Jacot JG, McCulloch AD and Omens JH. Substrate stiffness affects the functional maturation of neonatal rat ventricular myocytes. *Biophys J*. 2008;95:3479-87.
36. McDevitt TC, Angello JC, Whitney ML, Reinecke H, Hauschka SD, Murry CE and Stayton PS. In vitro generation of differentiated cardiac myofibers on micropatterned laminin surfaces. *Journal of Biomedical Materials Research*. 2002;60:472-479.

37. McDevitt TC, Woodhouse KA, Hauschka SD, Murry CE and Stayton PS. Spatially organized layers of cardiomyocytes on biodegradable polyurethane films for myocardial repair. *Journal of Biomedical Materials Research Part A*. 2003;66A:586-595.
38. Ribeiro AJS, Ang Y-S, Fu J-D, Rivas RN, Mohamed TMA, Higgs GC, Srivastava D and Pruitt BL. Contractility of single cardiomyocytes differentiated from pluripotent stem cells depends on physiological shape and substrate stiffness. *Proceedings of the National Academy of Sciences of the United States of America*. 2015;112:12705-12710.
39. Chrobak MO, Hansen KJ, Gershlak JR, Vratsanos M, Kanellias M, Gaudette GR and Pins GD. Design of a Fibrin Microthread-Based Composite Layer for Use in a Cardiac Patch. *ACS Biomaterials Science & Engineering*. 2017;3:1394-1403.
40. Black LD, Meyers JD, Weinbaum JS, Shvelidze YA and Tranquillo RT. Cell-Induced Alignment Augments Twitch Force in Fibrin Gel-Based Engineered Myocardium via Gap Junction Modification. *Tissue engineering Part A*. 2009;15:3099-3108.
41. de Boer TP, van Rijen HVM, van der Heyden MAG, de Bakker JMT and van Veen TAB. Adrenergic regulation of conduction velocity in cultures of immature cardiomyocytes. *Netherlands Heart Journal*. 2008;16:106-109.
42. Stein M, van Veen TAB, Hauer RNW, de Bakker JMT and van Rijen HVM. A 50% Reduction of Excitability but Not of Intercellular Coupling Affects Conduction Velocity Restitution and Activation Delay in the Mouse Heart. *PLoS ONE*. 2011;6:e20310.
43. van Rijen HVM, Eckardt D, Degen J, Theis M, Ott T, Willecke K, Jongsma HJ, Opthof T and de Bakker JMT. Slow Conduction and Enhanced Anisotropy Increase the Propensity for Ventricular Tachyarrhythmias in Adult Mice With Induced Deletion of Connexin43. *Circulation*. 2004;109:1048-1055.
44. van Veen TAB, Stein M, Royer A, Le Quang K, Charpentier F, Colledge WH, Huang CL-H, Wilders R, Grace AA, Escande D, de Bakker JMT and van Rijen HVM. Impaired Impulse Propagation in Scn5a-Knockout Mice. *Combined Contribution of Excitability, Connexin Expression, and Tissue Architecture in Relation to Aging*. 2005;112:1927-1935.
45. Lundy SD, Zhu WZ, Regnier M and Laflamme MA. Structural and functional maturation of cardiomyocytes derived from human pluripotent stem cells. *Stem Cells Dev*. 2013;22:1991-2002.
46. Lluçia-Valldeperas A, Soler-Botija C, Gálvez-Montón C, Roura S, Prat-Vidal C, Perea-Gil I, Sanchez B, Bragos R, Vunjak-Novakovic G and Bayes-Genis A. Electromechanical Conditioning of Adult Progenitor Cells Improves Recovery of Cardiac Function After Myocardial Infarction. *Stem cells translational medicine*. 2017;6:970-981.
47. Kroll K, Chabria M, Wang K, Häusermann F, Schuler F and Polonchuk L. Electro-mechanical conditioning of human iPSC-derived cardiomyocytes for translational research. *Progress in Biophysics and Molecular Biology*. 2017.
48. Ruan J-L, Tulloch NL, Razumova MV, Saiget M, Muskheli V, Pabon L, Reinecke H, Regnier M and Murry CE. Mechanical Stress Conditioning and Electrical Stimulation Promote Contractility and Force Maturation of Induced Pluripotent Stem Cell-Derived Human Cardiac Tissue. *Circulation*. 2016;134:1557-1567.

## 7 Specific Aim 3: Evaluate the use of fibrin microthread sutures to deliver hPS-CM to healthy cardiac tissue.

### 7.1 Introduction

hMSCs have been widely used in pre-clinical animal infarct models and human clinical trials; however, results from the clinical studies have only demonstrated minimal improvement in left ventricular function<sup>1, 2</sup>. The improvement of embryonic and induced pluripotent stem cell differentiation to cardiomyocytes<sup>3-5</sup> over the past decade have opened the doors to a new cell type that researchers can use for myocardial regeneration strategies<sup>5-11</sup>. Where an hMSC may reduce the harsh effect of the environment found post-infarct, an hMSC, which rarely differentiates into a cardiomyocyte<sup>12</sup>, will not be able to contribute to active mechanical function in a manner that an hPS-CM may, due to its contractile nature. Early studies using hPS-CM demonstrated that these cells are capable of engrafting in the heart and can attenuate infarct damage and improve function<sup>5, 7</sup>.

Many studies utilizing hPS-CM have focused on cell sheet, cardiac patch technology, or an ECM base to deliver cells<sup>11, 13-15</sup>. Wendel *et al.* created a cardiac patch utilizing hPS-CM and human pericytes entrapped in a fibrin gel, these patches were sutured to the epicardial surface of the left ventricle of an acutely infarcted rat heart<sup>11</sup>. Data at 4 weeks post implantation suggested survival of implanted cells, reduction in infarct size, and improvements in cardiac function. However, a thin collagen rich interface between the patch and epicardial surface of the ventricle mitigated any electromechanical coupling and thus improvements in function were likely due to paracrine effects and infarct stabilization from the patch. Cell sheet technology for hPS-CM delivery has been explored most notably by Masumoto *et al.* in which hPS-CM were used to create cardiac tissue sheets (hiPSC-CTS) that were transplanted onto the epicardial surface, without suturing, in a sub-acute rat infarct model<sup>13, 16</sup>. At 8 weeks post-implantation, viable cells were found with some evidence of neovascularization of host cells into grafts. Additionally, functional data indicated improvements in left ventricular systolic function by attenuating ventricular remodeling and improving fractional shortening. Ogasawara *et al.* delivered hPS-CM using a hyaluronan-based hydrogel (HyStem) or a pro-survival cocktail (PSC) combined with matrigel and injected the hydrogel/cell



combination into the infarct<sup>17</sup>. Graft sizes were significantly higher for cells delivered with PSC and matrigel rather than cells delivered with HyStem group alone. Additionally, no functional benefits were found for either group even given the larger graft sizes. These data suggest the need for improved methods to deliver hPS-CM without the use of matrigel or a PSC, due to the unregulated nature and high costs, or without a cell sheet or patch given the lack of cell migration into the damaged area.

The above studies suggest that hPS-CM may have the potential to improve function via attenuated left ventricular remodeling by paracrine effects and improvements in neovascularization<sup>11, 13</sup>. However, as a method to improve cell retention many studies transplanting hPS-CM in infarct models have done so in a cardiac patch or cell sheet form<sup>11, 13</sup>. These cell delivery methods have limited success due to the formation of collagen interfaces between the host and graft tissue, which limits the ability for graft cells to migrate into host tissue thus, limiting the potential for electrical integration. Other studies have delivered hPS-CM using more traditional delivery methods including intramyocardial injection without matrigel, however, as discussed in chapter 2 there are limitations on the delivery efficiency using an intramyocardial injection<sup>9, 18, 19</sup>. These low delivery efficiencies and in combination with using matrigel could be prohibitively expensive when considering the cost of some of these hPS-CM based cell therapies.

Previously, we have demonstrated that fibrin microthread based sutures can deliver cells with a 64% efficiency<sup>20</sup> and are capable of delivering hMSCs to an infarct<sup>21</sup>. In chapter 6 we demonstrated that hPS-CM are capable of attaching to and contracting on the fibrin microthread suture in a manner that does not impact functionality. In this objective, we aim to implant our hPS-CM seeded suture in healthy cardiac tissue and examine retention at 1 hour and 3 days post-delivery. The purpose of this aim is to determine the success of the fibrin suture delivery method on cell retention in healthy cardiac tissue. The cell type used in objective 2 will be used for aim 3; all microthreads used in this objective were produced as described in objective 1a and will be seeded as done for studies in objective 2b where individual threads were clamped into a bored out needle to facilitate implantation (Figure 7-1).



**Figure 7-1. Construct for implantation sutures. Three threads are clamped into a bored out needle and were individually glued to the PDMS washer to facilitate seeding.**

## 7.2 Materials and methods

### 7.2.1 Implant model

hPS-CM seeded microthreads were delivered to uninjured hearts for 1 hour, 8 hours, 1 day, and 3 days. (n=6 for all groups). Uninjured animals were used to assess the *in vivo* fate of the hPS-CM in a healthy heart before cells are delivered to an infarcted heart. Surgeries were completed as described in objective 1b without the LAD ligation. For the

1 hour time point animals were sacrificed 1 hour after hPS-CM implantation and the heart was extracted, bisected across the implanted suture and fixed overnight in 4% paraformaldehyde. For the 8 hour, 1 day, and 3 day time points, after hPS-CM are delivered, animals were closed and allowed to recover for the appropriate time. After 8 hours, 1day, or 3 days animals were anesthetized, reopened along previous suture lines, a 0.3mg/kg dose of Beuthanasia-D (390mg/mL pentobarbital sodium) was injected into the left atrium to arrest the heart, the heart was extracted, bisected and fixed in 4% paraformaldehyde. The protocol was approved by the Worcester Polytechnic Institute Institutional Animal Care and Use Committee.

### 7.2.2 Histological analysis

Twenty-four hours after fixation, the hearts were placed in 30% sucrose overnight and subsequently embedded in OCT for cryosectioning. A cryostat was used to obtain 10 $\mu$ m transverse sections across the entire region of the heart containing the biological suture. To assess the retention of hPS-CM, serial sections 60 $\mu$ m apart were stained for human Ku80 (rabbit anti-Ku80, ab80592 Abcam) to identify and quantify the presence of hPS-CM in the myocardium. These sections were imaged using a Leica TCP SP5 confocal laser scanning microscope. In each section imaged, the number of cells expressing Ku80 co-localized with Hoechst staining were counted. By averaging adjacent sections and using linear interpolation a total number of cells delivered was calculated. Given these results and the number of cells attached to the suture prior to implantation a cell delivery efficiency was also calculated. Additional sections were stained with sarcomeric  $\alpha$ -actinin (mouse anti-sarcomeric alpha actinin, Abcam) and

Connexin-43 (goat anti-Connexin 43, Abcam), or Hematoxylin and Eosin, or Masson's Trichrome according to the manufacturer's instruction.

### 7.2.3 In vitro cell delivery assay

To determine the fate of the cells after being delivered for an hour, an *in vitro* delivery assay was developed to mimic the conditions of cell delivery. The assay utilized a fibrin gel made by adding equal volumes of fibrinogen (70mg/mL) and thrombin (250U/mL) into a plastic mold (1.5x1.5x0.5cm)<sup>22</sup>. This formulation was chosen to mimic the stiffness of ventricular myocardium (>20kPa<sup>23</sup>) as the study using this formulation reported a Modulus of Elasticity of 27.5kPa<sup>22</sup>. 500µl of fibrinogen was added initially followed by 500µl of thrombin and a pipette tip was used to gently mix without the formation of air bubbles. After mixing, the gels were allowed to polymerize for 30 minutes and then were removed from the mold, placed in a petri dish and used in the assay.

hPS-CM were seeded onto fibrin microthreads attached to a suture needle as described previously. After 14 days of culture sutures were treated with one of three conditions to mimic the conditions cells would experience upon delivery to ventricular myocardium. Condition one examined the environmental effects the sutures that had been brought to the operating room (OR) and then brought back to the incubator may have experienced. Here, a 6 well plate containing the sutures was removed from the incubator and brought down one floor to the operating room, a process that takes around 2 minutes. The 6 well plate was then placed on the surgical table for 2 minutes, the approximate time required to prepare the suture for delivery. After those two minutes the sutures were then returned to their original incubator. During this entire process the sutures were never moved from the 6-well plate and remained in their standard medium consisting of RPMI with B27. Condition two simulated the effect of cell delivery by removing the suture constructs from the incubator and placing them in a biosafety cabinet. The microthreads were then clipped off the PDMS construct and needle drivers were used to grab the suture needle and sutured the construct completely through the fibrin gel. After which, the suture construct was

placed in standard RPMI-B27 medium in a 6 well plate and returned to the incubator for further incubation. Condition three simulated the effect of cell delivery in addition to the implantation effect. Here, the sutures were removed from the incubator, the threads were cut off the PDMS construct and were sutured through the gel. However, instead of being completely sutured through the gel as in condition two, sutures were left in the gel and were fully submerged in standard RPMI-B27 medium for further incubation. Controls included control seeded threads and control cells that were seeded on collagen IV coated tissue culture plastic, these controls were not exposed to any of the conditions. An additional control was used wherein cells seeded on collagen IV coated tissue culture plastic were exposed to the operating condition effects.

At 15 minutes, 30 minutes, 1 hour, 3 hours, and 6 hours sutures from each condition were stained using Annexin V and Propidium Iodide (PI) to examine apoptosis. Cells in the control conditions were also stained using Annexin V and PI. The sutures from the OR condition were clipped off the PDMS post and placed on a microscope slide, the sutures that had been pulled through the gel were also placed on a microscope slide, and the sutures remaining in the gel were pulled the remaining distance through the gel and were placed on a microscope slide. The Annexin V assay (V13241, Thermo Fischer) was run according to the manufacturers specifications, briefly, sutures were washed with cold PBS, then Annexin V binding buffer, and were stained with Annexin V (1:10) and Propidium Iodide (1.5:100 of 100 $\mu$ g/mL) at room temperature for 15 minutes. Sutures were then rinsed with Annexin binding buffer and stained with Hoechst 33342 (0.5 $\mu$ g/mL) for 4 minutes and then returned to Annexin binding buffer. Sutures were imaged using a Leica TCP SP5 confocal laser scanning microscope. Images were quantified using ImageJ to count for Hoechst, Annexin V, and/or PI positive cells for each group at each time point. Counts were then averaged and plotted as either a total number of cells or a percentage of the total cells present in each category: Annexin V + or PI + for each condition.

#### 7.2.4 Statistical analysis

Statistical analyses were performed using GraphPad Prism 6 (GraphPad Software, Inc.). Comparisons only between the 1 hour and 3 day delivery time points, due to low sample sizes in the 8 hour and 1 day group, were analyzed using an unpaired t-test. Cell retention is reported as mean±SEM. Significance was considered at  $p < 0.05$ .

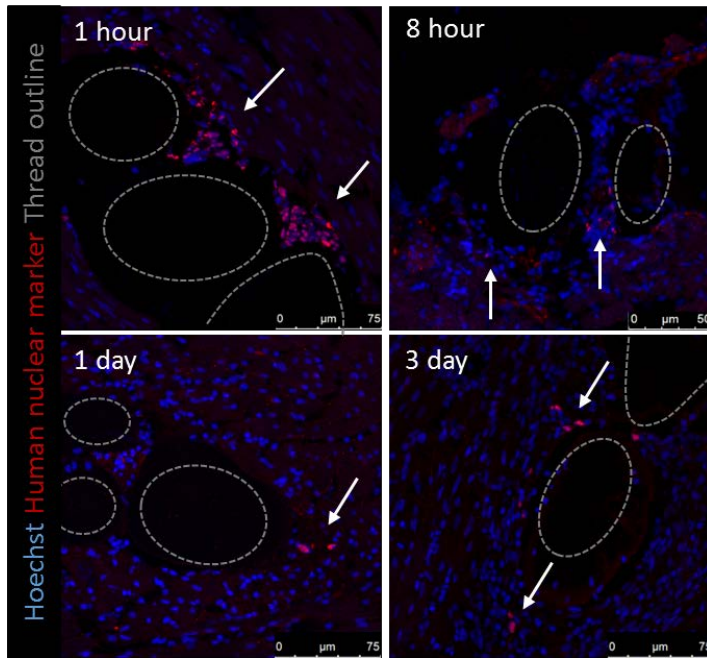


**Figure 7-2 hPS-CM persist in ventricular myocardium up to 3 days after delivery via a fibrin microthread suture.** PositiveKu80 staining (red) indicates cells persisting in the myocardium up to three days after delivery. Cells delivered at one hour were closely localized to the suture, however at later time points cells were found near the suture, but not as localized as in the one hour condition.

#### 7.3 Results

##### 7.3.1 Cell retention at 1 hour, 8 hours, 1 day, and 3 days

Cells expressing Ku80 co-localized with Hoechst staining were found around the suture area for all time points (Figure 7-2). At the one hour time point cells were found directly in contact and localized next to the suture, where as with other time points cells were found close to the suture, but not always in direct contact. The

numbers of cells delivered were quantified, using linear interpolation, through the entire section of the heart where the

sutures were delivered. At 1 hour an average of  $7602 \pm 2382$  cells were delivered equating to a delivery efficiency of  $67 \pm 17\%$  which was significantly higher than the average number of cells delivered at 3 days which was  $185 \pm 403$  with a delivery efficiency of  $1.3 \pm 3.9\%$  ( $p < 0.05$ , Figure 7-3). At 8 hours and 1 day an

average of  $1470 \pm 1470$  and  $256 \pm 196$  were delivered with delivery efficiencies of  $14 \pm 14\%$ , and  $1.9 \pm 2\%$ , respectively (Figure 7-3).

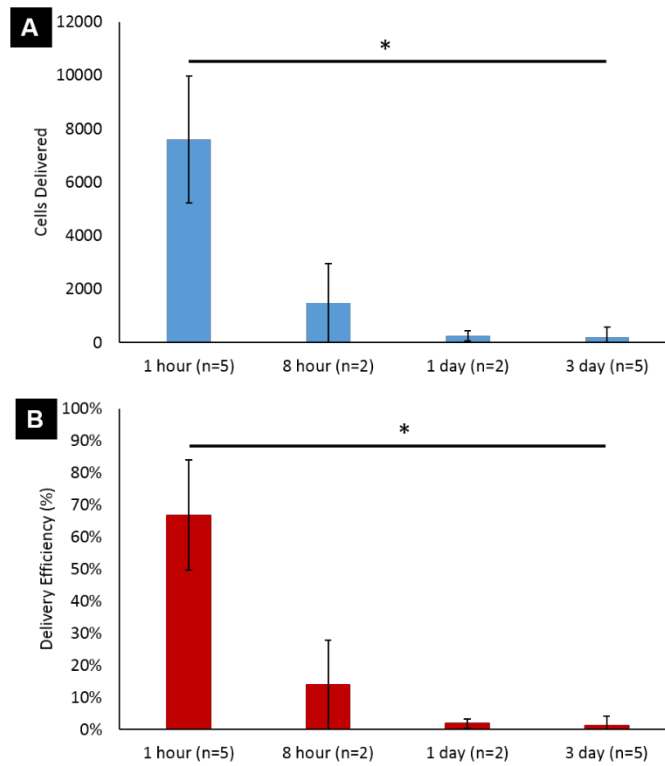


**Figure 7-3. hPS-CM can be delivered to healthy myocardium with a 67% delivery efficiency.** Cells were delivered with a 67% delivery efficiency one hour after delivery, however significantly fewer cells were retained at 3 days. Additionally, fewer cells were retained at 8 hours and 1 day post-delivery, however, significance was not reached due to a small sample size Mean±SEM, \*p<0.05. n=2-5

### 7.3.2 Cell distribution across the delivered area

Cell distribution was mapped along the entire delivery tract from entry to exit of the heart. For the 1 hour cell delivery group cells were found throughout the entire delivery tract (Figure 7-4A). Two hearts had higher cell retention at the entry point, however most hearts had relatively similar numbers of cells in every section. For the hearts that contained cells in the 8 hour and 3 day groups cell distribution was even and present along the entire delivery tract (Figure 7-4B, D). For the 1 day group, cell were only found in the entry half of the heart and no cells were found in the portion where the thread exited the heart (Figure 7-4C). These data demonstrate, that initially cells are delivered and are well distributed along the entire delivery tract from entry to exit with little effect of shearing resulting in higher cell number at the

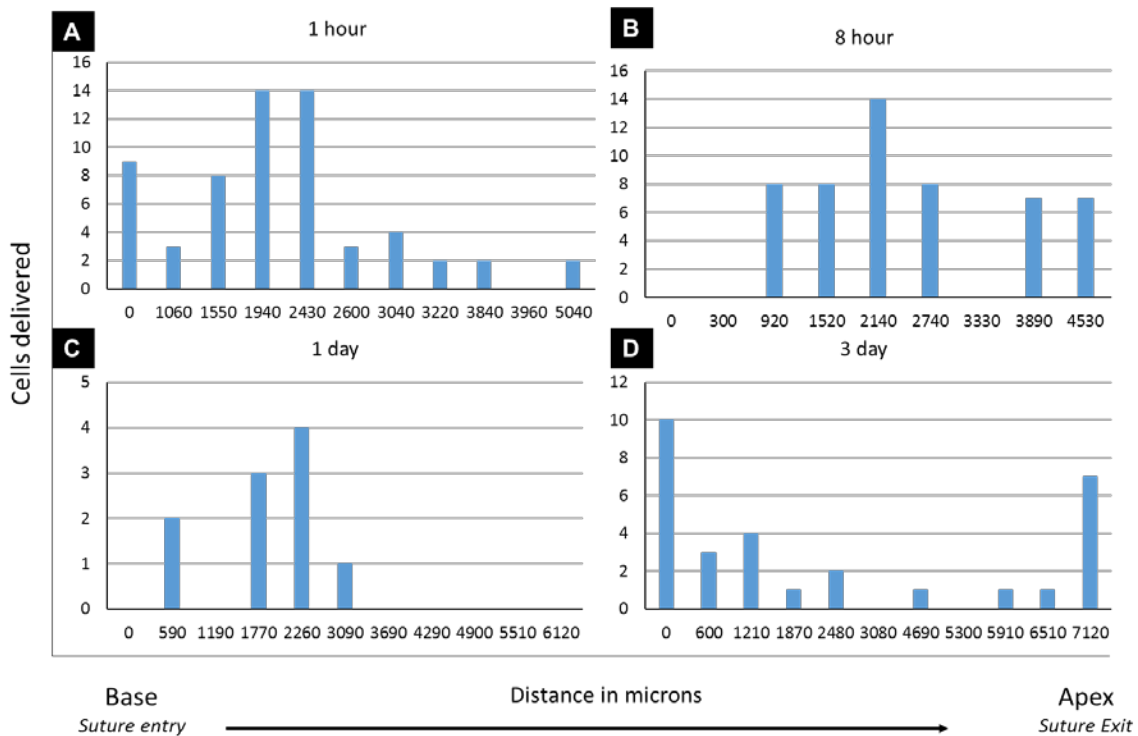


**Figure 7-4 Representative histograms indicate cells are distributed throughout the delivery track.** Histograms tracking cell delivery from suture entry to suture exit demonstrate cells present through the entire delivery track (A,B,D) with the exception of the cells delivered for 1 day (C). Histograms are representative of each time point and do not quantitatively describe the average cell distribution for each time point.

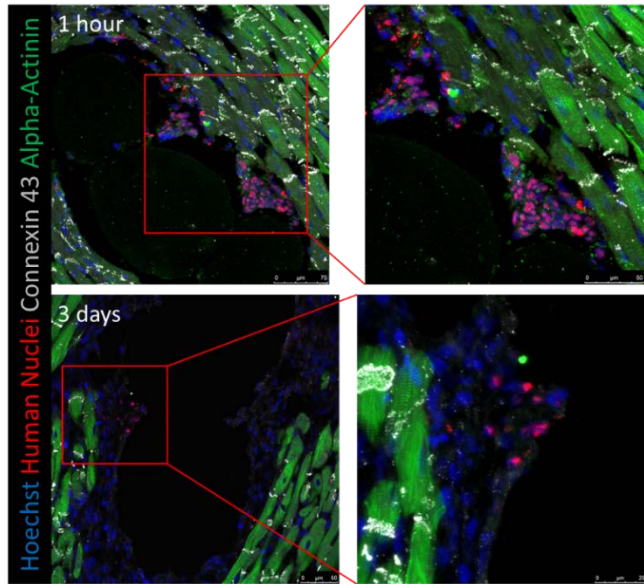


**Figure 7-5. Limited evidence of positive Connexin 43 staining between host tissue and graft tissue at 1 hour and 3 hours. Sections were stained with alpha-actinin and connexin 43 to examine the interface between host and graft tissue. Connexin 43 stained sections show limited staining between graft tissue, stained with Ku80, and host tissue indicating limited connection occurring between the graft and host cells**

entry. However, the decrease in cells present one hour after delivery compared to 3 days after delivery suggests a significant majority of cells are being retained in the heart for several days.

### 7.3.3 Cell morphology after delivery

Alpha actinin and Connexin 43 staining indicated limited positive signal between graft and host cells (Figure 7-5) indicating that the implanted cells are not making connections to the host tissue at the three day time point. Hematoxylin and Eosin stained sections indicated hyperchromatic cells and nuclear debris after 1 hour with high

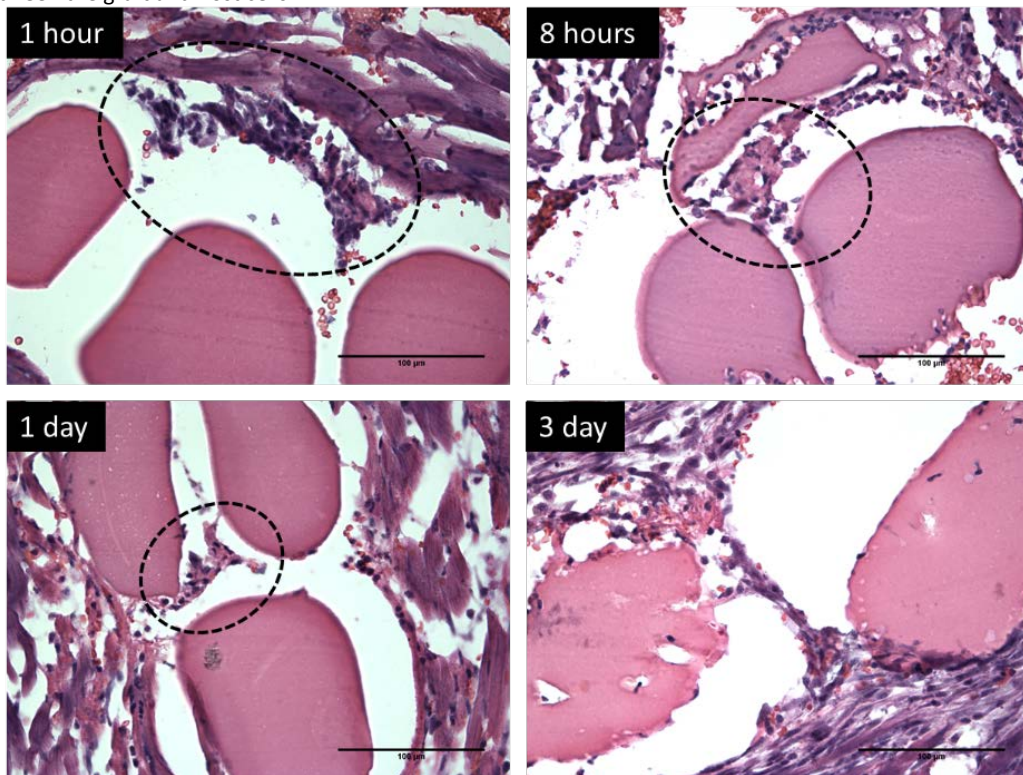


**Figure 7-6. Representative Hematoxylin and Eosin staining.** H&E stained sections indicate hyperchromatic cells with nuclear debris at 1 hour and neutrophil infiltration at 8 hours. Approximate location of delivered cells are outlined in black as determined by examining serial sections stained with Ku80.



neutrophil infiltration at 8 hours. These results indicate poor cell health post delivery and may explain why fewer cells were retained 8 hours to 3 days post-delivery (Figure 7-6). Additionally, Masson's Trichrome staining indicated increased collagen deposition around the suture by day 3 (Figure 7-7).

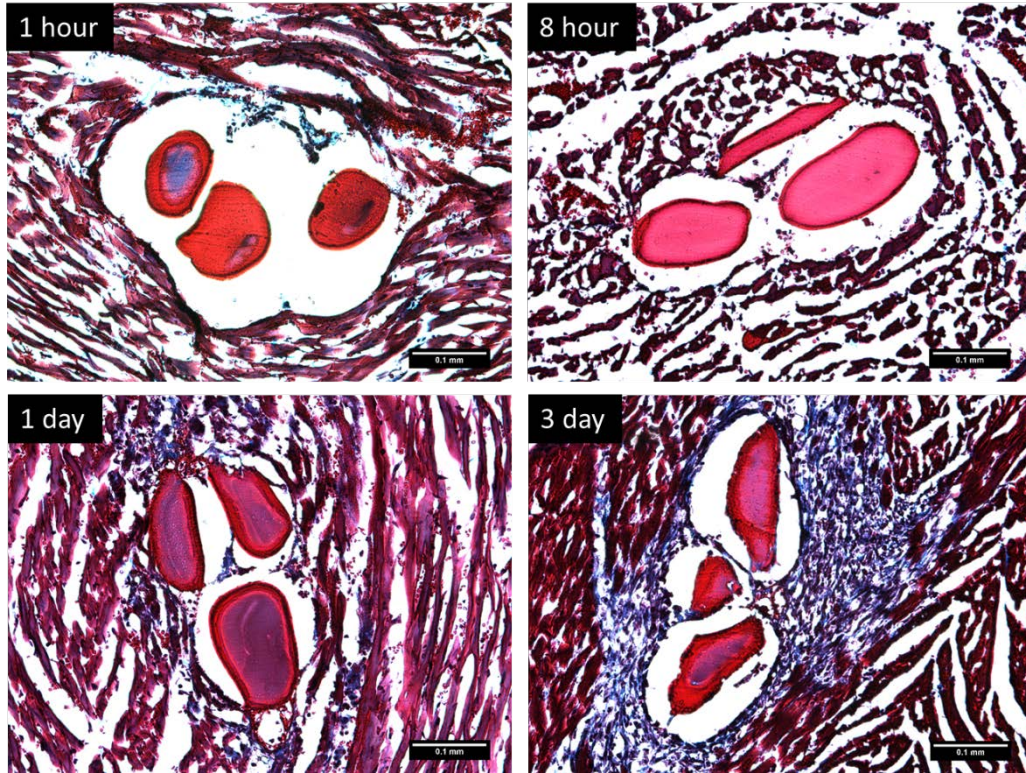


**Figure 7-7. Representative Masson's Trichrome stained sections.** Masson's Trichrome stained sections qualitatively indicate increased collagen deposition beginning at day 1 and out to day 3.

#### 7.3.4 In vitro cell delivery assay indicates apoptotic cells as early as 30 minutes post-delivery

We developed an *in vitro* cell delivery assay utilizing a fibrin gel which had a stiffness in the range of that of myocardium<sup>22</sup>. Cell seeded sutures were either brought to the operating room or delivered to the gel where the suture was pulled through the gel or kept in the gel until the appropriate time point. Annexin V and PI staining was used to visualize cell health in each condition (Figure 7-8) and was quantified to determine the percentage of apoptotic (Annexin V) and dead cells (PI) (Figure 7-9).

When examining the percentage of cells for Annexin V and PI expression we demonstrated that cells in control plates had low Annexin V and PI expression, however when the plate was brought to the OR, higher percentages of both apoptosis and PI positive cells were seen suggesting damaging effects of bringing the cells down to the OR (n=2, Figure 7-9A). Control sutures not exposed to any condition had

higher percentages of Annexin V and PI positive cells than those found for the cells in the control plate, but had lower expression than the sutures going through simulated delivery (n=2, Figure 7-9).

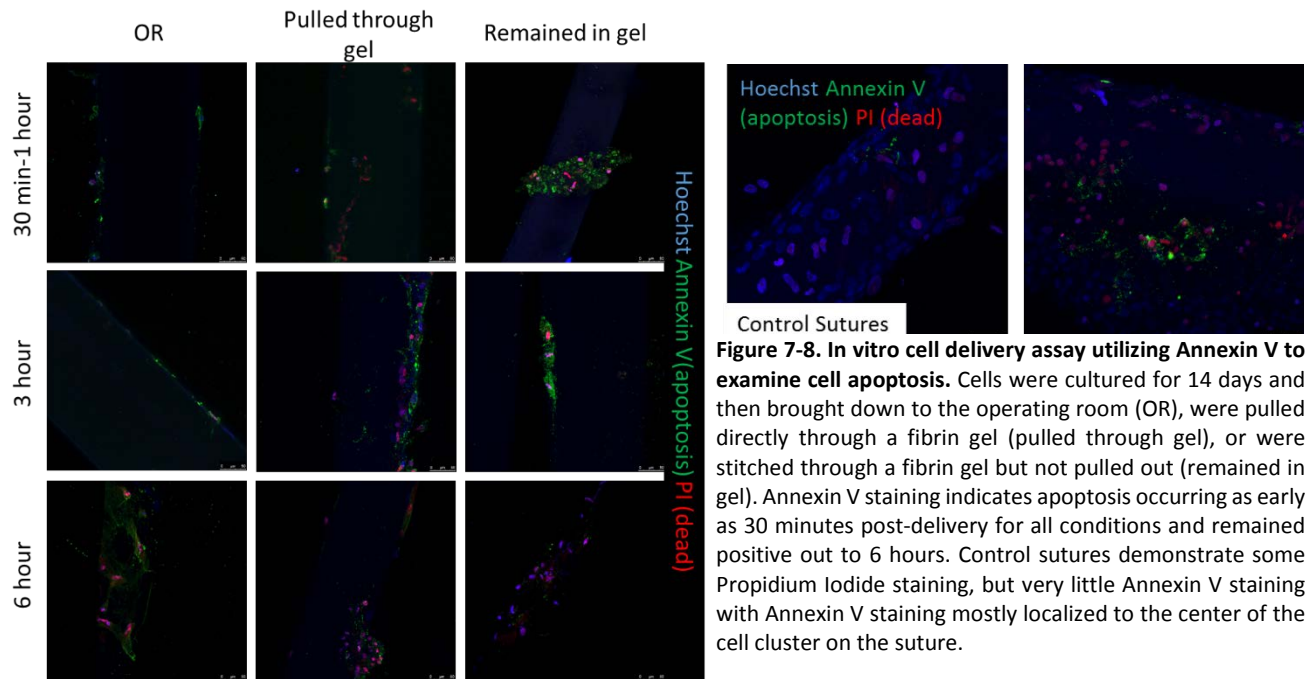


**Figure 7-8. In vitro cell delivery assay utilizing Annexin V to examine cell apoptosis.** Cells were cultured for 14 days and then brought down to the operating room (OR), were pulled directly through a fibrin gel (pulled through gel), or were stitched through a fibrin gel but not pulled out (remained in gel). Annexin V staining indicates apoptosis occurring as early as 30 minutes post-delivery for all conditions and remained positive out to 6 hours. Control sutures demonstrate some Propidium Iodide staining, but very little Annexin V staining with Annexin V staining mostly localized to the center of the cell cluster on the suture.

For the sutures that were brought to the OR there was a higher percentage of Annexin V cells at 30 minutes compared to controls, however Annexin V expression increased over 3 hours with PI positive expression remained the same over 6 hours indicating higher apoptosis occurring at later time points (n=2, Figure 7-9A,B). Sutures that were pulled through the gel and allowed to sit demonstrated decreased Annexin V expression over 6 hours, however PI expression was greater than 60% at all-time points (n=2, Figure 7-9C). A similar trend was observed for sutures that stayed in the gel until the appropriate time point, where there was a decrease in Annexin V expression over 3 hours, but a greater than 60% PI expression at all-time points (n=2, Figure 7-9D).

When examining Annexin V and PI expression by the number of cells present on the suture, we demonstrated that there were similar numbers of cells across all groups and all time points, such that no group had a higher number of cells which may have affected apoptosis. In the control groups, there were similar trends in Annexin V and PI expression compared to percentages where the control thread and

control plate had higher PI expression compared to Annexin V (n=2, Figure 7-10A). Additionally, Annexin V and PI expression was higher in the control plate exposed to the OR conditions indicating that the OR conditions had an effect on cell health (n=2, Figure 7-10A). For the threads exposed to the OR conditions a similar trend, compared with percentages, was found with low Annexin V initially, but higher at 1 hour and then decreasing over 6 hours with higher PI expression at later time points (n=2, Figure 7-10B). Again indicating low apoptosis occurring within the first 30 minutes post exposure to the OR conditions. For the threads that were pulled through gel all time points had similar cell numbers and consistent Annexin V and PI expression, with higher PI expression towards the 3 and 6 hour time point (n=2, Figure 7-10C). For threads that stayed in the gel there was higher Annexin V expression at 30 minutes that decreased over time, which may be due to a loss of cells as the cells on the threads had died and were no longer present on the threads when they were pulled through the gel at later time points (n=2, Figure 7-10D).

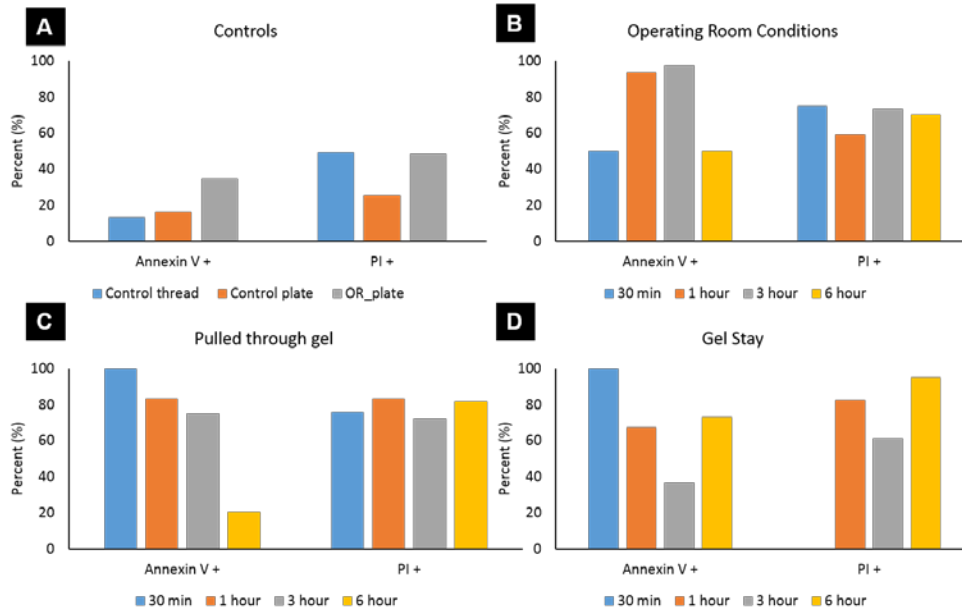


**Figure 7-9. Percentage quantification of the *in vitro* cell delivery assay utilizing Annexin V to examine cell apoptosis.** The percentage of Annexin V and PI positive cells were quantified for all conditions. Panel A indicated the control conditions where control threads and cells on a control plate with and without OR conditions exposure were used. Panel B indicated sutures exposed to the OR conditions, panel C indicated sutures that were pulled through the gel, and panel D indicated sutures that were stitched through a gel and were allowed to remain in the gel. The percentage of Annexin V or PI positive cells were plotted with respect to time. The controls indicate low Annexin V+ cells, however high PI positive percentages were demonstrated. Additionally, the OR cell plate control demonstrated higher Annexin V and PI positive cells over the non-exposed control plate alone. The gel conditions demonstrates decreased Annexin V expression over time, while the OR conditions demonstrated increased Annexin V expression over time. With the exception of the 6 hour time point. All time points saw high PI positive expression of greater than 50%. n=2 for each condition and time point.

#### 7.4 Discussion

These data demonstrate that hPS-CM are capable of being delivered with high efficiency to healthy cardiac tissue via a fibrin microthread suture. Other researchers have focused primarily on using cell sheet or cardiac patch technology to deliver hPS-CM, which have shown improved survival of grafted cells. However, these studies showed limited migration into host tissue because of a collagen interface that formed between graft and host tissue or because cells did not migrate from the graft<sup>11, 13</sup>. By using fibrin

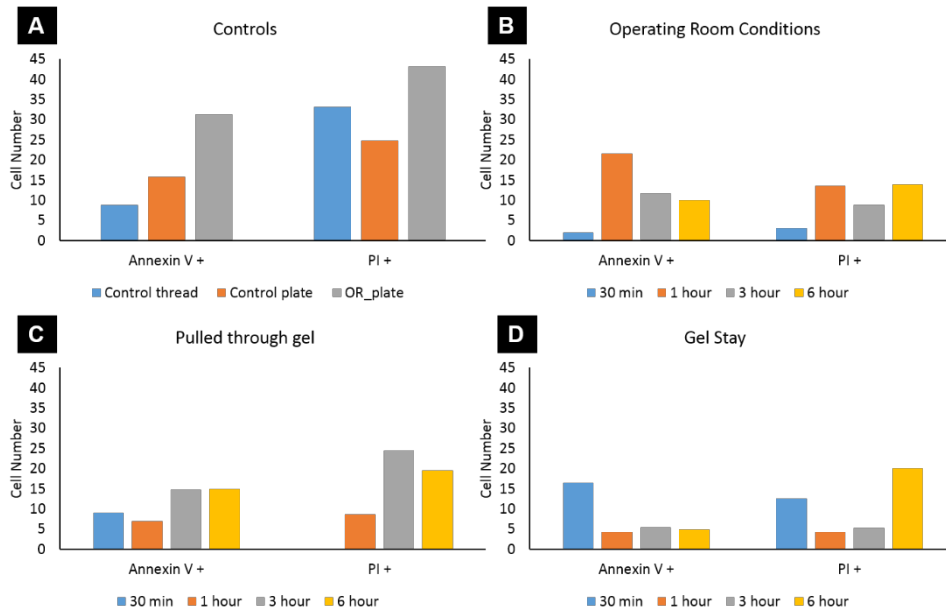


**Figure 7-10. Cell number quantification of the *in vitro* cell delivery assay utilizing Annexin V to examine cell apoptosis.** The number of Annexin V and PI positive cells were quantified for all conditions. Panel A indicated the control conditions where control threads and cells on a control plate with and without OP conditions exposure were used. Panel B indicated sutures exposed to the OR conditions, panel C indicated sutures that were pulled through the gel, and panel D indicated sutures that were stitched through a gel and were allowed to remain in the gel. The number of Annexin V or PI positive cells were plotted with respect to time. There were similar numbers of cells across all groups. In the control groups (A) there were similar trends compared to percentages with higher PI for control thread and control plate compared to Annexin V. Additionally, Annexin V and PI expression was higher in the OR plate. In the OR conditions (B) a similar trend, compared with percentages, was found with low Annexin V initially, but higher at 1 hour and then decreasing over 6 hours with higher PI expression at later time points. For the threads that were pulled through gel (C) all time points had similar cell numbers and had consistent Annexin V and PI expression at all-time points. For threads that stayed in the gel (D) there was higher Annexin V at 30 minutes that decreased over time. Additionally, over time there were fewer cells with the exception of high PI positive cells at 6 hours. n=2 for each condition and time point.

microthread sutures to deliver hPS-CM directly into the myocardium we aim to improve retention of the cells within the host tissue.

We begin the aim by delivering cells into the uninjured animal to investigate how the hPS-CM delivery on fibrin sutures compared to hMSC delivery. Results from these studies demonstrated the ability to deliver hPS-CM using the fibrin suture with a 67% delivery efficiency at 1 hour. This delivery efficiency aligned well with our previous data where hMSCs were delivered with a 64% delivery efficiency at 1 hour using the fibrin sutures. Additionally, cells that were delivered were delivered along the entire delivery tract of the suture indicating that cells were well distributed within the tissue and a high number of cells were not sheared off and retained at the suture entry point.

Next, we examined cell retention in host tissue 3 days after implantation in a non-infarcted environment. One hour was chosen in uninjured animals to look at immediate retention and viability in order to obtain an acute understanding of how the cells behave immediately after implantation. The 3 day time point in healthy animals was chosen to look at changes in cell retention that may occur after implantation. After delivering cells for 3 days we found very few cells present, thus we expanded our time points to include 8 hours and 1 day, which also demonstrated decreased retention. Using a Masson's Trichrome stain we indicated higher collagen deposition around the suture at day 3; a collagen interface between a biomaterial implant and the host myocardium has been demonstrated in other studies<sup>11</sup>. Moving forward, this collagen interface may be an issue, however as we only looked out to 3 days, further time points would be needed to elucidate the temporal progression, or regression, of further collagen deposition. While the suture was able to deliver hPS-CM with a high efficiency at 1 hour after 8 hours and out to 3 days post-delivery we saw a decrease in the number of cells that were retained. These data suggest that something is occurring to not allow sustained retention after the initial delivery period.

In order to investigate what may be occurring to cause the decrease in cells post-delivery we examined cell morphology. Through H&E staining, we determined that the cells that were present at 1 hour were hyperchromatic and there was nuclear debris in the sections. H&E stained sections also revealed high neutrophil infiltration by 8 hours. To further investigate what could be causing the poor cell health we developed an *in vitro* delivery assay using a fibrin gel and Annexin V/PI staining to examine apoptosis and cell death. We sought to examine the effects of bringing the sutures down to the operating room as was done for all implants, as well as the effects the mechanical delivery of the cells may have imparted on cell health. A fibrin gel was chosen due to ease of production and the ability to formulate the gel such that the stiffness mimicked what could be expected of ventricular myocardium. hPS-CM seeded sutures were either brought to the OR or were delivered to a fibrin gel and allowed to be pulled through the gel or remained in the gel. As we saw the highest drop in cell retention by 8 hour we chose time points of 30

minutes to 6 hours to examine acute and later stage cell health. Staining with Annexin V and PI allows us to discern which cells are going through apoptosis and which cells are already dead.

The results of the in vitro delivery assay indicated that a high number of cells on control sutures alone were already expressing PI. The decrease in Annexin V expression for both gel conditions suggest that the cells are apoptotic rather quickly after delivery and the cells either fall off the suture or are solely PI positive by 6 hours. The reverse is seen in the OR group where Annexin V expression increases, suggesting that the apoptotic effects of the OR take longer to occur in these cells. However, all groups did have high PI expression, over 60%, at all-time points, which may explain why the combination of bringing cells to the OR and then delivering them to cardiac tissue resulted in reduced retention 8 hours after delivery. While it is interesting to note the raw cell number data, the conclusions found remain the same as the conclusions drawn when examining the percentages of Annexin V and PI expression. All groups at all-time points had a similar range in the number of cells that were on the threads and showed positive Annexin V and PI expression indicating that cell number was not a major driver for apoptosis between the conditions. The controls and operating room conditions followed a similar trend when comparing cell number with the percentages. One interesting finding with the threads that remain in the gel is the higher Annexin V expression at the 30 minute time point that decreased over time. This finding indicates that as the cells are dying they may no longer be present on the thread after the thread is pulled through the gel resulting in a decreased number of Annexin V positive cells at the later time points. One thing to note with this set of data is the small sample number (2) run for this experiment. While trends are capable of being described using these sets of data, it will be necessary to increase the sample size to draw statistically significant conclusions.

This loss in viable cells is not unprecedented, several studies have demonstrated decreases in retention of hPS-CM over time<sup>24-28</sup>. A study by Funakoshi *et al.* delivered hPS-CM to healthy hearts using an intramyocardial injection and demonstrated up to a 75% decrease in retention 1 day and 3 days after

delivery<sup>25</sup>. They then tracked retention out to 56 days and saw increases in cell retention after 28 days suggesting a proliferative population in their delivered cells that was capable of surviving the initial cell delivery. Gao *et al.* delivered hPS-CM to infarcted cardiac tissue utilizing a scaffold patch approach; at 1 week they reported a delivery efficiency of 24.5% which was reduced to 11.2% by week 4<sup>26</sup>. A similar trend was observed by Rojas *et al.* when they delivered hPS-CM aggregates via intramyocardial injection to infarcted cardiac tissue; they reported a significantly reduced graft size from 7 to 28 days post-delivery<sup>27</sup>. Another study by Tachibana *et al.* saw very limited retention of hPS-CM at 2 weeks and even fewer cells at 4 weeks. These studies suggest that without a proliferative population, graft sizes of hPS-CM will decrease over time. Rojas *et al.* suggested that apoptosis due to weak cell-cell connections was a major driver for the decrease in cell retention. He attributed the weak cell-cell connections to the purity of the hPS-CM population in that there were limited fibroblasts that could improve structure and function of the delivered cells, as demonstrated by Kensah *et al.*,<sup>27, 29</sup> which may result in enhanced graft survival.

Even given limited and decreasing retention over time, all studies reported positive improvements in left ventricular function in terms of ejection fraction and decreases in infarct size. This suggests that high numbers of engrafted cells may not be necessary to obtain sustained improvements in left ventricular function post-infarct and that graft size may not correlate with functional improvements<sup>24</sup>. Additionally, studies did not demonstrate coupling between the host myocardium and the delivered cells suggesting that a paracrine effect from the remaining cells may be what is driving the improvement in LV function rather than regeneration and coupling from the delivered cells.

Here, we demonstrated that the fibrin suture is capable of delivering hPS-CM with a 67% efficiency, which is a similar efficiency as what was previously published when hMSCs were delivered using a fibrin suture. While the retention found with the fibrin suture decreased on a much quicker time scale than the decrease in retention found in other studies, it is encouraging that the other studies that indicated decreased retention still demonstrated improvements in left ventricular function. These data suggest that



the improvements in function may be due to a paracrine effect instead of cell replacement indicating that there is still an opportunity to increase restoration of contractile function through cell therapy. It will be important moving forward to ensure that the hPS-CM delivered are capable of being retained over time to allow them to couple and properly engraft with the host tissue to aid in regeneration and remuscularization. Studies have indicated the possibility for remuscularization. Chong *et al.* delivered hESC-CM to a non-human primate infarct model and showed significant remuscularization that was electromechanically coupled to the host tissue<sup>9</sup>. However, non-fatal ventricular arrhythmias did occur in the larger animal model. The incidence of ventricular arrhythmias was also found in a study by Shiba *et al.* where they delivered hPS-CM and demonstrated improved cardiac contractile function out to 12 weeks, however, this resulted in significantly higher incidences of ventricular arrhythmias compared to the control<sup>30</sup>. Future studies will need to be done to ensure the potential for the sustained retention of delivered cells as well as ensuring a low arrhythmogenic potential for these cell therapies.

## 7.5 References

1. Russo V, Young S, Hamilton A, Amsden BG and Flynn LE. Mesenchymal stem cell delivery strategies to promote cardiac regeneration following ischemic injury. *Biomaterials*. 2014;35:3956-3974.
2. Jakob P and Landmesser U. Current status of cell-based therapy for heart failure. *Current heart failure reports*. 2013;10:165-76.
3. Takahashi K and Yamanaka S. Induction of pluripotent stem cells from mouse embryonic and adult fibroblast cultures by defined factors. *Cell*. 2006;126:663-76.
4. Zhang J, Wilson GF, Soerens AG, Koonce CH, Yu J, Palecek SP, Thomson JA and Kamp TJ. Functional cardiomyocytes derived from human induced pluripotent stem cells. *Circ Res*. 2009;104:e30-41.
5. Laflamme MA, Chen KY, Naumova AV, Muskheli V, Fugate JA, Dupras SK, Reinecke H, Xu C, Hassanipour M, Police S, O'Sullivan C, Collins L, Chen Y, Minami E, Gill EA, Ueno S, Yuan C, Gold J and Murry CE. Cardiomyocytes derived from human embryonic stem cells in pro-survival factors enhance function of infarcted rat hearts. *Nature biotechnology*. 2007;25:1015-24.
6. Caspi O, Huber I, Kehat I, Habib M, Arbel G, Gepstein A, Yankelson L, Aronson D, Beyar R and Gepstein L. Transplantation of human embryonic stem cell-derived cardiomyocytes improves myocardial performance in infarcted rat hearts. *Journal of the American College of Cardiology*. 2007;50:1884-93.
7. van Laake LW, Passier R, Monshouwer-Kloots J, Verkleij AJ, Lips DJ, Freund C, den Ouden K, Ward-van Oostwaard D, Korving J, Tertoolen LG, van Echteld CJ, Doevendans PA and Mummery CL. Human embryonic stem cell-derived cardiomyocytes survive and mature in the mouse heart and transiently improve function after myocardial infarction. *Stem cell research*. 2007;1:9-24.
8. Fernandes S, Naumova AV, Zhu WZ, Laflamme MA, Gold J and Murry CE. Human embryonic stem cell-derived cardiomyocytes engraft but do not alter cardiac remodeling after chronic infarction in rats. *Journal of molecular and cellular cardiology*. 2010;49:941-9.
9. Chong JJ, Yang X, Don CW, Minami E, Liu YW, Weyers JJ, Mahoney WM, Van Biber B, Cook SM, Palpant NJ, Gantz JA, Fugate JA, Muskheli V, Gough GM, Vogel KW, Astley CA, Hotchkiss CE, Baldessari A, Pabon L, Reinecke H, Gill EA, Nelson V, Kiem HP, Laflamme MA and Murry CE. Human embryonic-stem-cell-derived cardiomyocytes regenerate non-human primate hearts. *Nature*. 2014;510:273-7.
10. Shiba Y, Fernandes S, Zhu WZ, Filice D, Muskheli V, Kim J, Palpant NJ, Gantz J, Moyes KW, Reinecke H, Van Biber B, Dardas T, Mignone JL, Izawa A, Hanna R, Viswanathan M, Gold JD, Kotlikoff MI, Sarvazyan N, Kay MW, Murry CE and Laflamme MA. Human ES-cell-derived cardiomyocytes electrically couple and suppress arrhythmias in injured hearts. *Nature*. 2012;489:322-5.
11. Wendel JS, Ye L, Tao R, Zhang J, Zhang J, Kamp TJ and Tranquillo RT. Functional Effects of a Tissue-Engineered Cardiac Patch From Human Induced Pluripotent Stem Cell-Derived Cardiomyocytes in a Rat Infarct Model. *Stem Cells Transl Med*. 2015;4:1324-32.
12. Grinnemo KH, Månsson-Broberg A, Leblanc K, Corbascio M, Wårdell E, Siddiqui AJ, Hao X, Sylvén C and Dellgren G. Human mesenchymal stem cells do not differentiate into cardiomyocytes in a cardiac ischemic xenomodel. *Annals of Medicine*. 2006;38:144-153.
13. Masumoto H, Ikuno T, Takeda M, Fukushima H, Marui A, Katayama S, Shimizu T, Ikeda T, Okano T, Sakata R and Yamashita JK. Human iPS cell-engineered cardiac tissue sheets with cardiomyocytes and vascular cells for cardiac regeneration. *Scientific Reports*. 2014;4:6716.
14. Higuchi T, Miyagawa S, Pearson JT, Fukushima S, Saito A, Tsuchimochi H, Sonobe T, Fujii Y, Yagi N, Astolfo A, Shirai M and Sawa Y. Functional and Electrical Integration of Induced Pluripotent Stem Cell-Derived Cardiomyocytes in a Myocardial Infarction Rat Heart. *Cell Transplant*. 2015;24:2479-89.
15. Ye L, Chang Y-H, Xiong Q, Zhang P, Zhang L, Somasundaram P, Lepley M, Swingen C, Su L, Wendel JS, Guo J, Jang A, Rosenbush D, Greder L, Dutton JR, Zhang J, Kamp TJ, Kaufman DS, Ge Y and Zhang J. Cardiac repair in a porcine model of acute myocardial infarction with human induced pluripotent stem cell-derived cardiovascular cells. *Cell Stem Cell*. 2014;15:750-61.

16. Masumoto H, Matsuo T, Yamamizu K, Uosaki H, Narazaki G, Katayama S, Marui A, Shimizu T, Ikeda T, Okano T, Sakata R and Yamashita JK. Pluripotent stem cell-engineered cell sheets reassembled with defined cardiovascular populations ameliorate reduction in infarct heart function through cardiomyocyte-mediated neovascularization. *Stem cells*. 2012;30:1196-205.
17. Ogasawara T, Okano S, Ichimura H, Kadota S, Tanaka Y, Minami I, Uesugi M, Wada Y, Saito N, Okada K, Kuwahara K and Shiba Y. Impact of extracellular matrix on engraftment and maturation of pluripotent stem cell-derived cardiomyocytes in a rat myocardial infarct model. *Scientific Reports*. 2017;7:8630.
18. Carpenter L, Carr C, Yang CT, Stuckey DJ, Clarke K and Watt SM. Efficient differentiation of human induced pluripotent stem cells generates cardiac cells that provide protection following myocardial infarction in the rat. *Stem Cells Dev*. 2012;21:977-86.
19. Hou D, Youssef EA, Brinton TJ, Zhang P, Rogers P, Price ET, Yeung AC, Johnstone BH, Yock PG and March KL. Radiolabeled cell distribution after intramyocardial, intracoronary, and interstitial retrograde coronary venous delivery: implications for current clinical trials. *Circulation*. 2005;112:1150-6.
20. Guyette JP, Fakhrazadeh M, Burford EJ, Tao ZW, Pins GD, Rolle MW and Gaudette GR. A novel suture-based method for efficient transplantation of stem cells. *Journal of biomedical materials research Part A*. 2013;101:809-18.
21. Hansen KJ, Favreau JT, Guyette JP, Tao Z-W, Coffin ST, Cunha-Gavidia A, D'Amore B, Perreault LR, Fitzpatrick JP, DeMartino A and Gaudette GR. Functional Effects of Delivering Human Mesenchymal Stem Cell-Seeded Biological Sutures to an Infarcted Heart. *BioResearch Open Access*. 2016;5:249-260.
22. Sierra DH, Eberhardt AW and Lemons JE. Failure characteristics of multiple-component fibrin-based adhesives. *Journal of Biomedical Materials Research*. 2002;59:1-11.
23. Radisic M and Christman KL. Materials Science and Tissue Engineering: Repairing the Heart. *Mayo Clinic proceedings Mayo Clinic*. 2013;88:884-898.
24. van Laake LW, Passier R, den Ouden K, Schreurs C, Monshouwer-Kloots J, Ward-van Oostwaard D, van Echteld CJ, Doevendans PA and Mummery CL. Improvement of mouse cardiac function by hESC-derived cardiomyocytes correlates with vascularity but not graft size. *Stem cell research*. 2009;3:106-12.
25. Funakoshi S, Miki K, Takaki T, Okubo C, Hatani T, Chonabayashi K, Nishikawa M, Takei I, Oishi A, Narita M, Hoshijima M, Kimura T, Yamanaka S and Yoshida Y. Enhanced engraftment, proliferation, and therapeutic potential in heart using optimized human iPSC-derived cardiomyocytes. *Scientific Reports*. 2016;6:19111.
26. Gao L, Kupfer ME, Jung JP, Yang L, Zhang P, Da Sie Y, Tran Q, Ajeti V, Freeman BT, Fast VG, Campagnola PJ, Ogle BM and Zhang J. Myocardial Tissue Engineering With Cells Derived From Human-Induced Pluripotent Stem Cells and a Native-Like, High-Resolution, 3-Dimensionally Printed Scaffold. *Circ Res*. 2017;120:1318-1325.
27. Rojas SV, Kensah G, Rotaermel A, Baraki H, Kutschka I, Zweigerdt R, Martin U, Haverich A, Gruh I and Martens A. Transplantation of purified iPSC-derived cardiomyocytes in myocardial infarction. *PLoS ONE*. 2017;12:e0173222.
28. Tachibana A, Santoso MR, Mahmoudi M, Shukla P, Wang L, Bennett M, Goldstone AB, Wang M, Fukushi M, Ebert A, Woo YJ, Rulifson E and Yang PC. Paracrine Effects of the Pluripotent Stem Cell-Derived Cardiac Myocytes Salvage the Injured Myocardium. *Circ Res*. 2017.
29. Kensah G, Roa Lara A, Dahlmann J, Zweigerdt R, Schwanke K, Hegermann J, Skvorc D, Gawol A, Azizian A, Wagner S, Maier LS, Krause A, Dräger G, Ochs M, Haverich A, Gruh I and Martin U. Murine and human pluripotent stem cell-derived cardiac bodies form contractile myocardial tissue in vitro. *European heart journal*. 2013;34:1134-1146.
30. Shiba Y, Gomibuchi T, Seto T, Wada Y, Ichimura H, Tanaka Y, Ogasawara T, Okada K, Shiba N, Sakamoto K, Ido D, Shiina T, Ohkura M, Nakai J, Uno N, Kazuki Y, Oshimura M, Minami I and Ikeda U.

Allogeneic transplantation of iPS cell-derived cardiomyocytes regenerates primate hearts. *Nature*. 2016;538:388-391.

## 8 Conclusions and future work

### 8.1 Conclusions

Heart disease continues to be a leading cause of death in the United States. Heart disease can lead to a myocardial infarction where a significant portion of the myocardium dies resulting in decreased cardiovascular function and an increased potential for heart failure. Cell based therapies have been proposed as a treatment strategy for myocardial infarction. Initial clinical data using human mesenchymal stem cells have shown the delivery of hMSCs to be safe, however no company has received FDA approval for hMSC cell therapy for MI due to the lack of efficacy data in late stage clinical trials<sup>1, 2</sup>. More recent studies have begun utilizing human pluripotent stem cell derived cardiomyocytes as a new cell source and have demonstrated their potential for improving cardiovascular function in pre-clinical animal models of MI<sup>3-5</sup>. While there is still significant excitement for cell based therapies to be a treatment strategy for cardiac disease, improvements in how cells are delivered to the damaged myocardium must be made.

A limitation of cell based treatments for myocardial infarction is the inefficient retention of cells delivered to the infarcted tissue. A number of delivery methods have been used with intramyocardial injections<sup>6</sup> and transendocardial<sup>7</sup> delivery resulting in the highest retention rates of 10 and 19%, respectively. In this dissertation we sought to build upon a fibrin based scaffold that has been shown to support hMSC attachment and can deliver hMSCs with a 64% retention rate to cardiac tissue<sup>8, 9</sup>.

This body of works aims to forward the use of the fibrin suture based delivery method for delivering hMSCs and hPS-CM which may aid in improving cardiovascular function post-MI by following two different paradigms. The first is that the hMSC will provide a pro-healing environment such that inflammation is decreased leading to a smaller infarct. The second is that a hPS-CM could provide a cell replacement strategy by coupling with the host myocardium and contributing to the active mechanical function lost after an infarct. This work explores both cell types and their potential for use in cardiovascular regeneration strategies.

Utilizing the fibrin based scaffold as a suture we further defined the seeding parameters of cell concentration and incubation time for hMSC attachment. A seeding concentration of 100 $\mu$ L of a 1.0 $\times$ 10<sup>6</sup> cells/mL concentration allowed to incubate for 24 hours resulted in an attachment of 17,887 $\pm$ 2,746 hMSCs per linear centimeter of the fibrin suture. These seeding parameters were used to deliver hMSCs to a rat model of myocardial infarction to examine how the delivery of an hMSC affected regional mechanical function. Here, we demonstrated that hMSCs persisted in the myocardium for 1 week and were found in regions away from the suture, suggesting their propensity to migrate from the suture into the damaged tissue. Delivery of biological sutures seeded with hMSCs partially restored regional mechanical function, in terms of RSW, to the injured region compared to infarct alone ( $p=0.07$ ). While the unseeded-suture group showed improvements in regional mechanical function over the MI group, the hMSC-seeded sutures demonstrated slightly higher function. This suggests that the biological suture alone has the ability to improve regional mechanical function in the infarct zone as supported by other studies demonstrating that biomaterial delivery, with no cells, to an infarct can improve mechanical function<sup>10-12</sup>.

While we demonstrated limited improvement by delivering an hMSC to an infarct the paradigm behind the MSC is that this cell type will act to reduce inflammation and decrease scar size post-infarct, however this cell cannot contribute to active mechanical function as it does not transdifferentiate into a myocyte *in vivo*. A cell type that could contribute to the active mechanical function lost after an infarct is that of a hPS-CM. hPS-CM are capable of spontaneous contraction in culture and literature has suggested their ability to couple with host myocardium and contract *in vivo*<sup>13</sup>. Here, we sought to determine if the fibrin microthread suture would support hPS-CM attachment and contraction and if the fibrin suture could be utilized to deliver hPS-CM to healthy cardiac tissue with a delivery efficiency similar to what was published for hMSCs.

To characterize the contractile behavior of hPS-CM we first developed a system in objective 2a that allowed us to quantify the mechanical contraction and calcium transients of hPS-CM over time. Systems

exist to measure and quantify contractile function, however many of these systems such as traction force or MEA arrays require a specific substrate for the cells to be cultured on which in turn imparts a secondary effect on the cells function<sup>14-16</sup>. Here, we sought to create an aseptic optical system where we could apply high density mapping (HDM), a speckle tracking algorithm used previously to examine regional cardiac function, to contracting clusters of hPS-CM to examine contractile behavior over time. We defined the analysis parameters of the HDM function and examined the techniques ability to quantify contractile behavior of hPS-CM seeded on TCP over 21 days in culture. Additionally, we developed an imaging technique capable of rapidly (>120fps) alternating bright field and fluorescence to capture mechanical contraction and calcium transient activity of fluo-4 AM dye loaded hPS-CM. While other optical systems exist to perform a similar function, many of the systems do not have the capability to simultaneously record brightfield and fluorescent channels, thus they only provide strain/force measurements or calcium/voltage measurements<sup>17</sup>. Additionally, many of the systems only examine beat velocity and do not provide quantitative information about the cells contractility over time<sup>14, 17</sup>.

Once we had defined a system to measure contractility we focused on defining the seeding conditions necessary to seed hPS-CM onto fibrin microthreads. We found that a collagen IV protein coating assisted hPS-CM attachment and that hPS-CM were capable of contracting on the microthreads. We then applied HDM to high speed (60fps) videos of hPS-CM contracting on the fibrin microthreads and characterized their contractile behavior, in terms of contractile strain, maximum strain, and beat frequency, over 21 days in culture. In terms of beat frequency, both cells on TCP and fibrin microthreads increased beat frequency over 21 days and up to physiologically relevant levels, a finding similar to other groups<sup>18, 19</sup>. Contractile strain and maximum strain were found to decrease over 21 days for hPS-CM seeded on TCP. hPS-CM seeded on fibrin microthread exhibited an opposite trend, where contractile and maximum strains increased over 21 days. By day 21, hPS-CM on fibrin microthreads produced maximum strains around 18%, which is near the strains found in ventricular myocardium (19%) suggesting that the cells

seeded on the microthreads are capable of contracting on a level found *in vivo*<sup>20</sup>. Over 21 days in culture it was found that cell contraction direction aligned more to the thread, suggesting that as these cells contract in a direction more aligned with the microthreads they are able to produce higher strains. Using the calcium transient activity we were able to calculate the conduction velocity of hPS-CM seeded sutures and found that conduction velocities increased over time. While the conduction velocity values were half of what is found in human ventricular myocardium, the values we reported are similar to other groups who are creating engineered cardiac tissue<sup>21</sup>. These findings suggest that the fibrin microthread is a suitable scaffold for hPS-CM attachment and contraction and that extended culture promotes cell alignment along the length of the suture as well as improvements in contractile function in terms of contractile strain and conduction velocity.

In the final aim of this dissertation we utilized the fibrin suture to deliver hPS-CM to healthy myocardium and examined cell retention at 1 hour to 3 days post-delivery. We demonstrated that after 1 hour post-delivery hPS-CM were delivered with a 67% delivery efficiency, an exciting finding as this matches very closely to the 64% delivery efficiency we found with hMSCs. However, when we examined retention after 8 hours and out to 3 days post-delivery we found that retention had significantly decreased. In order to determine why the cells were not being retained at later time points we developed an *in vitro* assay to simulate the conditions of delivery and examine at apoptosis. We demonstrated that the conditions of bringing cells to the OR as well as the delivery of cells through a gel increased the number of cells that were either undergoing apoptosis or were already dead as confirmed by Annexin V and Propidium Iodide staining. These results help elucidate the finding of reduced cell retention after the initial 1 hour delivery period. While these results were unexpected, they are certainly not unprecedented with what has been demonstrated in literature. Many studies delivering hPS-CM to cardiac tissue have reported decreased cell retention within a couple days after delivery to a month after delivery<sup>22-24</sup>. While cell retention was decreased over time, these studies still indicated improvements in function post-infarct.



This would suggest that the cells are having a larger paracrine effect than integrating with the damaged tissue to contribute to active mechanical function that is lost post-infarct.

## 8.2 Future work

In this dissertation, we demonstrated that delivering hMSCs to a rat infarct model have the ability to improve regional function. We chose to only examine function 1 week after the infarct was created and the cells were delivered. We chose this time point to look at any acute functional effects the therapy imparted; however, many rodent studies delivering cells chose to examine function out to 1 month after infarct creation as remodeling is mostly complete by this time point in a rat model<sup>25</sup>. In future studies it will be important to examine function at longer time points to understand how the delivery of cells will impact function at later time points. The fibrin suture will degrade over time in the myocardium; however, we demonstrated that cell loaded sutures preserved the area of suture compared to unseeded sutures. It is then possible that the retention of the biomaterial in the infarct had an impact on function over the cells alone. By examining function out to 1 month the fibrin suture should be completely degraded and we would have a better understanding of functional outcomes without the prolonged presence of the biomaterial. In addition to functional benefits, more work could be done at the tissue level to understand the role of inflammation and angiogenesis, utilizing immunohistochemical techniques, at both the one week and one month time points. This would provide more information on how the hMSCs are functioning in the infarct environment and how they and the fibrin suture are resulting in improvements in function in terms of modulating inflammation and driving angiogenesis.

For the studies utilizing hPS-CM, we demonstrated that the cells align along the suture and that contractile strains increase over 21 days. The cells seeded on tissue culture plastic did not have any dominate alignment and decreased strains over 21 days. It is possible that the stiffness differences alone led to the ability for the cells to generate greater strains on the fibrin microthreads over the very stiff TCP. While studies suggest that cells in an unaligned fibrin gel are not capable of generating higher strains and

that aligned softer substrates are more contractile, it remains important to examine the cells temporal contractile function in a softer environment<sup>26, 27</sup>. We chose to utilize collagen IV coated TCP as controls for our experiments, however a fibrin gel may have been a more relevant choice to examine functional contraction of the hPS-CM. Thus future studies will look at temporal changes in hPS-CM function when seeded in a fibrin gel.

While we demonstrated that the hPS-CM were capable of aligning along the microthread and increasing contractile strain and conduction velocities over 21 days we did not see any changes in Connexin 43 localization. In a mature adult cardiomyocyte Connexin 43 is polarized to the intercalated discs to allow for faster cardiac conduction. Many studies utilizing hPS-CM have suggested that hPS-CM are a relatively immature cell type in terms of sarcomere length, Connexin 43 localization, electrophysiology, and force production among other markers of maturity<sup>28, 29</sup>. One of the challenges within the field of regenerative medicine to utilize hPS-CM to their full potential is to create culture methods to mature hPS-CM. Studies have indicated that substrate stiffness, ECM incorporation, alignment, time in culture, and electrical and mechanical conditioning can mature hPS-CM<sup>16, 30-33</sup>. Future studies could use the fibrin suture as a maturation platform by integrating cardiac ECM into the suture, providing electrical and mechanical conditioning and examining functional maturation over time.

One of the challenges of working with pluripotent stem cell derived cardiomyocytes is the batch-to-batch variability that may occur due to the starting cell line or how the cells are differentiated. The differentiation process is a very sensitive process that even with the best, controlled methods can still lead to differences in differentiation efficiencies. It is possible that these changes in differentiation efficiencies can then affect how the cells respond out of cryopreservation in terms of viability, how they reattach to substrates, and how well they function. Thus, it will be important in future studies to ensure that similar levels of viability, attachment, and function are demonstrated with multiple batches. Additionally, it will be interesting to examine the effect of cryopreservation on cell attachment and

viability by examining freshly differentiated and dissociated cells from cells that came out of cryopreservation. We can repeat many of the same experiments done in objective 2a to determine the effects of different batches of cells as well as freshly dissociated cells on cell attachment, viability, and function. In order to truly consider stem cell therapy for myocardial infarction treatment it is necessary to create a highly controlled process that produces the same results time after time without having fluctuation in cell performance using different batches of cells.

In this dissertation we demonstrated that the fibrin suture was capable of delivering hPS-CM to healthy cardiac tissue with a 67% delivery efficiency, very similar to that found for delivering hMSCs. While this is an exciting finding, when we examined retention at later time points we saw a decrease in the number of cells retained by 3 days. By using an Annexin V *in vitro* delivery assay we demonstrated that viability for the cells was low after simulated delivery conditions. Thus, future studies will need to address this issue and improve cell viability. Methods for improving cell viability could incorporate improving cell attachment as well as heat shock or treating with a type of pro-survival cocktail as has been done in previous studies delivering this cell type to myocardial tissue<sup>3,34</sup>. Once the issue of cell viability is resolved and we have a system in place to ensure sustained cell retention, we can then begin delivering these cells to an infarct model. The rat infarct model is not an ideal model to study the regenerative effects of hPS-CM due to the large mismatch in beating rates (60 vs 400 bpm). Thus, larger animal models such as a rabbit or guinea pig, which have slower heart rates, could be used to examine how the delivery of hPS-CM seeded fibrin sutures affect functional regeneration post-infarct.

In order to use a larger animal model several questions regarding the delivery of the microthreads need to be addressed such as the number of threads that would be delivered. Larger animals have larger hearts than rats and thus higher numbers of cells delivered via more microthreads could be used in those systems. The number of microthreads that could be delivered could be determined by direct scale differences between the rat and the larger animal model, such that if a pig heart is five times larger than

a rat heart then five times more threads could be delivered. However, we have not examined the functional impact of the delivery of more than one suture to the ventricular myocardium of a rat and it is possible that the myocardium can support the delivery of more than one suture. Thus, future studies could be completed to examine the functional impact of delivering multiple sutures, as well as modulating the number of threads incorporated into the suture, to the rat heart and use the results to better inform how to scale up the technology for use in larger animal models. Additionally, future studies should take into consideration the depth into and length along the ventricular myocardium that the suture can penetrate in a larger heart. Finally, for true clinical translation a catheter based delivery system should be developed to allow the sutures to be delivered into the endocardial wall using a catheter lab instead of relying on using open heart surgery techniques for epicardial suture placement and cell delivery.

### 8.3 References

1. Hare JM, Traverse JH, Henry TD, Dib N, Strumpf RK, Schulman SP, Gerstenblith G, DeMaria AN, Denktas AE, Gammon RS, Hermiller JB, Jr., Reisman MA, Schaer GL and Sherman W. A randomized, double-blind, placebo-controlled, dose-escalation study of intravenous adult human mesenchymal stem cells (prochymal) after acute myocardial infarction. *Journal of the American College of Cardiology*. 2009;54:2277-86.
2. Behfar A, Crespo-Diaz R, Terzic A and Gersh BJ. Cell therapy for cardiac repair-lessons from clinical trials. *Nat Rev Cardiol*. 2014;11:232-246.
3. Laflamme MA, Chen KY, Naumova AV, Muskheli V, Fugate JA, Dupras SK, Reinecke H, Xu C, Hassanipour M, Police S, O'Sullivan C, Collins L, Chen Y, Minami E, Gill EA, Ueno S, Yuan C, Gold J and Murry CE. Cardiomyocytes derived from human embryonic stem cells in pro-survival factors enhance function of infarcted rat hearts. *Nature biotechnology*. 2007;25:1015-24.
4. Chong JJ, Yang X, Don CW, Minami E, Liu YW, Weyers JJ, Mahoney WM, Van Biber B, Cook SM, Palpant NJ, Gantz JA, Fugate JA, Muskheli V, Gough GM, Vogel KW, Astley CA, Hotchkiss CE, Baldessari A, Pabon L, Reinecke H, Gill EA, Nelson V, Kiem HP, Laflamme MA and Murry CE. Human embryonic-stem-cell-derived cardiomyocytes regenerate non-human primate hearts. *Nature*. 2014;510:273-7.
5. Gao L, Kupfer ME, Jung JP, Yang L, Zhang P, Da Sie Y, Tran Q, Ajeti V, Freeman BT, Fast VG, Campagnola PJ, Ogle BM and Zhang J. Myocardial Tissue Engineering With Cells Derived From Human-Induced Pluripotent Stem Cells and a Native-Like, High-Resolution, 3-Dimensionally Printed Scaffold. *Circ Res*. 2017;120:1318-1325.
6. Hou D, Youssef EA, Brinton TJ, Zhang P, Rogers P, Price ET, Yeung AC, Johnstone BH, Yock PG and March KL. Radiolabeled cell distribution after intramyocardial, intracoronary, and interstitial retrograde coronary venous delivery: implications for current clinical trials. *Circulation*. 2005;112:1150-6.
7. Vrtovec B, Poglajen G, Lezaic L, Sever M, Socan A, Domanovic D, Cernelc P, Torre-Amione G, Haddad F and Wu JC. Comparison of transendocardial and intracoronary CD34+ cell transplantation in patients with nonischemic dilated cardiomyopathy. *Circulation*. 2013;128:S42-9.
8. Proulx MK, Carey SP, Ditroia LM, Jones CM, Fakhrazadeh M, Guyette JP, Clement AL, Orr RG, Rolle MW, Pins GD and Gaudette GR. Fibrin microthreads support mesenchymal stem cell growth while maintaining differentiation potential. *Journal of biomedical materials research Part A*. 2011;96:301-12.
9. Guyette JP, Fakhrazadeh M, Burford EJ, Tao ZW, Pins GD, Rolle MW and Gaudette GR. A novel suture-based method for efficient transplantation of stem cells. *Journal of biomedical materials research Part A*. 2013;101:809-18.
10. Christman KL, Vardanian AJ, Fang Q, Sievers RE, Fok HH and Lee RJ. Injectable fibrin scaffold improves cell transplant survival, reduces infarct expansion, and induces neovasculature formation in ischemic myocardium. *Journal of the American College of Cardiology*. 2004;44:654-60.
11. Dai W, Wold LE, Dow JS and Kloner RA. Thickening of the Infarcted Wall by Collagen Injection Improves Left Ventricular Function in Rats: A Novel Approach to Preserve Cardiac Function After Myocardial Infarction. *Journal of the American College of Cardiology*. 2005;46:714-719.
12. Rane AA and Christman KL. Biomaterials for the Treatment of Myocardial Infarction A 5-Year Update. *Journal of the American College of Cardiology*. 2011;58:2615-2629.
13. Shiba Y, Fernandes S, Zhu WZ, Filice D, Muskheli V, Kim J, Palpant NJ, Gantz J, Moyes KW, Reinecke H, Van Biber B, Dardas T, Mignone JL, Izawa A, Hanna R, Viswanathan M, Gold JD, Kotlikoff MI, Sarvazyan N, Kay MW, Murry CE and Laflamme MA. Human ES-cell-derived cardiomyocytes electrically couple and suppress arrhythmias in injured hearts. *Nature*. 2012;489:322-5.
14. Huebsch N, Loskill P, Mandegar MA, Marks NC, Sheehan AS, Ma Z, Mathur A, Nguyen TN, Yoo JC, Judge LM, Spencer CI, Chukka AC, Russell CR, So PL, Conklin BR and Healy KE. Automated Video-Based Analysis of Contractility and Calcium Flux in Human-Induced Pluripotent Stem Cell-Derived Cardiomyocytes Cultured over Different Spatial Scales. *Tissue Eng Part C Methods*. 2015;21:467-79.

15. Asakura K, Hayashi S, Ojima A, Taniguchi T, Miyamoto N, Nakamori C, Nagasawa C, Kitamura T, Osada T, Honda Y, Kasai C, Ando H, Kanda Y, Sekino Y and Sawada K. Improvement of acquisition and analysis methods in multi-electrode array experiments with iPSC cell-derived cardiomyocytes. *Journal of pharmacological and toxicological methods*. 2015;75:17-26.
16. Jacot JG, McCulloch AD and Omens JH. Substrate stiffness affects the functional maturation of neonatal rat ventricular myocytes. *Biophys J*. 2008;95:3479-87.
17. Rajasingh S, Thangavel J, Czirok A, Samanta S, Roby KF, Dawn B and Rajasingh J. Generation of Functional Cardiomyocytes from Efficiently Generated Human iPSCs and a Novel Method of Measuring Contractility. *PLoS One*. 2015;10:e0134093.
18. Hescheler J, Halbach M, Egert U, Lu ZJ, Bohlen H, Fleischmann BK and Reppel M. Determination of electrical properties of ES cell-derived cardiomyocytes using MEAs. *Journal of electrocardiology*. 2004;37, Supplement:110-116.
19. Eng G, Lee BW, Protas L, Gagliardi M, Brown K, Kass RS, Keller G, Robinson RB and Vunjak-Novakovic G. Autonomous beating rate adaptation in human stem cell-derived cardiomyocytes. *Nat Commun*. 2016;7.
20. Taylor RJ, Moody WE, Umar F, Edwards NC, Taylor TJ, Stegemann B, Townend JN, Hor KN, Steeds RP, Mazur W and Leyva F. Myocardial strain measurement with feature-tracking cardiovascular magnetic resonance: normal values. *European Heart Journal - Cardiovascular Imaging*. 2015;16:871-881.
21. Bursac N, Parker KK, Iravanian S and Tung L. Cardiomyocyte Cultures With Controlled Macroscopic Anisotropy. *A Model for Functional Electrophysiological Studies of Cardiac Muscle*. 2002;91:e45-e54.
22. Funakoshi S, Miki K, Takaki T, Okubo C, Hatani T, Chonabayashi K, Nishikawa M, Takei I, Oishi A, Narita M, Hoshijima M, Kimura T, Yamanaka S and Yoshida Y. Enhanced engraftment, proliferation, and therapeutic potential in heart using optimized human iPSC-derived cardiomyocytes. *Scientific Reports*. 2016;6:19111.
23. Tachibana A, Santoso MR, Mahmoudi M, Shukla P, Wang L, Bennett M, Goldstone AB, Wang M, Fukushi M, Ebert A, Woo YJ, Rulifson E and Yang PC. Paracrine Effects of the Pluripotent Stem Cell-Derived Cardiac Myocytes Salvage the Injured Myocardium. *Circ Res*. 2017.
24. Rojas SV, Kensal G, Rotaermel A, Baraki H, Kutschka I, Zweigerdt R, Martin U, Haverich A, Gruh I and Martens A. Transplantation of purified iPSC-derived cardiomyocytes in myocardial infarction. *PLoS ONE*. 2017;12:e0173222.
25. Krzeminski TF, Nozynski JK, Grzyb J and Porc M. Wide-spread myocardial remodeling after acute myocardial infarction in rat. Features for heart failure progression. *Vascular pharmacology*. 2008;48:100-8.
26. Chrobak MO, Hansen KJ, Gershlak JR, Vratsanos M, Kanellias M, Gaudette GR and Pins GD. Design of a Fibrin Microthread-Based Composite Layer for Use in a Cardiac Patch. *ACS Biomaterials Science & Engineering*. 2017;3:1394-1403.
27. Black LD, Meyers JD, Weinbaum JS, Shvelidze YA and Tranquillo RT. Cell-Induced Alignment Augments Twitch Force in Fibrin Gel-Based Engineered Myocardium via Gap Junction Modification. *Tissue engineering Part A*. 2009;15:3099-3108.
28. Lundy SD, Zhu WZ, Regnier M and Laflamme MA. Structural and functional maturation of cardiomyocytes derived from human pluripotent stem cells. *Stem Cells Dev*. 2013;22:1991-2002.
29. Yang X, Pabon L and Murry CE. Engineering adolescence: maturation of human pluripotent stem cell-derived cardiomyocytes. *Circ Res*. 2014;114:511-23.
30. Baharvand H, Azarnia M, Parivar K and Ashtiani SK. The effect of extracellular matrix on embryonic stem cell-derived cardiomyocytes. *Journal of molecular and cellular cardiology*. 2005;38:495-503.
31. Nunes SS, Miklas JW, Liu J, Aschar-Sobbi R, Xiao Y, Zhang B, Jiang J, Masse S, Gagliardi M, Hsieh A, Thavandiran N, Laflamme ML, Nanthakumar K, Gross GJ, Backx PH, Keller G and Radisic M. Biowire: a

platform for maturation of human pluripotent stem cell-derived cardiomyocytes. *Nat Methods*. 2013;10:781-786.

32. Ruan J-L, Tulloch NL, Razumova MV, Saiget M, Muskheli V, Pabon L, Reinecke H, Regnier M and Murry CE. Mechanical Stress Conditioning and Electrical Stimulation Promote Contractility and Force Maturation of Induced Pluripotent Stem Cell-Derived Human Cardiac Tissue. *Circulation*. 2016;134:1557-1567.

33. Mihic A, Li J, Miyagi Y, Gagliardi M, Li SH, Zu J, Weisel RD, Keller G and Li RK. The effect of cyclic stretch on maturation and 3D tissue formation of human embryonic stem cell-derived cardiomyocytes. *Biomaterials*. 2014;35:2798-808.

34. Ogasawara T, Okano S, Ichimura H, Kadota S, Tanaka Y, Minami I, Uesugi M, Wada Y, Saito N, Okada K, Kuwahara K and Shiba Y. Impact of extracellular matrix on engraftment and maturation of pluripotent stem cell-derived cardiomyocytes in a rat myocardial infarct model. *Scientific Reports*. 2017;7:8630.

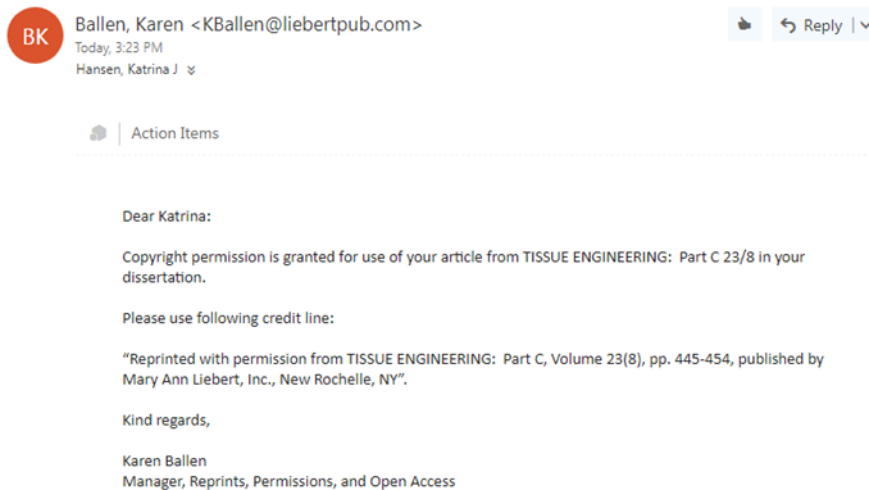
## 9 Appendix

### 9.1 Reprint Permissions

*Reprint permission for work included in chapters 3 and 4, from the publisher's website:*

"BioResearch Open Access publishes articles under the liberal CC-BY license. This means that articles can be freely redistributed and reused by the author and others as long as the article is properly cited. Published articles in *BioResearch Open Access* can be deposited immediately into an online repository or social network without an embargo. *BioResearch Open Access* articles can be emailed to colleagues, printed, archived in a collection, included in course-packs, and distributed without restrictions. Please read the full [Creative Commons license](#) for further information."

Reprint permission for work included in chapter 5:



### 9.2 Protocols

Protocols listed here:

- 1.2.1. Seeding fibrin sutures with hMSCs
- 1.2.2. Masson's Trichrome
- 1.2.3. Cardiac regional mechanics using HDM
- 1.2.4. GCaMP Scope /GCaMP analysis
- 1.2.5. Contractile strain analysis using HDM
- 1.2.6. Seeding fibrin threads with hPS-CM
- 1.2.7. Ku80 staining, Alpha-actinin and Connexin 43
- 1.2.8. Annexin V assay

#### 9.2.1 Protocol for seeding fibrin sutures using rotator method

##### **Materials:**

- Sterile thread-bundle in Bioreactor
- Sterile PBS
- Sterile 1 mL syringe (3)
- Cell Suspension (100,000 cells/100  $\mu$ L or 50,000/100  $\mu$ L, or 25,000/100  $\mu$ L)
- 50 mL vented conical tube
- Tube rotator (fully charged!)

##### **Procedure:**



1. Use a sterile syringe to inject sterile PBS into bioreactor (by attaching syringe to the already inserted 27G needle).
2. Ensure all bubbles are eliminated from the bioreactor.
3. Attach slide clamp and remove/discard syringe. (Keep syringe needle in the bioreactor).
4. Allow 20 min for hydration
5. While bundle hydrates prepare cell suspension according to cell passaging protocol
6. Use new syringe to expel all sterile PBS from the bioreactor before seeding. For this, remove the slide clamp at the end opposite to the needle, draw air into a new sterile syringe and push the air into the bioreactor to expel all the PBS.
7. Use a new syringe (1 cc maximum) to inject cell suspension into the bioreactor. For this, hold the bioreactor such that the open end of the bioreactor (one without slide clamp) remains elevated such that the cell suspension doesn't spill out while being injected. After 100  $\mu$ L of cell suspension is injected into the bioreactor, close the end opposite the needle by sliding the clamp onto the tubing.
8. After injecting the cell suspension and adding the slide clamp, remove the 27G needle from the bioreactor.
9. Place the bioreactor into a gas permeable 50 mL conical tube.
10. Place the bioreactor into the MACSmix tube rotator and rotate at 4 RPM (lowest setting) for 1-24 hours.

For cells destined to be implanted make sure they are Quantum dot loaded 24 hours before hand. Sutures seeded for implants are seeded at a concentration of 100,000cells/100 $\mu$ L for 24 hour before implantation.

### 9.2.2 Masson's Trichrome staining

#### **Reagents:**

- Bouin's Solution (sigma HT10-1-128)
- Weigert Iron Hematoxylin
  - Solution A (sigma HT107-500mL)
  - Solution B (sigma HT109-500mL)
  - Working Solution: Mix equal parts of solutions A and B
- Biebrich Scarlet-Acid Fuchsin Solution (HT151-250 mL)
  - 1% Biebrich Scarlet
    - Biebrich Scarlet-----2g
    - Distilled water -----198 mL
  - 1% Acid Fuchsin
    - Acid Fuchsin-----1g
    - Distilled Water-----99 mL
  - Working Solution:
    - 1% Biebrich Scarlet -----180 mL
    - 1% Acid Fuchsin -----20 mL
    - Glacial acetic acid-----2 mL
- Phosphomolybdic/phosphotungstic Acid Solution
  - Working Solution:
    - Using Solutions:
      - 1 Part Phosphomolybdic acid solution (HT156-250 mL)
      - 1 Part Phosphotungstic acid solution (HT152-250 mL)
      - 2 Parts Distilled Water
    - or-----
    - Using Powders:
      - Phosphomolybdic acid -----5g
      - Phosphotungstic acid -----5g
      - Distilled Water -----200 mL
- Aniline Blue Solution 1%
  - Aniline Blue-----5g

- Glacial Acetic Acid-----4 mL
- Distilled Water-----200 mL
- Acetic Acid Solution 1%
  - 1 mL: Glacial Acetic Acid
  - 99 mL: Distilled Water

**For frozen sections:**

1. Rinse slides in distilled water (5 mins)
2. Mordant the sections in Bouin solution for 1 hour at 60 degC
3. Remove slides from oven, wash in running water (10min)
4. Stain sections in Weigert hematoxylin for 10 minutes **Discard solution**
5. Wash in warm running tap water for 10 minutes
6. Stain sections in Biebrich Scarlet-Acid Fuchsin Solution for 10 minutes **Reuse solution**
7. Rinse in distilled water (2 minutes)
8. Place slides in Phosphomolybdic/phosphotungstic acid solution for 10 minutes, **Reuse solution**
9. Stain sections in aniline blue solution for 10 minutes. (Increase time for greater blue color) **Reuse solution**
10. Rinse slides in running water 2 minutes
11. Place slides in 1% acetic acid solution for 5 minutes. **Discard this solution**
12. Dehydrate through graded alcohols, clear in two changes of xylene and mount with cytoseal

**Results:**

Nuclei: Black

Collagen and Mucus: Blue

Cytoplasm, Keratin and Muscle fibers: Red

**9.2.3 High density mapping for regional cardiac function analysis**

All raw images should be saved in raw data folder under the experiment number for the animal (Eg Exp0404). All images and pressure files should be saved in a separate data set folder under the Experiment folder (Eg Exp0404\_ds1).

1. Open matlab under the Gaudette lab analysis environment (Session start is saved in projects under ~GCE folder and labeled GCE\_sessionstart)
2. Open to projects and the folder of the experiment you are analyzing
3. Batch your tiffs into avis
  - a. `tiff2avi_batch([],250,250,20, 11)`
  - b. 250= frame rate and sample rate
  - c. 20 = output frame rate
  - d. 11=the minimum number of tiffs in the folder to run the avi function
  - e. You will have to self-select the folder, by using the batch function you can select all data sets within one experiment and matlab will create avis for all of them
4. Name your dataset
  - a. 'Exp0404ds1'
  - b. This names the data set you want to analyze
5. Run heart mechanics code
  - a. `Heart_mechanics(ds, [beatgroups] , 'camera', 'fastcam')`
  - b. Beat groups = ]1, 2, 3, etc)...you will have to watch the video and select which beats you want to analyze. Don't analyze beats with a lot of movement/when the animal is breathing.
  - c. Only need to use 'camera' and 'fastcam' if you are analyzing videos taken with the old camera
  - d. In this analysis function the automatic settings are subimage: 32, shift: 16 and roi: poly
  - e. You will have to self-select the dataset folder where the tiff images are stored
6. Once the figure comes up...select the region you want to analyze, then close the region, then close the figure

7. Matlab will run the analysis and will output all data (SAC, RSW, pressure, heart rate etc) into a 'heart\_summary' spreadsheet and will continue to add to it per data set you analyze

#### 9.2.4 Dual imaging scope/setup parameters and analysis

Use the following specifications for 142 fps:

- Bin 2
- 1024x512
- Pulse: 2
- Exposure: 7ms

1. Turn on camera (Hamamatsu orca flash 4)
2. Turn on scope- in the back
3. Turn on power bar – powers LED and digital controller
4. Turn on fluorescence (camera (-), fluo (+))
5. Open micromanager  
Make sure correct program is loaded (100fps program...)
6. Go to device property browser in micromanager (under tools)  
change to “programmable” (DCAM- output trigger) Trigger output 1-0.5us  
make all polarity negative

To change the region of interest...go live...then hit expand...then stop live...and drag the square all the way to the right and left...then go live again. Do all of this in Bin 1 and then change to Bin 2.

#### **For GCaMP analysis**

All videos taken will be saved as tiff stacks and in order to use them you need to make substacks and separate out the tiffs.

1. Split stacks into substacks. Drag stack into ImageJ  
Image – stacks- tools – make substack  
If you have 1000 frames...do 1-1000-2....then next substack will be 2-1000-2 (this will separate out every other frame starting at 1 or 2)
2. Open brightness and contrast dialogue in ImageJ (Image – adjust – brightness/contrast). Adjust brightness and contrast by sliding the frame slider to the brightest point and hit 'auto' on brightness/contrast dialogue.
3. Change to an 8 bit file type  
Image – type- 8 bit  
Hit Apply on Brightness/contrast
4. Save substack in a new folder (label one brightfield, label one fluo)

In matlab:

1. Split the stacks into tiffs  
`split_tiff_stack ('name', [], [0 1])`
2. Run HDM on the brightfield images.  
Pull rawhdm.mat file (under matlab folder) into the workspace to define the ROI for the GCaMP analysis.

#### **GCaMP analysis**

Run: `gcamp_intensity2 (ds, roi, and x: y)`

x:y eg 5:20- frames...they don't matter at all, just pick random numbers

Outputs are an intensity.xlsx spreadsheet which does  $\Delta F/F_0$

#### **GCaMP heatmap production**

1. Run: `edit gcamp_intensity2`

2. hit debug at line 102 – this is at the end of intensity heatmap section, imwrite...

3. Run: `gcamp_intensity2(ds, roi, and x: y)`

If done correctly, a bunch of variable should pop up in the workspace

4. Run: `colormap (jet), imagesc (perinc)`

Your heatmap should come up as a figure...save this figure

5. To change the scale and remove the border...

run: `set(gca, 'position', [0 0 1 1], 'units', 'normalized')`

to scale down to ex. `1125x512 .... [0 0 0.46875 0.2843]`

6. Save

run: `print ('name', 'dtiff', '-r300')`

saves to your working directory

### 9.2.5 High density mapping for contractile cell analysis

All raw images should be saved in raw data folder under the experiment number for that cell thaw (Eg Exp4158).

All images should be saved in a separate data set folder in a separate day folder (Eg D7) under the Experiment folder explaining the conditions examined (Eg Exp4158\_thread1\_1).

1. Make tiffs into AVIs

a. Save under projects folder

For single AVIS use

`tiff2avi(ds, record rate, sample rate, output rate)`

eg. `tiff2avi(ds,60,60,30)` for 60 fps

For batch code

`tiff2avi_batch([], record rate, sample rate, output rate, min tiffs)`

eg. `tiff2avi_batch([], 60, 60, 30, 11)`

It will have you self-select the folder (in raw images) that contain the tiffs you want to make into avis

2. If you need to split the tiffs use:

a. `split_tiff_stack('name', [], [0 1])`

i. 0 and 1 control for brightness

3. Define your data set which is whatever the folder name is that you are analyzing

4. **\*\*Run HDM**

a. `hdm2(ds, frame rate, frames to use, subsize, shift)`

b. Eg `hdm2(ds, 60, 3:500, 16, 8)`

c. It will have you self-select your folder (in raw data) that contains the tiff images you want to analyze

d. **\*\*make sure you are analyzing in projects\*\***

5. To output to excel

a. `hdm2_avgstrain(ds,1)`

6. to rezero

a. `hdm2_cyclicstrain(ds, 'E2', 'maxfreqmaxs')`

i. this rezeroes it to your E2 strain

7. For heatmaps

a. `hdm2_strainfield_beatavg(ds, resolution, ranges, scale, color)`

b. eg `hdm2_strainfield_beatavg(ds, 5, {6:12, 40:47...}, [-0.1 0.1], '-jet')`

i. always use 5 as your resolution if you use a 16, 8 subimage and shift

ii. ranges are the zero to peak frame #s of a contraction

iii. scale is the strains you want to visualize between (eg -10 and 10% = [-0.1 0.1])

iv. color is the color map that will be output...'-jet'...blue is not contracting, red is contraction (for E2)

8. to quantify strain values

a. open heatmap folder...open beat avg folder...drag strain.mat into the workspace

i. `e2=straindata.E2`

- ii.  $I_c = e_2 < -0.05$  (this is your “noise” threshold value...aka less than 0.5% strain)
  - iii.  $\text{mean}(\text{mean}(e_2(I_c)))$  this is your avg strain aka Contractile strain
  - iv.  $\text{min}(e_2(I_c))$  this is your maximum contractile strain
9. to find the percentage that the region is contracting
- a. `percentcontract(threshold, straindata)`
    - i. eg `percentcontract(-0.05, straindata.E2)`

Here E2= contraction

E1= relaxation

\*\*for batch HDM analysis

1. Have all your folders that you want to analyze in one master folder
2. `Hdm2_batch([], frame rate, subimage size, shift)`
  - a. It will have you self-select the folder that contains all folders with the tiffs you want to analyze. Just select all the folders and hit okay
  - b. It will then analyze the folders and bring up the first images of each folder one by one
  - c. Select the region of interest you want to analyze, close the region, then close the image...it will then bring up the next image...

Then analyze folders for excel/quantifying as described above

#### 9.2.6 Protocol for seeding microthreads with hPS-CM

##### **Materials:**

- Sterile thread construct in 6 well plate with coating platform (sterilize using ETO)
- Extra 6 well plate with seeding platform
- Sterile PBS
- Sterile forceps
- Cell Suspension (200,000 cells/150  $\mu$ L) in 50ug/mL Aprotinin supplemented RPMI-B27 media +10% FBS + 1% Rock inhibitor (Sigma, Y0503, 1mg)

##### **Procedure:**

11. Add 2 mL of sterile PBS to each 6 well that had a thread construct
12. Allow 20 min for hydration
13. While threads hydrate prepare your ECM coating solution
  - a. Typically use Collagen IV (10ug/mL)
14. Use sterile forceps to place construct on the coating platform making sure all threads are draped across the coverslip
15. Add 150uL of Collagen IV solution onto coverslip ensuring all solution stays on the coverslip
  - a. Also prepare a control 96 well plate with just cells (150,000 cells/cm<sup>2</sup>)
16. Keep in biosafety cabinet for 2 hours
17. During the coating period prepare your cell suspension by thawing a vial of cells and reconstituting in Aprotinin supplemented RPMI-B27 media
18. Move constructs from coating platforms to seeding platforms
19. Add 150uL of cell suspension to each thread construct
20. Place the constructs with cell suspensions into the incubator at 37C with 5% CO<sub>2</sub> for 18 hours
21. After 18 hours, carefully remove constructs from seeding platform and place in a new 6 well plate with 1-2mL of Aprotinin supplemented RPMI-B27 media, enough to cover all the threads
22. Change media every 2-3 days

#### 9.2.7 Ku80, Alpha-actinin, and Connexin 43 staining

##### **Reagents**

- 5% Normal Donkey Serum

- In 5% donkey serum - primary
  - Rabbit monoclonal anti-Ku80 nuclei 1:250 (Abcam ab80592) in your blocking agent
  - Mouse anti-sarcomeric alpha actinin 1:100 (Abcam 9465) in blocking agent
  - Goat anti-connexin 43 1:100 (Abcam 87645)
- In 5% donkey serum - secondary
  - 1:400 donkey anti-rabbit Alexa Fluor 488
  - 1:400 donkey anti-goat Alexa Fluor 568
  - 1:400 donkey anti-mouse Alexa Fluor 647
- Hoechst
  - 0.0167% Hoechst dye in PBS
  - 0.5ul in 3000ul PBS

**Double boil antigen retrieval:**

1. Thaw slides in DiH2O
2. Add 70ml DiH2O + 656ul vector antigen to a big coplin jar
3. Place coplin jar in a beaker with 400ml of DiH2O
4. Heat to 95-98C without boiling
5. Add slides and leave for 30 minutes
6. Remove from heat for 20 min
7. Resume staining

**Procedure (for fixed tissue samples)**

1. Thaw tissue in PBS 5 minutes (or after antigen retrieval)
2. 0.25% Triton-X-100 10 minutes
3. 3 washes PBS, 5 minutes each
4. Block with 5% Normal Donkey Serum 45 minutes
5. Leave serum on negatives but aspirate serum off the positives
6. Primary 1 hour room temp
7. 3 washes in PBS, 5 minutes each
8. Secondary antibody 1 hour at room temperature in the dark
9. 3 washes PBS, 5 minutes each
10. Hoechst – 1:6000 in PBS, 5 minutes
11. 3 washes in PBS, 5 minutes each
12. Coverslip

**Results:**

Human Nuclei: Green

Alpha-actinin: Far red – have to use confocal to visualize

Connexin 43: Red

Nuclei: Blue

**9.2.8 Annexin V Assay**

**Make Fibrin gels**

1. Thaw fibrinogen (70mg/mL standard) and thrombin (250U/mL – have to make)
2. Add 500uL of fibrinogen to an embedding cassette then add 500uL of thrombin (100uL of 250U/ml thrombin + 425uL of 40mM CaCl<sub>2</sub>). Add quickly and carefully avoiding air bubbles
3. Let gels polymerize for 30 minutes

\*Don't need to do aseptically...but you can filter both thrombin and fibrinogen using a 0.22um filter prior to gel formulation

**Annexin V staining**

Prepare 1X Annexin-binding buffer. For example, to make 1 mL 1X buffer, add 200  $\mu$ L 5X Annexin-binding buffer (Component C) to 800  $\mu$ L deionized water.

**Protocol:**

1. Induce apoptosis using 10mM Staurosporine (Billiar lab) in cells cultured on TCP. Prepare a negative control by incubating cells in the absence of the inducing agent. 1 hour
2. After the incubation period, wash the cells in cold PBS.
3. Aspirate PBS and add 1X Annexin-binding buffer.
4. Prepare a 100  $\mu$ g/mL working solution of PI by diluting 5  $\mu$ L 1 mg/mL PI stock solution (Component B) in 45  $\mu$ L 1X Annexin-binding buffer. Store the unused portion of this working solution saved for future experiments
5. Add 10 $\mu$ L of the Annexin V conjugate (Component A) and 1.5 $\mu$ L of the 100  $\mu$ g/mL PI working solution (prepared in step 4) to each 100  $\mu$ L cells in media.
6. Incubate the cells at room temperature for 15 minutes.
7. Wash the cells with 1X Annexin-Binding buffer.
8. Observe the fluorescence using appropriate filters
9. Fix using 4% PFA for 10 minutes

The cells should separate into three groups: live, apoptotic, and dead. Live cells show only weak Annexin V staining of the cellular membrane, while apoptotic cells show a significantly higher degree of surface labeling. Dead cells show both membrane staining by Annexin V and strong nuclear staining from the Propidium iodide.